Structure-Function Study of Human Glucose Transporter 9 (hSLC2A9)

by

Wentong Long

A thesis submitted in partial fulfillment of the requirements for the degree of

Doctor of Philosophy

Department of Physiology
University of Alberta

Abstract

Abnormal serum uric acid (urate) is found related to many medical complications, such as hypertension, gout and kidney stones. Both Single Nucleotide Polymorphism and genome wide association studies demonstrated that the glucose transporter 9 (hSLC2A9) is highly associated with abnormal human plasma urate levels, indicating that hSLC2A9 has an essential physiological role in urate regulation in the human body. Human SLC2A9 is certainly a hexose and urate transporter. However, investigations are still being undertaken to try to reveal the mechanisms of how hSLC2A9 transports hexoses and urate. As a result, this thesis explores the possible pathway of urate translocation mediated by hSLC2A9. We applied site-directed mutagenesis, followed by functional studies with radiolabelled fluxes and electrophysiological measurements to screen several possible groups of residues predicted by our homology hSLC2A9 computer model, which might be involved in urate transport. We hypothesized that the hydrophobic residues I335 and W110, cysteine residues C181, C297, C301, C398, C451, and C459, transmembrane helix 7 (H7), and two residues, Y298 and N429, predicted to be in the binding sites are important for hSLC2A9 urate transport. The results indicate that the I335V mutant transports urate similarly to the wild type hSLC2A9; however, I335 is necessary for urate/fructose trans-acceleration exchange to occur. In addition, tryptophan 110 (W110) is a critical site for urate transport. Two homology computer models of hSLC2A9 and hSLC2A5 reveal that I335 (or the homologous I296 in hSLC2A5) is a key component for protein conformational changes when the protein translocates substrates and W110 is a critical site that could directly

interact with urate during transport. Our results for the cysteine residues in hSLC2A9 demonstrated that C181 and C398 are important for urate translocation while C297 and C451 are not required. Mutation of either C301 or C459 significantly reduced urate transport. Combining the computer model analysis, we suggest that C181 is the residue with which pCMBS reacts; C301 and C459 could plausibly have an intermolecular disulfide interaction, which serves as a central core for the protein structure, thus, also critical for urate transport. Analysis of the chimæric proteins, hSLC2A9$_{(7)5}$ and hSLC2A5$_{(7)9}$ indicate that helix H7 is necessary for urate transport in hSLC2A9b, but not sufficient to allow hSLC2A5$_{(7)9}$ to gain urate transport. *In silico* docking and functional studies allow us to postulate that N429 is a key residue that could form part of the urate binding.

Preface

Some of the research conducted for this thesis forms part of a research collaboration with Professor M. J. Lemieux at the University of Alberta. The electropyhsiological study apparatus referred to in **Chapter 2** and **3** was provided with the assistance of Professor Xing-Zhen Chen at the University of Alberta. The data analysis in **Chapter 2** and **3** are my original work, as well as the literature review in **Chapter 1**.

Part of **Chapter 1.2** is accepted for publication as Wentong Long and Chris I. Cheeseman. 2015. Structure and functional insight into the GLUT family of membrane transporters. Review. *Cell Health and Cytoskeleton.* I was responsible for manuscript composition, and C. Cheeseman contributed to manuscript edits.

Chapter 2 of this thesis has been published as Long W, Panwar P, Witkowska K, Wong K, O'Neill D, Chen X, Lemieux, MJ, Cheeseman, CI. Critical Roles of Two Hydrophobic Residues within Human Glucose Transporter 9 (hSLC2A9) in Substrate Selectivity and Urate Transport. *J Biol Chem*. 2015;290(24):15292-15303.I was responsible for the data collection and analysis as well as the manuscript composition. P. Panwar assisted with the data collection in the protein computer modeling and contributed to manuscript edits.

To my parents, Rui Lian and Jin Yuan, for all the great support and love throughout my studies and work in Canada

Acknowledgements

Life is fascinating.

As a girl grew up in a village surrounding by mountains, I was amazed by all the living organisms found in the forest. I am very lucky that I have the opportunity to study biology and physiology in this wonderful country and university. In the past five years of study, I have gained not only knowledge, but also patience, confidence, friendships, and all the skills I need for research and life. Here, I have to thank many people who give me support and love.

First of all, I would like to express the sincerest appreciation to my PhD supervisor, Dr Chris I. Cheeseman, who has been support me with his patience, trust, and wisdom. I thank him for taking me as his last PhD student, for giving me lots of freedom to work independently, for always encouraging me to have more ideas, for raising concerns of my data if they were confusing, for encouraging me to be more confident, for showing me that presenting our works to the world is as important as doing the experiments in the lab, and for turning a science lover into a real scientist.

Second, I need to thank my PhD committee members, Dr. Elaine Leslie and Dr. Todd Alexander. Todd gave me suggestions on my data and experiments. He was the one who always reminded me that I have to look at the big picture in my research. Elaine also has been always encouraging and giving me advice on my data. She is also a role model for me that a woman with children can also be a success in research.

I also need to thank the PhD thesis external examiners, Dr. Joseph Casey and Dr. Kelle Moley, for taking their valuable time to evaluate my thesis. I also thank Dr. Moley for traveling a long way to attend my defense.

A special thank you goes to Dr. Xing-Zhen Chen. Dr. Chen, who have been gave me lots of support on my research since my undergraduate study. I thank him for showing me all the new techniques in electrophysiology, for teaching me to look at the probability

of my statistic analysis when I am not sure which data to believe and for being very patient with me when I encounter problem in my experiments.

I also need to thank our collaborators Dr. M. Joanne Lemieux and her post-doc Dr. Pankaj Panwar. Without their help in the protein computer model, our publication is not possible.

Next, I need to thank Debbie O'Neill from the bottom of my heart. She is our lab technician and lab manager. I thank her for asking me to do a graduate study in the Cheeseman lab. Without her, I would never in my life have considered undertaking. She is my best companion in the lab and in Canada.

I also need to thank Kenneth Wong, who provided lots of technical support in my electrophysiology experiments. I also thank him for sharing lots of child education experiences.

I need to thank Kyla Smith for providing help with my electrophysiology studies, for teaching me how to set up the two micro-electrode voltage clamp, and lending me her chemicals whenever I had a shortage.

I also need to thank all my friends who gave me lots of support and love during my PhD study. They are:

- Kate Witkowska for getting me started on my research in the lab.
- Wang Zeng for the wonderful discussion on how to design primers for my chimæra mutants.
- Qian Wang for the discussion on how to do the biotinylation of my proteins.
- Olivier Soueidan for teaching me all the chemistry I needed for my experiments. I also thank him for being a good company during our conferences.
- Jeff Liang for babysitting whenever I need to stay late for my experiments.
- Isabella Cheng for lots of love and support for my family.

Next, I need to sincerely thank my husband and son, Sihua and Vincent. Sihua has given me much support during my PhD studies; he cooks the most nutritious food for

the family, and tries to help with house work whenever he can after his busy work and study. Vincent is the most understanding boy that will let mommy finished her work before asking to play.

Last but not least, I think I am most thankful to my lovely parents. I thank them for all the financial, emotional, spiritual supports. Whenever I encounter problem in Canada, they are always there to help. I thank them for always reminding me that they are proud of me.

Table of contents

List of tables

List of figures

List of symbols

µM – micromolar

2DOG – 2-deoxy-D-glucose

3OMG - 3-O-methyl-glucose

ABC – ATP-binding cassette

ABCG2 – Breast Cancer Resistance Protein (BCRP)

ATP – Adenosine triphosphate

BBMV – brush border membrane vesicles

BCRP – Breast Cancer Resistance Protein

cAMP – cyclic adenosine monophosphate

CB – Cytochalacin B

cDNA – complementary deoxyribonucleic acid

***cis* side** – one side of the cell membrane; usually the substrate presenting side

COS 7 – **C**V-1 in **O**rigin with a version of the **S**V40 genome (cell line derived from kidney cells of the African green monkey), form 7

cRNA – complementary ribonucleic acid

DHA – dehydroascorbic acid

DNA – deoxyribonucleic acid

EGF – epithelial growth factor

ER – endoplasmic reticulum

FucP – fucose tranporter

FDG – 18F-Fluorodeoxyglucose

Glcp – glucose / H^+ symporter

GlpT – glycerol-3-phosphate transporter

GLUT9b – GLUT9 with truncated animo terminus

GWAS – genome-wide association studies

h – human, referring to protein homologue

HEK 293 – human embryonic kidney cell line

HepG2 – human liver carcinoma cell line

HMIT – proton-coupled myo-inositol transporter

I-TASSER – Iterative Threading ASSEmbly Refinement

ICH – **Intracellular helical bundles**

IL-1β – interleukin 1β

INS 1 – rat pancreas insulin secreting beta cell

IP3 – inositol-3-phosphate

K_M – Michaelis-Menten kinetic constant representing half-maximal saturation of a carrier by a substrate, also referred to as apparent affinity of substrate for a given carrier

LacY – proton-coupled lactose transporter

m – mouse, referring to protein homologue

MBM- Modified Barth Medium

MCT – proton-coupled monocarboxylate transporter

MDCK – Madin Darby canine kidney cell line

MFS – Major Facilitative Superfamily

mM – millimolar

mRNA – messenger ribonucleic acid

MRP – Multidrug Resistance Protein

MRP4 – multiresistance protein transporter 4 (ABCC4)

MSD – membrane spanning domain(s)

NaDC – Sodium dicarboxylate contransporters

N-terminus – amino terminus

NBD – nucleotide binding domain(s)

NO – nitric oxide

NPT – sodium-phosphate cotransporter

OA^- - organic anion

OAT - organic anion transporter

PAH – *para*-aminohippurate

pCMBS - p-Chloromercuribenzene sulfonate

PCR – polymerase chain reaction

PCT – proximal convoluted tubule

PDZ – protein acronym: PDS-95, DLG1, ZO-1

PDZK1 – PDZ-domain binding protein 1

pH – measure of acidity or basicity of an aqueous solution

pKa – the symbol for the acid dissociation constant at logarithmic scale

PKA – Protein Kinase A

PKC – Protein Kinase C

PMA – Phorbol 12-myristate 13-acetate, Protein Kinase C activator

PZA – pyrazinamide

RAMP – a stepwise protocol used to access the urate conductance mediated by hSLC2A9 and its isoforms

R.M.S.D. – root-mean-square deviation

S.E.M – standard error of mean

Sf9 – *Spodoptera frugiperda* insect cells

SLC – Solute Carrier Proteins

SLC17A3 – sodium-phosphate cotransporter 4 (NPT4)

SLC22A12 – gene name URAT1

SLC2A – gene name for GLUT

SMCT1 – sodium-dependent monocarboxylate transporter

SNP – single nucleotide polymorphism

SSSF – Sodium/Solute Symporter Family

STM - Standard Transport Medium

TM – transmembrane helix

TEVC – Two microelectrode voltage clamping

***trans* side** – the other side of the cell membrane; usually the substrate absent side

UAT – urate transporter, also known as galectin 9

V_{MAX} – Michaelis-Menten kinetic constant representing maximal rate of carrier-mediated transport, also referred to as a carrier's capacity to transport a substrate

XylE - D-xylose transporter

WT – wild type

Chapter 1

Introduction and Literature Review

(A version of this chapter has been submitted as a review article:
Wentong Long and Chris I. Cheeseman. 2015. Structure and functional insight into the GLUT family of membrane transporters. Review. *Cell Health and Cytoskeleton.* Accepted.)

Chapter 1.1. Uric acid (Urate) and its transporters

1.1.1. Outline of introduction on urate transporter in humans

This section will outline the importance of urate as a metabolic end product in humans, and how it is regulated at the molecular level, in particular, how it is regulated in the proximal convoluted tubule (PCT) cell of the kidney. Discussion will be based on a proposed simplified human kidney proximal tubule cell model followed by examination of a more developed model. Attention will focus on transporter proteins, which have moderate to high association with human urate levels.

1.1.2. Introduction to urate and its physiological role in humans

Urate, also known as uric acid, is the end product of the metabolism of purine compounds or dietary food (**Fig. A.1 and Fig. 1.1**) (1). It is a heterocyclic compound composed of carbon, hydrogen, nitrogen, and oxygen molecules ($C_5H_4N_4O_3$). Urate is a weak acid with a pKa of about 5.75, and at physiological pH 7.4 circulates in the human body as the urate anion (2). It is interesting that the majority of mammalian species have extremely low levels of plasma urate (range from 30-80 μM), whereas primates and humans have much higher levels of plasma urate (240 to 350 μM) (3). This discrepancy in levels is because most mammals have an enzyme called uricase (4), which can convert urate into a highly soluble excretory product, allantoin. Primates and humans, on the other hand, have an inactivated uricase gene (5). Thus, urate is the final product before elimination from the human body.

Urate has a long history related to medical conditions. In 1679, Antoni van Leeuwenhoek was the first person who portrayed the appearance of the urate crystal from a gouty tophus (6). Leeuwenhoek was the inventor of the microscope, which he used to examined the "chalk" like substance extracted from a gouty person. As Leeuwenhoek describes in one of his letters:

" I observed the solid matter which to our eyes resembles chalk, and saw to my great astonishment that I was mistaken in my opinion, for it consisted of nothing but long, transparent little particles, many pointed at both ends and about 4“axes” of the globules in length, others shorter and a few only half as long" (6).

However, Leeuwenhoek did not know the chemical properties of this unknown substance yet. Almost a century later, German-Swedish chemist Karl Wilhelm Scheels isolated an acidic substance from a bladder stone and named it "lithic acid" (from Greek "lithos" meaning “stone”) (7). According to George Pearson and Antonine Fourcroy in the 18th centry this substance is one of the basic component of urine stones, and they named it uric acid (known as urate today) (7). Although studies in the 21th centry indicated that kidney stones consist of only 8% of urate (8), these early discoveries established that urate is a common component and the first identified metabolite in human urine.

In 1848, Alfred B. Garrod, an English physician, described the causation of gout as excessive urate in blood (9). Currently, this is known as a medical condition called hyperuricemia. Hyperuricemia not only can lead to diseases like gout, but also has a possibly pathogenic role in cardiovascular diseases,

hypertension, diabetes and metabolic diseases (9–13). Gout, for the first example, was recognized as a painful joint disease back in 2000 BC when the Egyptians categorized this disease as "podagra", which means acute gout occurring in the first metatarsophalangeal joint (14). Hippocrates, later in the fifth century BC, referred to this condition as "the unwalkable disease" (14). Today, gout affects 3% of Canadians and 5% of the overall north Americans (15, 16). Studies have shown that men have a three times higher risk of developing gout than women (16). In 2003, the Feig and Johson pointed out that 89% of hypertension patients have elevated plasma urate levels (17). On the contrary, when urate is excessive in urine, it will develop a condition called hyperuricosuria, which will lead to urate crystallization in the kidney and cause kidney stone (18). As a result of these debilitating medical complications, it is very important to understand how urate is actually regulated in our body.

The human plasma urate level is tightly regulated by its production and elimination from the body, where it maintains a steady state concentration. Since little urate is contained in food, the bulk amount of urate in the human body is produced by endogenous synthesis of xanthine, a metabolic product of purine (**Fig. 1.1**) (1, 2). This urate biosynthesis process is catalyzed by an enzyme known as xanthine oxidase; the process takes place primarily in the liver, with a small contribution from the muscles and the intestines (3). Purine, on the contrary, is richly found in a majority of dietary foods; together with the endogenous synthesis of purine, these components serve as the sole source for urate production in humans. Studies have shown that elimination of dietary purines in

normal people for 10 days can lessen both serum urate level and urinary urate excretion by 25% and 50%, respectively. *De novo* purine synthesis is also important for urate production; however, this multi-step process is energy costly. Thus, it requires a well-organized biochemical system, which can reuse and interchange purine nucleotides, nucleosides, and bases to save cellular energy. Since humans do not have uricase to further degrade urate into allatoin, which is the end metabolite in the purine degradation pathway in other mammals, like mouse. As a result, the human body needs to eliminate the excessive formation of urate, and the kidney is the major organ that can excrete urate.

In humans, the kidney is responsible for two thirds of the urate excretion, whereas the intestinal tract is accountable for the other one third of the elimination (19). Intensive studies have been conducted to identify the urate transporters in the human kidney to discover the mechanisms of how urate is regulated in the body. In 2009, Cheeseman proposed a simple model of urate reabsorption and excretion at the epithelial membrane of PCT in the human kidney (**Fig. 1.2**) (20). He suggested that an organic anion exchanger 1 (URAT1) is responsible for the majority of urate uptake into epithelium. This process is believed to be electroneutral in that URAT1 exchanges urate for intracellular monocarboxylates accumulated by sodium-coupled transporters, SMCTs. Urate exit from the epithellial cells into the peritubular (blood) is facilated by human glucose transporter 9 full length isoform a (encoded by hSLC2A9a), which can exchange glucose for urate in an electrogenic manner. Urate excretion is thought to be mediated by glucose transporter 9 truncated N- termus isoform b

(hSLC2A9b) on the apical membrane, where hSLC2A9b can transport urate out into the PCT lumen with exchange of glucose from the lumen. Therefore, the differential expression of hSLC2A9a and hSLC2A9b on PCT may play an essential role of urate reabsorption and excretion. In addition, the PCT is the site responsible for 90% of glucose reabsorption (21). The presence of hSLC2A9b with the ability to exchange urate and glucose at the site may serve as a main determinant in terms of glucose and urate regulation in the human body.

Later, research effort was focused more on the urate transport mechanism in humans; thus, more molecular members were added to the urate regulation model in the human PCT. Bobulescu and Moe (22) reviewed the most of the possible urate transporter proteins of human PCT in their 2012 article, and they pointed out that the apically localized hURAT1 and the basolateral localized hSLC2A9 are still the most important urate handling candidates. Other players include: the organic anion transporter family (OATs): OAT1, OAT3, OAT4 and OAT10; the Sodium phosphate cotransporters (NPTs): NPT 1 and NPT4; and the ATP-binding cassette transporters: ABCG2 and MRP4 (ABCC4) (22) (**Fig. 1.3**).

Bobulescu and Moe also included the human homologue of rat urate transporter in the model (hUAT, also known as galectin 9). Nevertheless, the functional study of urate transport mediated by hUAT was conducted only in an artificial lipid bilayer system, and no *in vivo* study has been conducted to date to illustrate how hUAT regulates urate in cell or tissues (22). In 2004, Bannasch *et al.* (23). excluded the possibility of hUAT as a urate transporter in Dalmatian dogs,

which have hyperuricosuria due to a genetic defect. As well, another two classes were mentioned in their proposed model, the SMCTs and Sodium dicarboxylate contransporters 1 and 3 (NaDC1/3), all of which demonstrated weak evidence in direct association of urate handling (22). Both SMCTs and NaDC1/3 were believed to function as couplers for the organic anion exchangers (URAT1 and OATs) to translocate urate in human PCT by generating intracellular gradients for monocarboxylates and dicarboxylates (24, 25).

1.1.3. Urate handling members in PCT with moderate to strong research evidence

1.1.3.1. Organic anion transporters family (OATs)

The human organic anion transporters, the OATs family, are encoded by the subfamily of hSLC22A genes, and they are believed to regulate body homeostasis by eliminating endogenous metabolites and foreign chemicals, such as urate and toxic chemicals. You *et al.* (26) and Kuze *et al.* (27) predicted that OAT has 12 transmembrane helices. The predicted topology of OATs reveals a conserved cluster of glycosylation sites on the extracellular loop that connects H1 and H2. Studies have shown that these glycosylation sites are critical for protein trafficking to the cell membrane (28). In addition, OATs contain several phosphorylation sites, which implies a possible phosphorylation provoked functional regulation (29, 30).

OAT1 and OAT3

The cDNAs of hOAT1 (hSLC22A6) and hOAT3 (hSLC22A8) were cloned at the same time in 1999 and encode proteins of 550 and 568 amino acids,

respectively (31, 32). They were both found located on chromosome 11 and expressed on the basolateral membrane of the proximal tubule in the human nephron. Both hOAT1 and hOAT3 showed moderate urate uptake in exchange with dicarboxylate anions when expressed in *Xenopus* oocytes (32–34). Furthermore, both hOAT1 and hOAT3 knockout mice showed evidence of decrease of renal secretion of urate (22). Therefore, these two proteins were hypothesized to be responsible for urate secretion in the human kidney. However, this assumption has only been tested with *in vitro* studies, but not *in vivo* (22, 32–35).

OAT4 and OAT10: Facilitate urate reabsorption

Human OAT4 was found to be expressed on the apical side of the epithelial cell of the proximal tubule in humans (19, 34). The cDNA of OAT4 (hSLC22A11) encodes a 550 amino acid protein, and it shares 44% identity with hOAT1 and hOAT3 (36). Human OAT4 was the first multispecific organic anion transporter that expresses in the kidney as well as in the placenta. hOAT4 is also a low affinity urate exchanger that exchanges urate with organic anion; however, OAT4 exchanges these organic anions in an asymmetrical manner (37–39). Hagos *et al.* demonstrated that hOAT4 expressed *Xenopus* oocyte exemplified only efflux transport activity of *p*-aminohippurate (PAH) but no uptake activity; and this PAH efflux could trans-stimulate urate uptake into the oocytes (39). In the same study, the experimental results elucidated that a diuretic compound called hydrochlorothiazide (HCTZ) can also trans-stimulate urate uptake from the intracellular side, but, again, not from the extracellular side. In a mammalian cell,

it is believed that HCTZ enters the cell through OAT1 at the basolateral membrane, and it can provoke hyperuricemia. Consequently, Hogos *et al.* (39) assumed that this process is due to the cell using OAT4 to release HCTZ into urine, directing the re-absorption of urate. Therefore, they hypothesized that OAT4 is a low affinity urate anion exchanger responsible for urate reabsorption at the apical membrane of the proximal tubule cell.

Human OAT10 was also found expressed on the apical side of the epithelial cell of the proximal tubule in humans (19, 34). Human OAT10 was initially identified as a multifunctional organic-cation transporter similar to hORCTL3 (human organic cation transporter like 3) (40). However, Bahn *et al.* (41) in 2008 renamed it hOAT10 (human organic anion transporter 10, gene name hSLC22A13) when they discovered this 551 amino acid protein was highly expressed at the apical membrane of the renal proximal tubule cell. Human OAT10 has 44% sequence homology to hOAT1 and 33% identical to URAT1(22, 41). Most importantly, they noticed that hOAT10 is a urate transporter and could facilitate urate exchange with other organic anions, such as nicotine, PAH, lactate, and so on. Together, both hOAT4 and hOAT10 were hypothesized for urate reabsorption at the kidney proximal tubules (22).

1.1.3.2. Urate anion exchanger 1 (URAT1): A urate reabsorption transporter

The urate-anion exchanger 1 (URAT1) is the first urate specified transporter found on the proximal tubule of the human kidney. Discovered by Enomoto *et al.* in 2002 (42), URAT1 is a 553 amino acid protein and encoded by SLC22A12. URAT1 has 42% amino acid sequence identity with that from organic

anion transporter 4 (OAT4). URAT1 has a 12 transmembrane helix topology, which is similar to others in the OAT family. URAT1 is known as a urate/monocarboxylate exchanger that exchanges urate with intracellular organic anion when expressed in *Xenopus* oocytes (24). In human nephron, URAT1 expresses mainly on the apical membrane of the proximal tubule but not on the distal tubule. Moreover, on the basis of results from functional studies, Enomoto *et al.* (42) proposed that URAT1 is a urate transporter responsible for urate reabsorption.

Mutations, such as G774A and W258stop, in URAT1 were known SNPs to associate with hypouricemia and acute renal failure (43–45). Genome wide association studies, undertaken by Tin *et al.* (46) *in 2011,* demonstrated a loss of function allele, G65W, of URAT1 in a large group of African Americans. Moreover, evidence showed that urate uptake by URAT1 was inhibited by many uricosuric drugs, such as indomethacin, salicylate, phenylbutazone, probenecid, sulphinpyrazone, and benzbromarone (47). Benzbromarone gave the most potent inhibition effect. More recently, a Japanese group found an interesting fact that whisky can lower serum urate levels in humans, and the urate elimination mechanism is believed to be a direct inhibition on URAT1 (48, 49). As a result, URAT1 is speculated as a high affinity urate exchanger responsible for urate reabsorption in humans (33).

1.1.3.3. Sodium phosphate cotransporters (NPTs): NPT1 and NPT4

Both sodium phosphate cotransporters 1 and 4 are located at the apical membrane of human PCT, and they were first discovered as sodium phosphate

transportersencoded by SLC17A1 and SLC17A3 in rabbit kidney cortex (50–52). Nevertheless, molecular studies and GWAS indicated that both NPT1 and 4 are urate transporters and associated with human plasma urate levels. Iharada *et al.* exposed that NPT1 is a chloride dependent urate transporter when they reconstituted NPT1 in proteoliposomes (53). Miyaji *et al.* also revealed that NPT1 is a membrane potential-driven urate efflux pump when expressed in *Xenopus* oocytes (54). Missense mutant T269I was reported with 30% lower urate transport activity compared to the wild type protein (54). In addition, human patients who carried this T269I were believed to have a high risk of gout(53). Hollis-Moffatt *et al.* confirmed that NPT1 is associated with gout in both Caucasian and Polynesian patients (55). On the other hand, Dehghan *et al.* pointed out a weak association of NPT4 to hyperuricemia patients (56). Jutabha *et al.* (57) demonstrated that three SNPs, V257F, G279R, and P378L, from the public SNP database of NPT4. These SNPs were found to lower the urate transport activities compared to the wild type NPT4 when expressed in oocytes (57, 58). Therefore, it is hypothesized that both NPT1 and 4 could play an important role in urate secretion on the apical membrane at the PCT of the human kidney.

1.1.3.4. ATP-binding cassette transporters (ABC transporters)

The ATP-binding cassette (ABC) transporters belong to the ABC super family, whose proteins were found in most living organisms (59, 60). Unlike OATs and URAT1, these transporters use adenosine triphosphate (ATP) to generate energy to translocate their substrate across biological membranes. Secondary

structures vary among the ABC proteins. A common feature of these transporters is that they are formed by multiple membrane span domain(s) (MSD), which consist of four to six transmembrane helix transmembrane helices, plus multiple subunits with nucleotide binding domain(s) (NBD) (59, 61). For example, ATP-binding cassette subfamily G protein (ABCG2) consists of one NBD and one MSD (NBD-MSD) domain; thus, it is known as a typical "reverse half-transporter" (61). On the other hand, the multidrug resistant protein 4 (MRP4/ABCC4) has a typical four domain structure with MSD-NBD-MSD-NBD (62). ABC tranporters transport a wide range of molecules like lipids, metabolites, and xenobiotics. In 1976, Juliano and Ling first described the drug resistant membrane protein conferring P glycoprotein in (ABCB1) in a drug selected Chinese hamster ovary cells (63). Later, Kathawala *et al.* and Kool *et al.* illustrated that ABC transporters are involved in cancer tumor resistance; that is, these transporters could transport the anti-cancer drugs out of the tumor (60). More recently, researchers found that some ABC transporters are engaged in urate transport in the human kidney (56, 64, 65).

ATP-Binding Cassette Subfamily G protein 2 (ABCG2) was first described as a ABCP transporter encoded by 655 amino acids over expressing in human placenta in 1998 (66, 67). Later, the HUGO Gene Nomenclature Committee assigned it into ABCG2 (68). ABCG2 was also over expressed in multidrug resistant breast cancer cell lines and colon carcinoma cells (67, 69). These observations allowed researchers to speculate that ABCG2 is an efflux pump for xenobiotics, which could prevent foreign toxins from entering the cells. More

recently, Dehghan *et al.* (56) conducted Genome-wide association studies (GWAS) to reveal that ABCG2 is related to urate level and gout. They also found that a missense SNP of ABCG2, Q141K, is directly associated with urate level and gout.

The multidrug resistance protein 4 (MRP4) is an ATP-binding cassette transporter (gene name ABCC4); thus, it also utilizes adenosine triphosphate (ATP) as its energy to transport its substrate across the cell membrane. Using membrane vesicles prepared from Sf9 cells, Van Aubel *et al.* (65) demonstrated that MRP4 can transport urate when ATP was present. In the same study, the authors demonstrated that MPR4 is a unidirectional urate efflux pump when the authors overexpressed MRP4 in the human embryo kidney cell line (HEK293 cell line). Moreover, MRP4 was originally known as a multispecific organic anion transporter B (MOAT-B) and found widely expressed in different human tissues, including kidney and liver (70, 71). More recently, MRP4 was located in the apical membrane of the proximal tubule cell in the kidney as well as the basalateral membrane of liver cell (72). As a result, it was hypothesized that MRP4 is another urate exporter responsible for urinary urate excretion and hepatic urate secretion from the liver cells to blood.

1.1.3.5. Glucose transporter 9 (hSLC2A9)

Human glucose transporter 9 is encoded by human Solute Linked Carrier family 2, subfamily A gene family, SLC2A, member 9 (hSLC2A9). Human GLUT9 was initially characterized as a high affinity-low capacity hexose transporter, but more recently it was determined to be a high capacity urate transporter for which

hexoses can trans-stimulate urate transport (73). Genome-wide association studies reported that hSLC2A9 has the strongest direct association with human plasma urate level, which is associated with gout and cardiovascular complications. Studies unveiled that the Single Nucleotide Polymorphisms (SNPs) of hSLC2A9 are highly associated with human serum urate level (74). Currently, thirteen hSLC2A9 mutations have been found in patients who developed critical renal hypouricemia condition (74–79). Ten of these mutants are missense/nonsense mutations, one small insertion, one large duplication, and one deletion. I will discuss structure function studies of GLUT9 in the next section, The Glucose Transporters.

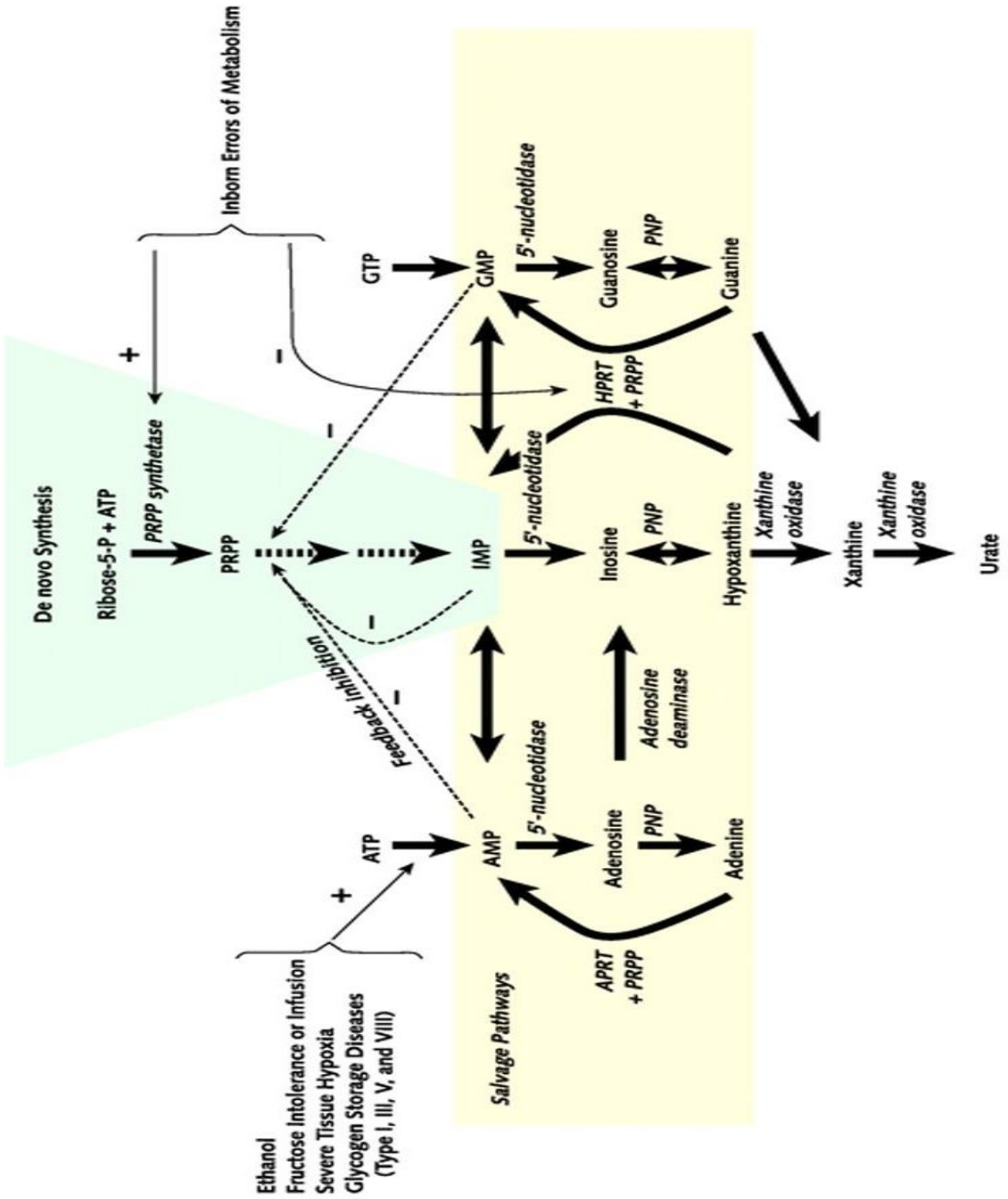

Figure 1. 1. *De novo* synthesis of urate in human body.

Adapted from (1).

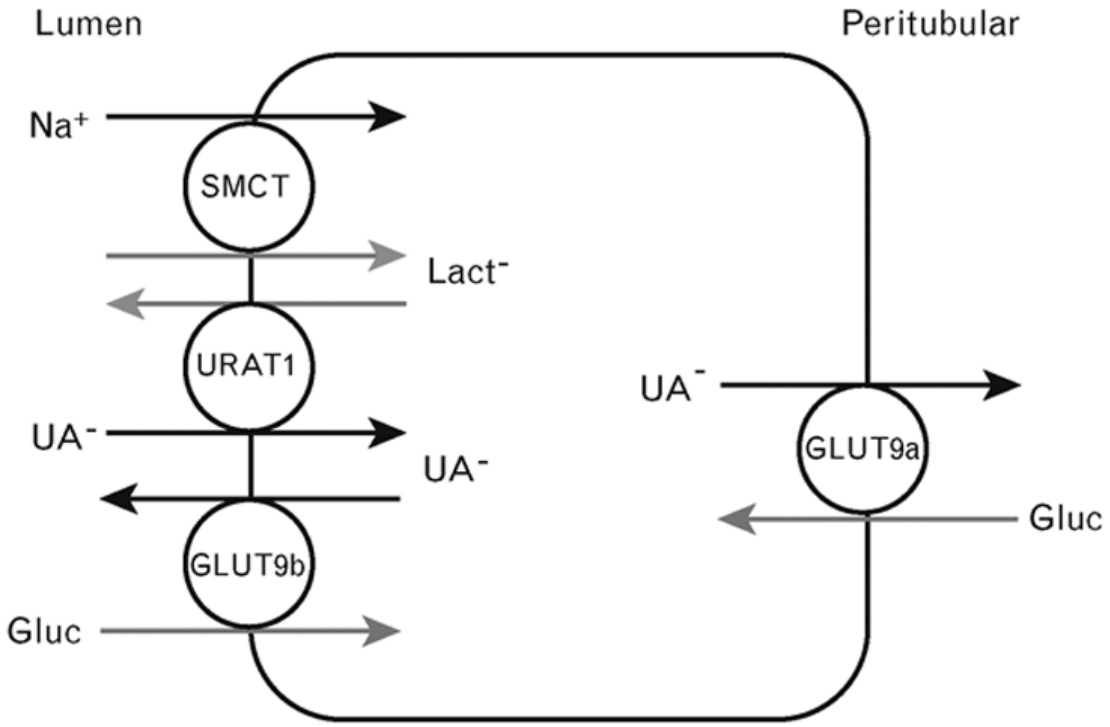

Figure 1. 2. . A proposed simple model of urate absorption and secretion in human proximal renal tubule.

Note: $Lact^-$ is lactate acid anion; Na^+ is sodium cation; UA^- is uric acid anion; Gluc is glucose molecule(s).Adapted from (20).

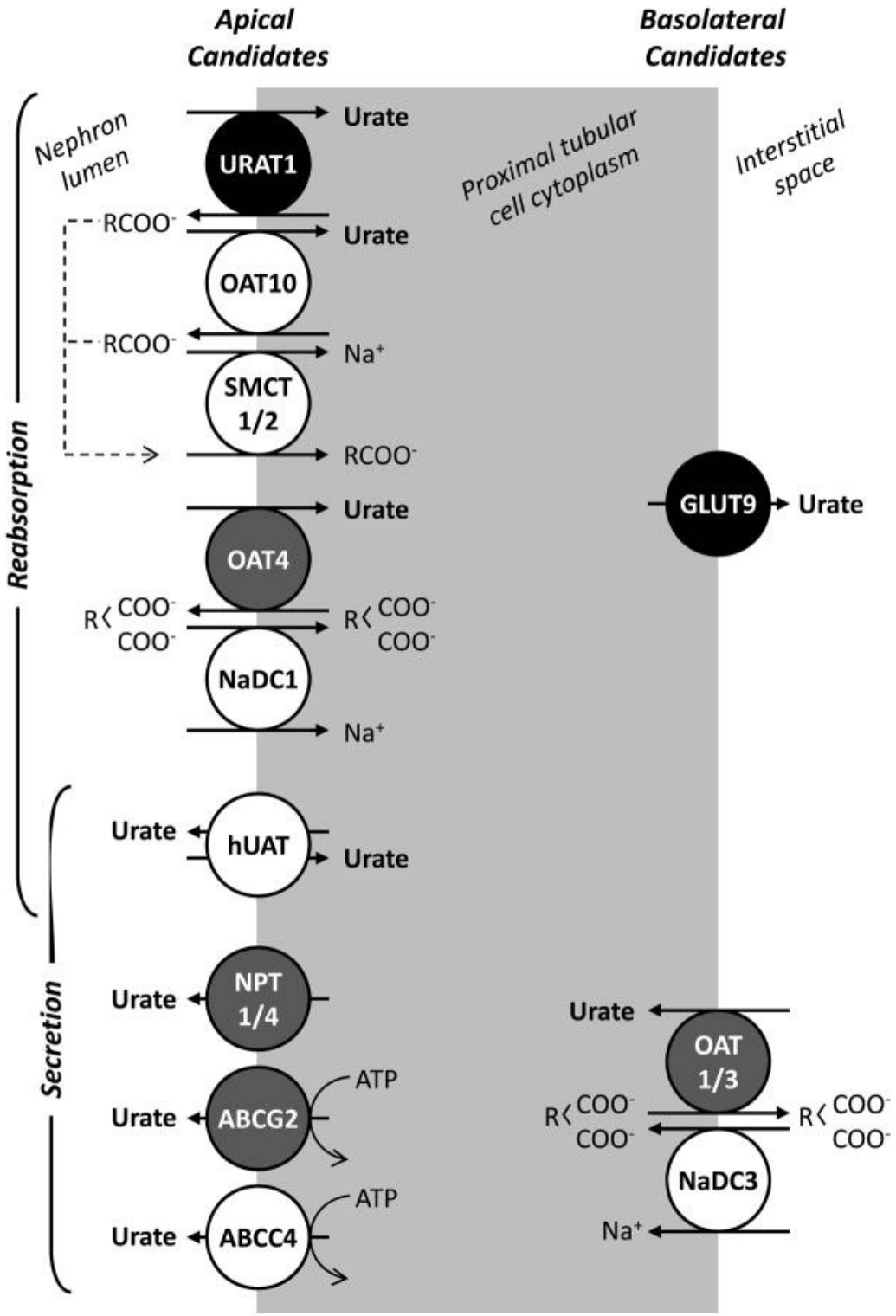
Apical Candidates
Basolateral Candidates
Nephron lumen
Proximal tubular cell cytoplasm
Interstitial space
Reabsorption
Secretion
URAT1
Urate
RCOO-
OAT10
SMCT 1/2
Na+
GLUT9
OAT4
R COO- COO-
NaDC1
hUAT
NPT 1/4
ABCG2
ATP
ABCC4
OAT 1/3
NaDC3

Figure 1. 3. The possible urate transporter proteins of human proximal convoluted tubule reported in 2012.

Note: URAT1 is urate-anion exchanger 1; OAT is organic anion transporter; SMCT is sodium monocarboxylate transporter; NaDC is sodium dicarboxylate contransporters; hUAT is human urate transporter; NPT is sodium phosphate cotransporters; ABCG2 is ATP-binding cassette subfamily G transporter 2; ABCC4 is ATP-binding cassette subfamily C ransporter 4; and GLUT9 is the glucose transporter 9. $R\text{-}COO^-$ represent a carboxylate ion with the conjugate base of a carboxylic acid. Adapted from (22).

Chapter 1.2. Human glucose transporter

1.2.1. Outline introduction of human glucose transporters

Hexoses are an essential carbon and energy source for the cells of the human body and so their entry and exit across the plasma membrane is critical for life (80). There are now known to be at least two distinct transporter gene families responsible for the handling of hexoses in mammalian cells. The first family is the sodium/glucose co-transporters, SGLTs, which are secondary active transporters which use the sodium gradient across the cell membrane to drive glucose and galactose uptake (81, 82). In contrast, GLUTs are passive transporters that use either chemical or electrochemical gradients to transport hexoses or other substrates (83, 84).

This section of the introduction will discuss the discovery of glucose transporters, the GLUTs, in humans. Since the glucose transporters are membrane proteins that belong to the sugar porter family (SP) within the Major Facilitator Superfamily (MFS), I will review the properties of the MFS superfamily and the SP family. Then, I will examine the details of the glucose transporters in terms of their cloning, structure, the possible transport mechanisms, subcellular trafficking, and the pathophysiological relevancies of some GLUTs. Moreover, I will focus on the recent findings of my protein of interest, the human glucose transporter 9, hGLUT9 (hSLC2A9), with emphasis on the structure-function studies.

1.2.2. Major facilitator superfamily (MFS)

The major facilitator superfamily is one of the two largest membrane transporter protein superfamilies (83). The MFS transporter proteins express ubiquitously from prokaryotic to eukaryotic organisms. Currently, 29 transporter families have been identified in MFS (84). These transporter proteins can be uniporters, proteins that transport one substrate; symporter, proteins that transport two substrates in the same direction; or antiporters, proteins that transport two substrates in opposite directions. Protein sizes of MFS range from 300 amino acids to about 800 amino acids, a discrepancy due to the difference among proteins' C- and N- termini, and sometimes, the difference among the transmembrane helices. One distinct characteristic of MFS is that these proteins all have 12 transmembrane helices (Hs), except for three families that have 14 TMs within one single polypetide chain (83). The 12 TMs of the MFS arise from two of the six-TMs units of the proteins through evolutionary processes (85). In some cases, e.g., family 2, the drug / proton antiporter, two additional TMs were formed to meet the additional structure and function needs (83).

Originally, it was assumed that sugar was the only substrate for MFS; however, subsequent research revealed that other molecules, like drugs and metabolites, can also be transported by this superfamily (86, 87). Now, we know that other small molecules, such as amino acids, nucleotides, and vitamins, are also involved (88, 89). Unlike ABC transporter protein superfamily (mentioned in Chapter 1.1), MSF proteins use the electrochemical gradients of their substrate as the driving force to translocate the substrates across cell membranes (83). In

this thesis, I will focus on the hexose and urate transport mediated by the monosaccharide transporter in family 1, the sugar porters.

1.2.3. Sugar porter family

The first and largest identified family in MFS is the Sugar Porter family (SP), which consists of 133 members (83). The SP proteins express widely in almost all organisms from Archaea, Bacteria, to plant and animals. Some examples include the galactose permease (Galp) and D-xylose transporter in *Escherichia coli,* and the glucose transporters (GLUTs) in humans. Besides sugar, some transporters in this SP family can transport other substrates, like urate and inositols. The size of the SP proteins ranged from 404 to 818 amino acids. They all have 12 transmembrane helices (Hs) with both C- and N- termini present intracellularly.

1.2.4. Glucose transporters

The glucose transporter proteins are encoded by the Solute Carrier family 2, subfamily A gene family, SLC2A. Up until today, there are 14 mammalian facilitative glucose transporters and they belong to the sugar porter family in the Major Facilitator Superfamily (MFS) (Table 1) (83, 84, 90). The original name glucose transporter is somewhat misleading as many of them have substrates other than hexoses (21, 91). They are subdivided into three classes based on their protein sequence and structural similarity (**Fig. 1.4, Table 2**) (90). Class I, the “glucose transporters” include GLUT1, 2, 3, 4, and 14; Class II glucose transporters include GLUT 5, 7, 9, and 11, and they are known to transport fructose as well. Class III is made up of GLUT 6, 8, 10, 12 and 13 (HMIT1); this

Class is believed to be the most ancient group with largely as yet unknown substrates.

1.2.5. Molecular discoveries of Class I, II, III GLUTs

Class I GLUTs were all cloned in the 1980's. Human GLUT1 protein was purified by Kasahara and Hinkle in 1977 from human erythrocytes, in which GLUT1 has very high expression levels. The molecular weight of the transporter protein was identified as a 55,000 Dalton band on a sodium dodecyl sulfate-polyacrylamide gel, sometimes referred to as Band 3 (92, 93). After reconstitution into liposomes, this protein was able to show the transport activities for D-glucose but not L-glucose. Furthermore, ninety percent of the D-glucose transport activity was inhibited by low concentrations of cytochalasin B, a cell permeable mycotoxin. In 1985, Mueckler's research team obtained the complete gene and protein sequence of GLUT1 from the human HepG2 hepatoma cell line (94). Northern blot analysis demonstrated that it is expressed in most tissues and cell types in mammals (21, 94). Consisting of 492 amino acids it was predicted to have 12 putative membrane spanning domains (MSD) with both the C- and N- termini in the cytoplasm, and a putative glycosylation site Asn45 on the first extracellular loop (94).

Human GLUT2 was cloned from rat and human liver cDNA libraries in 1988 (95, 96). Human GLUT2 having 524 amino acids and an 80% homology and 55% identity with GLUT1. It is found mainly in the intestine, liver, kidney and islet cells and was shown to transport both glucose and fructose with relatively low affinities, an important feature of liver hexose transport (97–99). Kayano *et al.*

indentified Human GLUT3 in 1988 (100). GLUT3 is a 496 amino acid protein and was cloned from a human fetal skeletal muscle cDNA library (97). It has 64.4% and 51.6% identity with GLUT1 and GLUT2, respectively and expresses mostly in the brain, in particular in the frontal lobe of the cerebrum (97, 100–102). Its primary substrate is also glucose (97). GLUT14 was identified by Wu and Freeze as a duplicon of GLUT3 with 94.5% identity (103). It appears to be exclusively expressed in the human testis. Human GLUT4 was cloned from the human small intestine and skeletal muscle by Fukumoto *et al.*. in 1989 (96). It is a 509 amino acid protein that has 65.3, 54.3, 57.5% identity with GLUT1, GLUT2 and GLUT3, respectively. The majority of human GLUT4 is expressed in cardiac and skeletal muscle and adipose tissue, and glucose transport activity is highly insulin sensitive (104).

Class II GLUTs are comprised of 5, 7, 9 and 11, and they all transport fructose and to some degree glucose. Human GLUT5 was cloned from small intestinal cDNA, and was proposed as a second hexose transport system in the brush border (apical) membrane of intestinal epithelial cell along with SGLT1 (105). GLUT5 is a 501 amino acid protein expressed mostly in human small intestine and at low levels in kidney, skeletal muscle and adipose tissues. GLUT5 has 41.7, 40.0, 38.7 and 41.6% identities with GLUT1, GLUT2, GLUT3 and GLUT4, respectively. The use of 2-deoxy-D-glucose as a substrate indicated that GLUT5 was also a very low affinity glucose transport system in the brush border membrane. However, its primary substrate is fructose and it is responsible for much of the fructose uptake at the apical surface of the intestine (106).

Initially, Waddell *et al.* described GLUT7 in 1992 as a hepatic microsomal transporter protein, which had 68% identity with GLUT2 (107). Subsequently, it was reported to be a cloning artifact, and its mRNA could not be found in either human or rat liver (108). In 2004 human GLUT7 was the last member of the GLUTs to be cloned using an intestinal cDNA and a PCR-based strategy (109). Having 528 amino acids, GLUT7 shares 68% similarity and 53% identity with GLUT5 and is predominantly expressed at the apical membrane of the enterocytes in the small intestine. This GLUT can transport both glucose and fructose when expressed in *Xenopus* oocytes with high affinity, but with very low transport capacity, and it is not sensitive to cytochalasin B (109). It is likely that its correct physiological substrate has yet to be identified (see GLUT9 below).

In 2000, Moley *et al.* cloned human GLUT9 from cancer tissues, using PCR-based methods (110). GLUT9 has two splice variants, a 540 amino acid length transporter (hSLC2A9a), which is targeted to basolateral membranes in the liver and kidney and a N terminal truncated form (hSLC2A9b) which is found in the renal apical membrane, apparently in the distal convoluted tubule (111). It shares 38% and 44% identity with GLUT1 and GLUT5, respectively. Human GLUT9 was initially shown to be a high affinity/ low capacity glucose and fructose transporter, but more recently as a consequence of a series of genome wide association studies identified as a high capacity urate transporter (73, 112–114).

Human GLUT11 was cloned from the human heart in 2001 and shares 35% and 41.9% identity respectively with GLUTs 1 and 5 (115). To date, it has only

been detected in heart and skeletal muscle and has three splice variants of unknown function. GLUT11 transports glucose and fructose when expressed in Cos-7 cells.

Class III GLUTs include 6, 8, 10, 12 and 13 (HMIT). A non-functional pseudo gene called GLUT6 with high sequence identity to GLUT3 was initially identified in 1990(105). Subsequently, the functional human GLUT6 was cloned in 2000 from leucocytes but initially named GLUT9 (112). Later, the gene was designated as SLC2A6 (GLUT6) by the HUGO Gene Nomenclature committee (113). Human GLUT6 is a 507 amino acid protein, and has high sequence identity with GLUT8 (44.8%) and has 28.5% identity with GLUT1. It appears to be exclusively expressed in the brain and lymphoid tissues and transports glucose when reconstituted into COS-7 membrane vesicles. GLUT8, another glucose transporter, was cloned from the human testis, its primary expression site, and has 477 amino acids with 29.4% sequence identity to GLUT1 (112, 116, 117).

GLUT10 was cloned from human liver cDNA as a 541 amino acid protein with 29.7% and 33.6% sequence identity with GLUT3 and GLUT8 respectively (118). GLUT10 expressed in most human tissues with the highest level found in the liver and pancreas. GLUT10 displays very low transporter activity and high affinity for 2-deoxyglucose when expressed in *Xenopus* oocytes (119). Human GLUT12 was identified using a malignant breast cancer cell line (MCF-7) as a 617 amino acid protein(120). GLUT12 shares 40% and 29% sequence identity with GLUT10 and GLUT4, respectively. Immunocytochemistry assays indicated

that GLUT12 is expressed in skeletal muscle, small intestine and adipose tissue. Other studies indicated that GLUT12 was also found in heart, prostate, brain, placenta, and kidney tissues (121–124). GLUT12 shows glucose transporter activity when expressed in *Xenopus* oocytes and this activity is inhibited by other hexoses, including fructose, galactose and 3-O-methyl-glucose (3OMG) suggesting that they may also be substrates (125).

Human GLUT13, is also known as the H^+-myo-inositol transporter, HMIT for its proton coupled activity. GLUT13 was cloned at the same time from rat spleen (126). While the rat cDNA encoding a 618 amino acid protein, the human GLUT13 has 629 amino acids. GLUT13 expressed mainly in the brain, in particular in ganglian cells and some neurons (126). GLUT13 is the only GLUT which has the specific electrogenic transport activity for myo-inositol. To date, no glucose transport activity has been reported for GLUT13, although it does appear to mediate inositol-3-phosphate (IP3) movement (126).

1.2.6. Structural comparisons between class 1, 2 and 3 GLUT transporters

Hydropathy analysis of all GLUTs reveals that they all have 12 predicted transmembrane helixtransmembrane helices with both C- and N- termini and a long loop connecting the H6 and H7 present on the cytosolic side (127–130) (**Fig. 1.5**) Protein sequence alignments of all GLUTs reveal that many amino acids are conserved among these proteins. Good examples are PMY in H4, PESPRY/FLL in H7, GRR in Loop8, GPGPIP/TW in H10, VPETKG in the C terminus (Fig. 1.6) (131). These motifs are considered to be the signature characteristics of glucose

transporters. Other residues, like R92 in Loop 2, E146 and R153 in Loop 4, Y293 in Loop 7, E329, R333, and R334 in Loop 8, E393 and R400 in Loop10 and P385 in H10, are also highly conserved in all the GLUT members. (Note: all amino acid residue numbers are assigned according to the corresponding residues in GLUT1). Mutations of these residues in GLUT1 reduced or abolished glucose transport activity with or without affecting cytochalasin B binding (131–134).

Structure of Class I glucose transporters Although the Class I GLUTs have a similar putative topology, only 38% of all the amino acids are conserved in GLUT1 - 4(135). They all appear to have a single *N*-linked glycosylation site on the extracellular loop 1, which connects H1 and H2 (94, 96, 97, 102, 136). A glutamine residue (part of the QL motif) in H5 is shared among Class I GLUTs, which suggests this motif may be important for glucose recognition (137). The serine-threonine-serine (STS) motif in extracellular Loop 7 between H7 and H8 is also conserved in Class I GLUTs (138). Mutation of these serine or threonine residues locks the protein conformation， suggesting that this is a critical site for conformation change. Another highly conserved motif is GPXXXP in H10, where a tryptophan appears immediately after (139, 140). It has been proposed that this tryptophan is a crucial residue for binding the inhibitors, cytochalasin B and forskolin, without directly affecting glucose transport. In addition, a QLS motif in H7 is only present in transporters like GLUT1, 3, and 4 which carry glucose, but not in those which transport fructose, including GLUT2, suggesting that this motif is involved in glucose and fructose selectivity (141).

Structure of Class II glucose transporters Class II GLUTs also have 12 transmembrane helices and a single N-linked glycosylation site on exofacial loop 1 between H1 and H2 (105, 109, 110, 112). A major difference between Class I and II is that Class II lacks the tryptophan residue after the GPXXXP motif (142). Another striking difference is that all Class II GLUTs have a single hydrophobic residue, isoleucine, in H7 associated with fructose/glucose selectivity (143). It was speculated that this residue was facing the aqueous pore at the exofacial vestibule of GLUT7 using a computer model of the GLUT7 protein based on the GlpT crystal structure (144). However, analysis using a GLUT9 computer model based on the recent GLUT1 crystal structure indicates that this isoleucine is more likely to be facing away from the aqueous pore and acting as a structural regulator through hydrophobic interactions with adjacent TMs (145). At the equivalent position in Class I GLUTs, (except for GLUT2 which can also transport fructose) there is a valine residue (91). This suggests that subtle interactions between TMs mediated by hydrophobic residues can affect substrate specificity within this family of transporters. Another important structural variation between Class I and II GLUTs is that Class II do not contain the QLS motif (141).

Structure of Class III glucose transporters Class III GLUTs have similar topology to the I& II and many of the motifs found in the other classes are conserved, such as the PESPR in H6 (GLUT6 and GLUT8), GRR in Loop 2 and Loop 8, PETKGR in H12, and arginine and glutamate residues in Loops 4 and 10 (112, 116, 118, 120, 125). Class III GLUTs also have a tryptophan residue after the GPXXXP motif in H10. But, one significant difference is that Class III

GLUTs do not have an *N*-linked glycosylation site in Loop 1 between H1 and H2. Instead, Loop 1 is shorter, and the predicted glycosylation sites are in the long Loop 9 between H9 and H10 (112, 116, 118, 120). GLUT13 (HMIT) is predicted to have more than one N-linked glycosylation site within this loop (125). In addition, GLUT6 has two arginine residues present in H7 and H8, which are absent in other GLUTs (113). Again, Class III GLUTs do not contain the QLS motif, which is unique to the Class I proteins (136).

1.2.7. Crystal structure of human GLUT1

Primary structure of GLUT1 Despite the amino acid sequence differences among all the GLUTs, the overall protein structure arrangements are very similar. The pioneer glucose transport protein for structure analysis is the first discovered GLUT, GLUT1. Extensive studies have been carried out to elucidate the structure function relationship using primarily GLUT1 since 1985. Most of the early research disclosed the primary structure of GLUT1 as a 492 amino acid protein, which has 12 TMs, with both C- and N- terminal tails and a long loop connecting H6 and H7 present in the cytoplasm. The *N*-linked glycosylation site is at Q45 in extracellular Loop 1 (94). The glycosylation of GLUT1 caused the protein to run as a 45-65 kDa smeared band when detected by Western blot (142). Moreover, glycosylation was found to be important for glucose transport mediated by GLUT1, but not to affect the targeting of GLUT1 to the cell membrane (146). The C- terminus was also found essential for glucose transport but not for protein trafficking (142).

The secondary structure of GLUT1 was first hypothesized by Mueckler *et al.* in 1985 (94). The study predicted that the 12 transmembrane helices of GLUT1 were α-helices with over half of GLUT1 protein residues as hydrophobic residues. Later, this secondary structure hypothesis was confirmed by fourier transform infrared spectroscopy, circular dichroism spectroscopy analysis, scanning glycosylation mutagenesis, and mass spectrometric analysis (144, 145).

The tertiary structure of GLUT1 Besides the secondary structure, the original paper of GLUT1 predicted the earliest tertiary structure of GLUT1. The original paper suggested that amphipathic helices H3, 5, 7,8, and 11 may form a central membrane aqeous channel allowing glucose to be translocated (94). Since then, conscientious studies have been conducted to disclose the accessibility of the GLUT1 aqueous transport pathway. The most thorough studies were performed by Mueckler's group, who utilized the cysteine scanning mutagenesis method wherein they mutate every single amino residue of each TM of GLUT1 into cysteine residue (147–158). These cysteine substituted mutants were subjected to either extra- or intracellular application of sulfhydryl-reactive molecules, such as p-Chloromercuribenzene sulfonic acid, pCMBS, to examine the changes in glucose transport. These experimental results allowed Mueckler *et al.* to locate all the plausible residues to where the solvent/substrate could bind within the aqueous environment of the protein. After scanning all the TMs in GLUT1, Mueckler and Makepeace proposed a GLUT1 model in which H2, 4, 5, 7, 8, 11 and possibly 1 and 10 were located in the center and forming an aqueous transport channel for both water and glucose molecules, whereas the H3, 6, 9

and 12 were lining the outside of the protein (159). Three amino acid residues that involved in substrate binding were also proposed in this model: Q161, Q282, and W412 (158).

Computer model of GLUT1 A three dimensional inward-facing computer GLUT1 model was created based on the GlpT crystal structure by Salas-Burgos *et al.* (160). This model confirmed most of the biochemical and molecular analysis and physiological data accumulated for GLUT1, which establish that it has 12 transmembrane helices and can be viewed as two symmetrical 6 α-helical bundles connected with a long intracellular loop between H6 and H7. The Salas-Burgos model supports the hypothesis that the 12-TM GLUT proteins arose from a gene duplication event from 6 TMs (161, 162). The model also confirms that H1, 2, 4, 5, 7, 8, 10, and 11 are surrounded in a box formed by TM 3, 6, 9, and 12. This finding is consistent with the predicted model proposed by Mueckler and Makepeace (163). Furthermore, the new model established that the central transport cavity was formed by H2, 4, 5, 7, 8, and 10. This model also concurred with the theories of the importance of the residues previously described as crucial for substrate/inhibitor transport/binding functions. These residues include Q161, R126, Q279, Q282, N317, T321, W65, W388, W412, and V165. However, the docking study for the binding site of the GLUT inhibitor, cytochalasin B, located it in the intracellular side, a positioning that contradicts the experimental data (160, 164).

Computer model of other GLUTs Other GLUTs such as GLUT3, 4, 5 and 9 were also constructed with the computer model based on Mechanosensitive ion channels of the MscI homolog from *Mycobacterium tuberculosis* (MscI), GlpT and an *Escherichia coli* homologue of GLUT1-4(XylE) (165–168). Nonetheless, the precision of the GLUT3 computer model is debatable in the field. This is because the authors of this study claimed that the MscI crystal resemble a 6-TM aquaporin protein, but this MscI channel is a 10-TM channel protein; therefore they have to apply few gaps to develop the model (169). The greatest controversy of the model, however, is the proposed glucose transport mechanism. The authors declared that glucose is transported by key flexible TM segments and a network of polar and aromatic residues with two different glucose binding sites on each site of the transport pathway other than an alternated access transport with one stable binding site (165). The GLUT4 model is based on GLUT1 experimental data and the GlpT pictured an inward facing computer. This GLUT4 model was very similar to the GLUT1 (based on GlpT) model with the same TM arrangement of conserved residues lined within the transporter cavity, and both ATP- and cytochalasin binding cites in the cytosolic side (166).

Computer model of GLUT5 In 2014, another GLUT1 and GLUT5 computer models were formed based on the XylE crystal structure, which is a bacterial D-xylose transporting homologue sharing high degrees of similarity and identity with GLUT1-4 (167). Parallel to other MFS protein transporters, the topology of the GLUT1 and 5 models fit in the common structure fold with 12 TMs. More importantly, this study proposed that the 12 TM topology of MFS may have arisen

by two gene duplication events through and initial triple-helix bundle into the six-helix bundle then became two pseudosymmetrical six-helix bundles (94). Thus, the alignment of the GLUT1 and GLUT5 sequences to XylE is in the triple-helix array. This modeling predicted that Asn411 in GLUT1 and His419 in GLUT5 are the corresponding substrate binding sites for glucose and fructose, respectively.

Computer model of GLUT9 More recently, the resulting GLUT9 model was also constructed based on XylE (168). The GLUT9 model topology is similar to the XylE structure with 12-TMs arranged in a 6-helical bundle arrangement. In the same study, single monomer GLUT9 protein was purified from the high GLUT9 expressing oocyte. Consequently, it allowed the construction of a low resolution crystal structure of GLUT9 . The structure revealed a transport cavity, which contains the plausible urate binding sites. The sites include amino acids H23, R31, L182, Q203, A206, Q328, L332, N333, F426, W459, and N462.

GLUT1 Crystal After almost four decades from the first purified GLUT, the first glucose transporter protein was crystallized in 2014. Human GLUT1 is the only glucose transporter that has a crystal structure, and it was produced by Deng *et al.* (170). This GLUT crystal was created from a purified GLUT1 protein generated in baculoviruses infected High five insect cells. This 3.2 Å resolution crystal structure reveals a partially open inward facing transport conformation of GLUT1, which was locked due to a single missense mutation E329Q. The structure demonstrated a 12 TM transporter protein formed by two 6-helical domains with cytoplasimic N- and C- domains. These two 6-helical domains are

connected with the intracellular helical bundles (ICH domain). This ICH domain was also found in other sugar transporter crystals, such as XylE and GlcP (171, 172), in which these ICH domains were believed to be unique in the sugar porter family but not found in other MFS. The crystal structure suggested that the ICH domain may function as a latch to ensure the closing of an intracellular gate in the inward facing conformation of GLUT1. Furthermore, the crystal illustrated that there is only one sugar binding site mainly on the C-terminaldomain of the transporter, at which sugar could alternate access from either side of the protein. The possible bindings observed from the crystal structure are Q 282/Q 283/N 288 from H7, N 317 from H8, and N 415 from H11. The N-terminal domain of the structure was related to the regulation of the conformation change during transport. Another notable feature of this GLUT1 crystal is the extracellular gate bridged by H1 and H7. N34 is an essential residue in H1 that serves as the center coordinator for hydrogen bonding between S294, T295 in H7 and T310 in H8.

1.2.8. Importance of transmembrane helix 7 (H7) in GLUTs

The GLUT1 crystal structure suggested that H7 is critical for both structure regulation and substrate binding. As mentioned above, H7 is forming an extracellular gate in the inward facing conformation GLUT1 (170). Most important, three potential substrate binding amino acid residues, Q282, Q283 and N288, were observed within the substrate bound crystal structure. The observed binding sites, and they matched the molecular data that obtained from Mueckler's cystine scanning mutagenesis studies (154). Substitution of these residues into cysteines

reduced the glucose transport substantially. However, only Q282/283 was shown facing the aqueous environment, but not N288. The motif QLS and the hydrophobic residue (V290, isoleucine in fructose transporters) were illustrated as critical determinants for substrate selectivity; however, they were not confirmed in the crystal structure. All these developments suggest that H7 is necessary for substrate translocation by GLUTs.

1.2.9. Hydrophobic residues in GLUTs

Hydrophobic residues, such as isoleucine, valine, leucine, and phenylalanine, are often clustered within active sites (173) , and known to be essential in protein structure-function relationships. A highly conserved motif 'QLS' in GLUTs was found adjacent to the postulated 'bottle-neck' region of the substrate transport pathway (141). Also, valine165 was predicted to locate near the exofacial surface of the substrate binding site (174). Subsequently, an isoleucine in H7 in the Class II GLUTs (5, 7, 9 and 11) was identified as a critical determinant for substrate selection. Substitution of this isoleucine into valine within these proteins significantly reduced or abolished fructose transport without affecting glucose fluxes (143, 144). The same study predicted that the isoleucine or valine might form a hydrophobic interaction across the translocation pore with a tryptophan in H2. However, the interaction of these hydrophobic residues with other substrates transported by GLUTs were not examined.

1.2.10. Cysteine residues in GLUTs

Cysteine residues in glucose transporters were believed to be important for hexose translocation in GLUT1 (175). Cysteine residues in the C-terminal half

of GLUT1 were observed in a moderate reduction in the 2-deoxy-D-glucose uptake. Cysteine 429, on the exofacial side of GLUT1, was identified to be responsible for the inhibitory effect by the thiol-group-reactive reagent, p-Chloromercuribenzene sulfonic acid (pCMBS) (176). However, Due *et al.* (177) demonstrated that the cysteine-less GLUT1 has similar 3-O-methylglucose transport activity as the wild type GLUT1. However, in multiple sequence alignments (**Fig. A.2**), we notice that Class I glucose transports (hSLC2A1, 2, 3 & 4) have no more than six cysteine residues in their sequences. hSLC2A1 has only four cysteine present in TMs, whereas hSLC2A4 has no cysteine in any of the TMs. This is one of the reasons why early research used cysteine mutagenesis scanning to investigate the aqueous pore facing residues in transmembrane helices (TMs) of GLUT1 (149, 163). Class II GLUTs, on the other hand, have more cysteine residues present in their sequences. GLUT9, for example, has eight cysteines, and GLUT11 has 16 cysteines. Nevertheless, no research has been conducted to examine the role of these cysteines in these Class II GLUTs.

1.2.11. Mechanisms of substrate transport by GLUTs

Although 14 GLUTs were identified, the mechanism of glucose transport has mainly been investigated using GLUT1. Initial explanations of how glucose is transported across the cell membrane were based on the mathematical analysis of hexose transport activity utilizing erythrocyte preparations. The fluxes were best fit with the Michaelis-Menten enzyme kinetics model (178–180), which predicts that the rate of hexose absorption depends on both the initial hexose

concentrations and the binding affinity of the protein for the substrate and that there is a maximum rate of transfer (rate of transfer is saturable) (181). The earliest mechanistic theory, the “Simple Carrier Model”, was proposed by Widdas and assumes four transport stages (**Fig. 1.7A**): 1. An empty carrier that opens to one side of the membrane (*cis* side), to which glucose can bind; 2. The substrate binding carrier has to translocate to the other side of the membrane (*trans* side); 3. The carrier releases the glucose on the *trans* side; 4. The empty carrier switches back to the *cis* side (181). Moreover, Widdas postulated that both phosphorylation and metabolism of glucose were the two possible mechanisms providing the necessary energy for the glucose transfer. Due to the complexities of the erythrocyte system, and the differences and difficulties in experimental methods, variation in experimental transport kinetic results are common. As well, many other models have been proposed over the same time period (182). These models include the following: the Regen-Tarpley asymmetrical carrier model (183); the Eilam mode l (184); the Lattice-pore model (185); the Tetramer model (186); and the introversion model (187). Despite the differences between these models, they all tried to explain two principle scenarios that occur during the glucose transfer: 1. the asymmetry of the transport affinities (K_M , substrate concentration at half the maximal transport rate) of zero *trans* between hexose influx and efflux. 2. the trans-acceleration occurs when hexose is present on the *trans* side (182, 188).

The purification and cloning of GLUT1, subsequently permitted a better picture of how glucose is transported to be proposed. Today there are two

popular models still under consideration. One is the two-site/fixed sites transporter, in which both substrate binding-sites are simultaneously available from either side of the membrane (**Fig. 1.7B**) (189–192). After binding, hexoses can then exchange between these sites and accelerate the binding process. In other words, this model suggests that GLUT1 can work as an antiporter (**Fig. 1.7C**). However, Human GLUTs (all except GLUT13) were thought to be uniporters (191), in which they transport one hexose molecule at a time in an unidirectional approach; whereas an antiporter (or exchanger) will simultaneously transport two molecules in opposite directions. It is argued that this two-site model can explain the complex asymmetry and multiphasic transport kinetics, while the simple carrier model cannot sufficiently explicate the incidences without violating the energy conservation law (188, 189). However, asymmetric glucose transport activities are not seen in hepatocytes or adipocytes which are mediated by GLUT2 and GLUT4, respectively (99, 193, 194). Several recent investigations also point out that GLUT1 can form oligomers, such as dimers or tetramers which could account for the three phases and asymmetric kinetics (195–197). Cloherty *et al.* (196) and De Zutter *et al.* (197) proposed that the glucose transporters in mammalian cells present as cooperative dimers or tetramers of GLUT1, and they hypothesized that one (or two in tetramer) exofacial and one (or two in tetramer) endofacial hexose binding site(s) present simultaneously. In both dimers and tetramers of GLUT1, cis-allosteric hexose transport was observed; i.e., hexose binds to one oligomer subunit induce the transport by other subunit(s). Therefore, the GLUT1 dimers are able to transport cis- hexose in exchange with the trans-

side substrate, which is similar to the two-state model assumption; the tetramer GLUT1 cooperative transporter could also further explain the observed multiphasic transport

Alternating-access mechanism Another proposed mechanism is the alternating-access model and this appears to be supported by the available MFS crystal structures (162, 170, 172, 198, 199). Jardetzky explained the assumptions of the mechanism as early as 1966 (200). They are the following three premises: 1. The transporter has a cavity to admit a small substrate; 2. the transporter contains a substrate binding site; 3. The transporter has two different configuration openings to one side of the cell membrane or the other. This alternating access mechanism supports the presumption that GLUT1 is an uniporter, and has only one binding site which substrate can alternately access from either side of the membrane in the course of conformational changes. The newly crystallized GLUT1 also fits with the alternating access mechanism (170), which predicts four conformational states during a complete hexose transport cycle (**Fig. 1.8**): 1) An empty outward-open transporter state, 2) ligand bound and occluded transporter state, 3) inward-open state and 4) ligand-free and occluded state. These four states appear as a slightly more detailed version of the original Simple Carrier Theory that Widdas proposed in 1952 (180). Additionally, the crystal structure of GLUT1 suggests that the transporter has a favorable conformation when it is substrate free.

Mechanism of trans-acceleration Another often observed property of GLUT dependent glucose transport is that of trans-acceleration. This was first observed in erythrocytes as uphill hexose counter flow (other terms include counter transport acceleration and trans-stimulation transport) (201, 202). In these experiments, hexose was detected flowing apparently against its concentration gradient from the *cis* side into the *trans* side of the membrane where hexose also present, and *vice versa*. Rosenberg and Wilbrandt argued that the phenomenon was due to two different transport systems present in the red cell, which Naftalin and Holman referred to as a two binding site carrier (182, 203). Furthermore, it was believed that hexoses could exchange freely between these two sites within the carrier cavity, a process that Naftalin *et al.* termed a geminate-exchange (182, 189, 204). Alternatively, others argued that the carrier contains only one binding site, and the carrier can move from outward facing to inward facing with and without substrate binding. It is the empty carrier that returns from the *trans*-side to the *cis*-side of the membrane that limited the rate of transport. Therefore, trans-acceleration occurs when hexose presented on the *trans*-side, which allows the carrier to return faster to the *cis*-side with a bound substrate (170, 191).

Currently, hexose/hexose trans-acceleration has only been shown in GLUTs 1, 3 and 9 (73, 191, 203, 204) and few studies have probed the mechanism at the molecular level. One study indicated that GLUT1 contains ATP-binding sites, which are amino acid residues necessary for glucose trans-acceleration to occur (205). The same study proposed that mutations in the ATP-binding sites would alter the tertiary structure of GLUT1; and thus, restrict the

flexibility of the transporter for sensing substrates on both sides of the membrane. A second study employed chimæras constructed from GLUT1 and GLUT4 expressed in the human embryo kidney cells (HEK-293) (204). It found that H6 of GLUT1 contains residues necessary for trans-acceleration with glucose-glucose exchange and is responsible for constraining the relaxation of GLUT1, but not direct binding or translocation of substrate during transport. Hence, this study was not able to distinguish between the simple carrier model or the two-site model to explain trans-acceleration. GLUTs 2 and 4 do not show trans-acceleration of hexose transport, instead, they show symmetrical transport in both the oocyte and mammalian cell systems (194, 206).

Human GLUT9 is the only Class II GLUT reported to show, not only hexose/hexose trans-acceleration activity, but also hexose/urate trans-acceleration using the *Xenopus* oocyte expression system (73).

GLUTs 5, 7, 11 and Class III GLUTs are not subjected to detailed molecular examination of their transport mechanisms or substrate binding pockets.

1.2.12. Subcellular trafficking of GLUT transporters

In the 1990s' it was discovered that while GLUT1 is primarily present in the plasma membrane, GLUT4 is mostly localized to intracellular compartments (194, 207–210). The C-terminus is primarily responsible for the differential targeting for the GLUTs (211–215), to the plasma membrane or intracellular vesicles that can translocate these proteins to other sites (216–220). GLUT1 and

GLUT4 are thought to be recycled by exocytosis and endocytosis between the plasma membrane and cytosol, but to varying degrees. Insulin promotes their surface expression, but the regulatory mechanisms are thought to be different for the two proteins (212, 216, 217, 219).

GLUT1 The cytoskeleton and microtubules within cells are important in regulating the trafficking of GLUT1. For example, GLUT1 carrying intracellular vesicles are up-regulated by protein kinase C and casein kinase substrate 3 (PACSIN3) in adipocytes and down-regulated by Syntaxin 1C (STX1C) in a lung epithelial cell line (221, 222). STX1C is a soluble syntaxin suppressing the stability of microtubules and vesicle-transport mobility, whereas PACSIN3 is an adaptor protein involved in the regulation of cellular cytoskeletal elements and the clathrin-coated pit pathway. Trafficking of GLUT1 from an intracellular pool to the plasma membrane is also increased by AMP kinase in murine brain microvasculature endothelium bEnd.3 cells (223). In the human megakaryocytic leukemia M07e cell line, GLUT1 trafficking is also influenced by the cytokine stem cell factor (SCF) and cholesterol depletion induced by methyl-β-cyclodextrin (MBCD) (190).

The most recent studies of subcellular trafficking of GLUT1 have focused on the phosphatidylinositol 3-kinase (PI3K)/protein kinase B (Akt) pathway (218, 224). Increased PI3K/Akt activity regulates GLUT1 trafficking and glucose uptake in T-cell/B-cells (225). Factors that activate the Akt pathway include the growth factors IL-7 and IL-3, granulocyte/macrophage colony-stimulating factor (GM-

CSF), the inhibitor of NF-kB-kinase b (IKKb), clusters of differentiation 28 (CD28), and Kaposi scarcoma associated herpes virus infection (225–229).

GLUT4 The targeting, trafficking and recycling of GLUT4 between the intracellular compartments and the plasma membrane have been reviewed extensively elsewhere (21, 188, 220, 230–232). Consequently, we will simply outline some of the key features of the GLUT4 trafficking process. Cushman and Waradzala (231) proposed the first schematic mechanism of how insulin stimulates GLUT translocation to and from the membrane in the rat adipose cell in 1980. This study hypothesized that vesicles containing glucose transporters were stimulated to bind and fuse with the plasma membrane by undefined "secondary messengers" upon insulin association with its receptor, and that when insulin disassociate with the receptor, the process reversed. Subsequently, numerous pathways involved in the insulin dependent pathway have been identified (230, 232). They include: insulin receptor substrate (IRS), phosphatidylinositol-3-kinase (PI3K) and its regulatory subunit, P85 and catalytic P110, protein kinase C (PKC), ADP-ribosylation factors (ARFs), phosphoinositide-dependent protein kinase 1(PDK1), Golgi-localized, g-ear-containing ARF-binding proteins (GGA) and protein kinase B (PKB or AKT) and its substrate protein of 160kDa (AS160) (233–243).

GLUT4 trafficking and recycling are also regulated independently from the insulin signal, which is referred to as a general pathway (insulin independent pathway) and that the movement of GLUT4 is controlled by muscle contraction.

Muscle contraction activates several signaling messengers, like calcium, nitric oxide, or reactive oxygen species within the muscle cells themselves that regulate glucose homeostasis endogenously (232, 244–246).

GLUT2 and GLUT3 There is good evidence that GLUT2 can be trafficked to the small intestinal enterocyte apical membrane under the influence of protein kinase C bII, which is activated by PMA, extracellular signal-regulated kinase p38 and glucagon-like-peptide 2 (GLP-2) in the rat intestine (246–251). In contrast, stress, a high fat diet and glucocorticoids inhibit GLUT2 trafficking to the brush border membrane (252–254). Most recently, subcellular localization studies using live cell imaging demonstrated that GLUT2 is endocytosed through a calveolae-dependent mechanism, which is partially recovered in Rab11A-positive recycling endosomes (255). However, what is still not entirely clear is what role this transporter plays while it is transiently localized at the cell surface. It was proposed that this transporter provides a high capacity entry pathway for glucose and fructose at the start of a meal when the luminal concentrations are high and then is withdrawn as the meal progresses, leaving SGLT1 to bring in the remaining hexose upward into the cells. Another theory is that apical GLUT2 provides a shunt moving glucose back out into the lumen providing an osmotic control during the absorptive process (256).

Trafficking of GLUT3 is mediated by intracellular carrying vesicles with a SNARE complex in the neuronal PC12 cell line, and it is possibly regulated by Rab11 in neurons from Huntington's diseased mice (189, 257). However, only a

few studies were conducted on the actual processes for these trafficking pathways.

GLUT8 Trafficking of GLUT8 is different from other GLUTs. GLUT8 expression levels at the plasma membrane are controlled by glucose and insulin, and a t-SNARE protein, syntaxin 4, which was found to be necessary for the fusion of GLUT8 carrying vesicles with the plasma membrane in blastocysts. Other targeting/trafficking studies show that GLUT8 distributes more to the intracellular compartment in neurons and blastocysts than at the cell surface (258–260). Piroli *et al.* (261) pointed out that in rat hippocampal neurons, GLUT8 rapidly translocated to the rough ER following peripheral glucose administration. Therefore, they hypothesized that GLUT8 transports glucose out of the rough ER into the cytosol to maintain cellular glucose homeostasis in neurons (258, 259). On the other hand, it has been observed that a highly conserved dileucine containing motif (DEXXXLLI) was critical for GLUT8 sorting to the late endosomal/lysosomal compartments in mouse blastocysts (261–265).

GLUT12 Similar to GLUT8, GLUT12 has the conserved dileucine motif (DEXXXLLI) in its sequence; however, this motif affects the cell surface expression level instead of directing GLUT12 to the intracellular compartment as seen for GLUT8 in mouse blastocysts (261, 263). In the case of MCF-7 cells, GLUT12 was localized perinuclearly when insulin was absent (120). However, the acute change of the GLUT12 subcellular distribution was not detected after

insulin treatments. Another study indicated that GLUT12 trafficking is influenced by the mTOR-raptor signaling pathway (121).

GLUT9 The only study of GLUT9 trafficking was done by Augustin *et al.* in 2004 (266). This study illustrated that the amino terminus (N-terminus) determines which membrane that GLUT9 travels to. The full length GLUT9 with the full size N-terminus travels to and expresses on the basolateral membrane; whereas the truncated N-terminus GLUT9 travels to and expresses on the apical membrane of the MDCK cells. However, future experiments are needed to reveal more information of the GLUT9 trafficking process.

1.2.13. Pathophysiologies associated with GLUT proteins

Given the essential roles played by this family of proteins in cellular metabolism, it is not surprising that there are really no common diseases associated with genetic mutations in the GLUTs. In most situations, such mutations would be lethal for the embryo and development could not occur. However, it is now becoming appreciated that there are a number of disease states in which the expression patterns of hexose transporters are altered providing an opportunity for diagnosis or even treatment. Therefore, this section will cover the few documented GLUT specific genetic diseases and then look at recent advances in diagnosis and treatment.

GLUT1 – deficiency syndrome

A limited number of patients (~250) have been described since 1991 with autosomal dominant haplo-insufficiency mutations in their hSLC2A1 gene leading

to reduced concentrations of glucose in cerebrospinal fluid (267). This mutation in turn results in seizures, delayed development and small brain size. The types of mutation are numerous and could affect functional activity of the protein directly or its ability to form dimers or tetramers or its trafficking to the plasma membrane, etc (121, 267–270).

GLUT2 –Fanconi-Bickel syndrome

This is an extremely rare glycogen storage disease for which a little over 100 patients worldwide have been reported, the first described in 1949 (271). Three mutations in hSLC2A2 responsible for this autosomal recessive disease were identified in 1997 and they appeared to result in a truncated non-functional protein (270). This would fit with a number of the clinical symptoms associated with the syndrome including glucosuria, presumably as a consequence of significantly impaired glucose reabsorption across the renal proximal convoluted tubular basolateral membrane where GLUT2 is expressed (270). Their diarrhea could be explained by poor hexose absorption in the small intestine, again resulting from the lack of GLUT2 in the epithelial BLM. Patients also suffer from poor regulation of blood glucose and galactose levels, which after a meal, rise rapidly and maintained for some time. This condition could result from both the inability of the liver to take up hexoses and store them as glycogen and also probably from impaired insulin release by pancreatic beta cells as GLUT2 forms part of the normal blood glucose sensing mechanism (272–274). Similarly, after a meal the liver would be unable to release glucose back into circulation, an inability that could be responsible for the severe accumulation of glycogen in this

organ seen in many patients. The lack of renal reabsorption of glucose will further exacerbate the situation leading to hypoglycemia. Patients with a variety of mutations in GLUT2 continue to be reported, some with full length, but a non-functional transporter, while in others the defective protein fails to be targeted to the plasma membrane (273, 275).

GLUT9 - Association with urate metabolism disorders

While GLUT9 can transport glucose and fructose, its primary physiological substrate appears to be the organic anion, urate. This observation is supported by reports of patients, primarily from Japan, who have mutations in the hSLC2A9 gene (111). Unlike the majority of mammals, humans maintain high plasma levels of urate, which is a result of their modified metabolic pathway that is missing the enzyme uricase. Consequently, this metabolite is retained in the body as opposed to being broken down to allantoin and lost in the urine. Plasma levels are regulated within narrow limits (250 – 300 μM) by secretion from the liver mediated by GLUT9 and by reabsorption in the kidney proximal convoluted tubule. Transport across the renal epithelium is achieved by the organic anion exchanger URAT1 in the apical membrane and by GLUT9a in the basolateral membrane. Loss of function of GLUT9 results in hypouricemia, presumably as a consequence of both reduced release of urate from the liver and poor reabsorption from the urine in the kidney (74–79, 276).

Elevated levels of plasma urate have also been associated with hypertension, gout and metabolic disease (277). A number of Genome Wide Association studies have identified polymorphisms in the hSLC2A9 gene(73).

Consequently, it has been proposed that GLUT9 in the kidney and liver may well play a role in these disease processes. However, to date, few, if any, single nucleotide polymorphisms have been demonstrated to have direct effects on the function of the protein when it is expressed *in vitro* (74–79). It is more likely that such mutations have subtle effects on levels of expression or interactions with other proteins in the cell.

GLUT expression in relation to disease

The most common and well described change of GLUT expression is in cancerous cells that switch their metabolism primarily to glycolysis which is far less energy efficient and requires far more substrate. This rapid metabolic change is often referred to as the Warburg effect (278, 279). To supply the greatly elevated need for glucose, the cells increase their expression of some GLUT proteins, particularly GLUT1. This observation has been used to develop imaging tools, such as Positron Emission Tomography (PET), to detect some cancers (280, 281). Patients are injected with a radioactively labeled glucose analogue, fluoro-deoxy-D-glucose, FDG, which is rapidly taken up by the tumor cells and then metabolically trapped after phosphorylation (282–284). Research efforts are also focusing on breast cancer cells, where in some subtypes of the disease, the cells over express GLUT5 rather than GLUT1 suggesting that fructose based probes may be of value (284, 285). However, this PET technique is expensive and the probes are very short lived. Thus, it led to efforts to develop fluorescently labelled hexose analogues that would be preferentially taken up by

tumor cells. There are no reports as yet of clinical trials for such compounds, but a number of reports have shown promising results obtained *in vitro* (286, 287).

Other studies observed that the GLUT1 gene rather than GLUT4 was predominantly expressed in the failing human heart, resembling the fetal stage heart (122). Several studies have also reported a similar phenomenon in the rodent heart (265, 288, 289). However, the actual cause of the heart failure in humans has not been directly determined. Some recent studies indicate that upregulated GLUT1 expression is related to HIV infection in T-cells (290–292). It was observed that increased gene expression of GLUT1 in IL-7 induced T-cells rendered the CD4 T-cells and thymocytes susceptible to HIV-1 infection (290, 291). These reports suggest that the GLUT1 mediated metabolic pathway is the major regulator in HIV infected cells (291). Thus, GLUT1 could be a potential marker of diseased hearts and inflammation in HIV-infected subjects (122, 287, 291).

Moreover, other GLUTs, such as GLUT4, were reported to be expressed on the myeloma cell membrane, in which it is responsible for cell glucose consumption (293). GLUT4 had increased and GLUT2 decreased expression levels in senescent hepatic cells and chronically diseased human liver tissues, which suggests that GLUT4 may play an important role in liver cirrhosis (294). In many studies, GLUT4 was also found to be associated with type 2 diabetes (232). While the expression level of GLUT4 did not change in type 2 diabetic rodents, the trafficking of GLUT4 was affected in these animals (295, 296).

It was reported that in joint disease the pattern of GLUT expression in cartilage changes, offering a possible tool for diagnosis and ultimately treatment. Pro-inflammatory cytokines have been shown to alter the expression pattern of GLUTs in primary cultured articular chondrocytes and the patterns are very different under anaerobic conditions that are normal for these cells (297).

1.2.14. Summary

The SLC2A family of transporter proteins are essential for the handling of hexoses and a variety of other substrates. They are expressed in numerous cell types, some almost ubiquitously, while others have very specialized cell localization and work with other protein families to perform a wide variety of functions. The recently reported first crystal structure of GLUT1 will undoubtedly lead to a better understanding of just how these proteins bind their substrates and move them across the cell membrane. Major genetic mutations are uncommon underlining the critical roles GLUTs play in metabolism; however, their patterns of expression can change significantly in disease. Currently, scientists focus more on developing the profile of alteration of GLUTs in the human dieseases. Thus, these profiles could possibly be used as diagnostic tools; or, even to develop treatments for a variety of conditions. However, careful deliberations have to put into future research of treatment based on GLUTs because of their ubiquitous expression and critical roles in the human body. Thus, it may prove possible in the future to develop inhibitors or activity modulators for GLUTs based on a detailed knowledge of their binding sites and how transport is mediated.

1.2.15. Hypothesis

The objective of this thesis is to further disclose the structure function of the urate/hexose transport mediated by human glucose transporter 9, GLUT9. (We use hSLC2A9 in the next chapters). We first examined the importance of the hydrophobic residues I335 and W110 of hSLC2A9 for urate transport and urate/hexose trans-acceleration exchange. For this, we constructed three point mutations of hSLC2A9: isoleucine 335 to valine (I335V) and tryptophan 110 to alanine (W110A) and phenylalanine (W110F). We hypothesized that I335V will have reduced urate/hexose trans-acceleration activity, whereas W110A and W110F will have reduced activities in both urate transport and urate/hexose trans-acceleration. The results of this study were published in the *Journal of Biological Chemistry, 2015,* and will be presented in Chapter 2 in this dissertation.

Secondly, we examined the roles of six cysteine residues: C181, C297, C301, C398, C451, and C459 in hSLC2A9b. With successful construction of the chimæric protein $hSLC2A9_{(7)5}$ (a hSLC2A9 chimeric protein with H7 replaced with that from hSLC2A5) and $hSLC2A5_{(7)9}$ (a hSLC2A5chimeric protein with H7 replaced with that from hSLC2A9), we also explored the role of H7 in urate transport in hSLC2A9. Collaborating with Dr. M. J. Lemieux's group in hSLC2A9 computer modeling and substrate docking, we were able to propose a possible binding site, N429, for urate transport in hSLC2A9. We hypothesized that mutation of all the hSLC2A9 cysteine residues into the corresponding residues from hSLC2A5 will change their urate transport abilities without affecting the fructose transport abilities. Since H7 was discussed as a very important residues

in all GLUTs, we hypothesized that replacing H7 in hSLC2A9 with that from hSLC2A5 will result in lost urate transport in the chimæric protein $hSLC2A9_{(7)5}$ but maintain fructose transport. Additionally, we hypothesized that $hSLC2A5_{(7)9}$ will obtain urate transport ability with a H7 from hSLC2A9 substituted into hSLC2A5. Finally, we assumed that N429H (histidine is from hSLC2A5) will lose urate transport ability if N429 is the long sought urate binding site.

Table 1. Summary of the GLUT family proteins and their characteristics. Note: GLUT14 is grouped together with GLUT3 because GLUT14 has 94.5% identity *with GLUT3.* N/A: No data available.

GLUT Classes	GLUT Isoforms	Gene Name	Tissue Distribution	Substrate specificity	Trans-acceleration	Crystal Structure/Computer Model
I	GLUT1	SLC2A1	Red blood cells, Ubiquitous	Glucose/Galatose/ Dehydroacetic Acid	Yes	Crystal structure
I	GLUT3 (GLUT14)	SLC2A3 (SLC2A14)	Neurons (Testis)	Glucose/Galatose/ Dehydroacetic Acid	Yes	Crystal Structure/Computer model
I	GLUT4	SLC2A4	Muscle cells, Fat cells (Adipocytes)	Glucose/ Dehydroacetic Acid	No	Computer model
I	GLUT2	SLC2A2	Intestine, Liver, Kidney, Beta-cells	Glucose/Fructose/ Galatose/ Glucosamine/ Dehydroacetic Acid	No	N/A
II	GLUT5	SLC2A5	Intestine, Kidney, Muscle, Sperm, Brain	Fructose	N/A	Computer model
II	GLUT7	SLC2A7	Intestine,Colon	Fructose/Glucose	N/A	Computer model
II	GLUT9	SLC2A9	Kidney, Liver, Intestine, Placenta, Colon,	Urate/Fructose/ Glucose	Yes	Computer model
II	GLUT11	SLC2A11	Muscle, Heart, Placenta, Kidney, Pancreas, Fat	Glucose	N/A	N/A
III	GLUT6	SLC2A6	Brain, Spleen	Glucose	N/A	N/A
III	GLUT8	SLC2A8	Testes, Brain, Fat, Liver, Blastocyst	Glucose/Fructose	N/A	N/A
III	GLUT10	SLC2A10	Heart, Lung	Glucose	N/A	N/A
III	GLUT12	SLC2A12	Insulin-sensitive tissues	Glucose/Fructose	N/A	N/A
III	GLUT13 (HMIT)	SLC2A13	Brain	Myo-inositol	N/A	N/A

Table 2. Comparison of sequence identity of human GLUT family.

	GLUT1	GLUT4	GLUT3 (GLUT14)	GLUT2	GLUT9	GLUT11	GLUT7	GLUT5	GLUT6	GLUT8	GLUT10	GLUT12	GLUT13
GLUT1	100												
GLUT4	65.45	100											
GLUT3 (GLUT14)	64.29	57.43	100										
GLUT2	55.94	54.97	52.24	100									
GLUT9	37.27	36.11	35.03	30.47	100								
GLUT11	35.4	35.5	33.75	32.02	40.4	100							
GLUT5	41.43	41.45	38.9	40.29	43.11	41.1	100						
GLUT7	38.41	38.1	37.9	36.33	42.41	39.92	59.08	100					
GLUT6	26.39	27.16	25.72	27.49	21.46	23.13	25	23.61	100				
GLUT8	27.88	29.21	30.95	27.94	24.01	25.97	28.05	25.56	44.65	100			
GLUT10	25.9	27.29	24.72	26.58	20.49	23.41	26.23	26.83	28.88	29.61	100		
GLUT12	25.27	27.27	27.37	27.72	18.92	19.37	22.92	23.83	23.06	27.06	41.26	100	
GLUT13	25.95	27.1	29.08	30.08	20.5	20.92	26.29	24.09	23.46	28.96	27.68	26.76	100

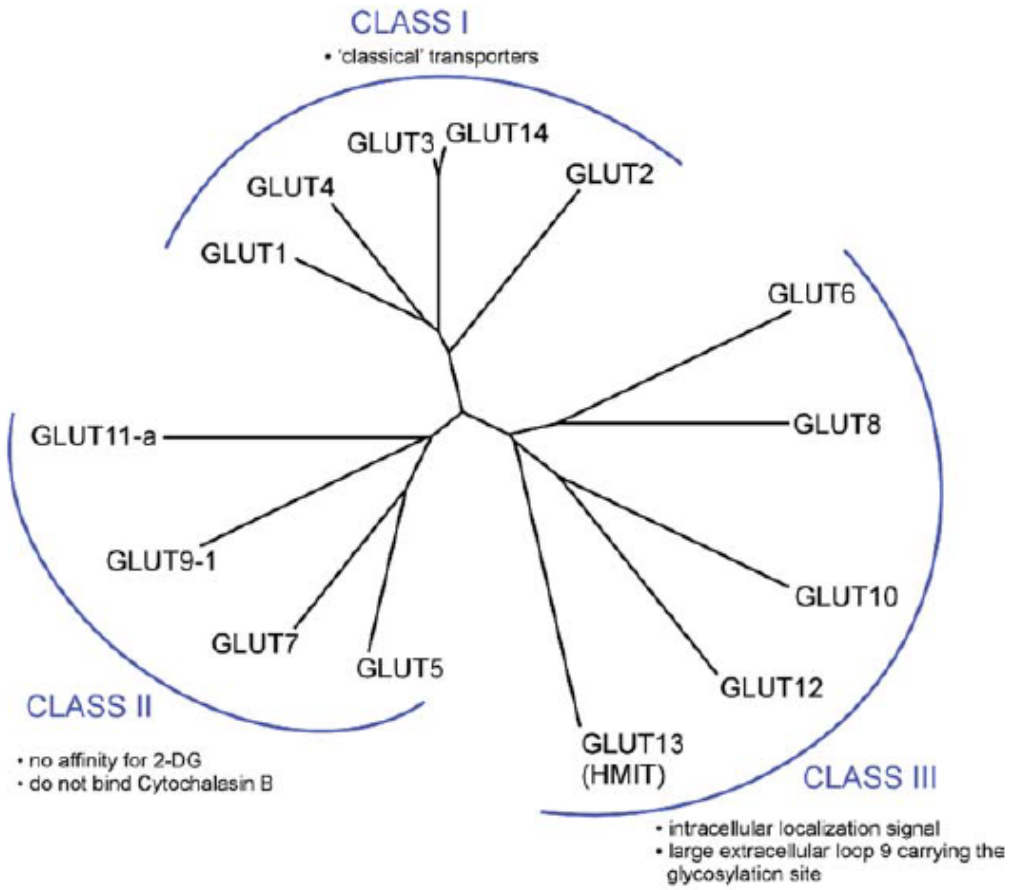

Figure 1. 4. Unrooted phylogenetic tree showing the relationship between the 14 human GLUT protein family members.
Adapted from (90).

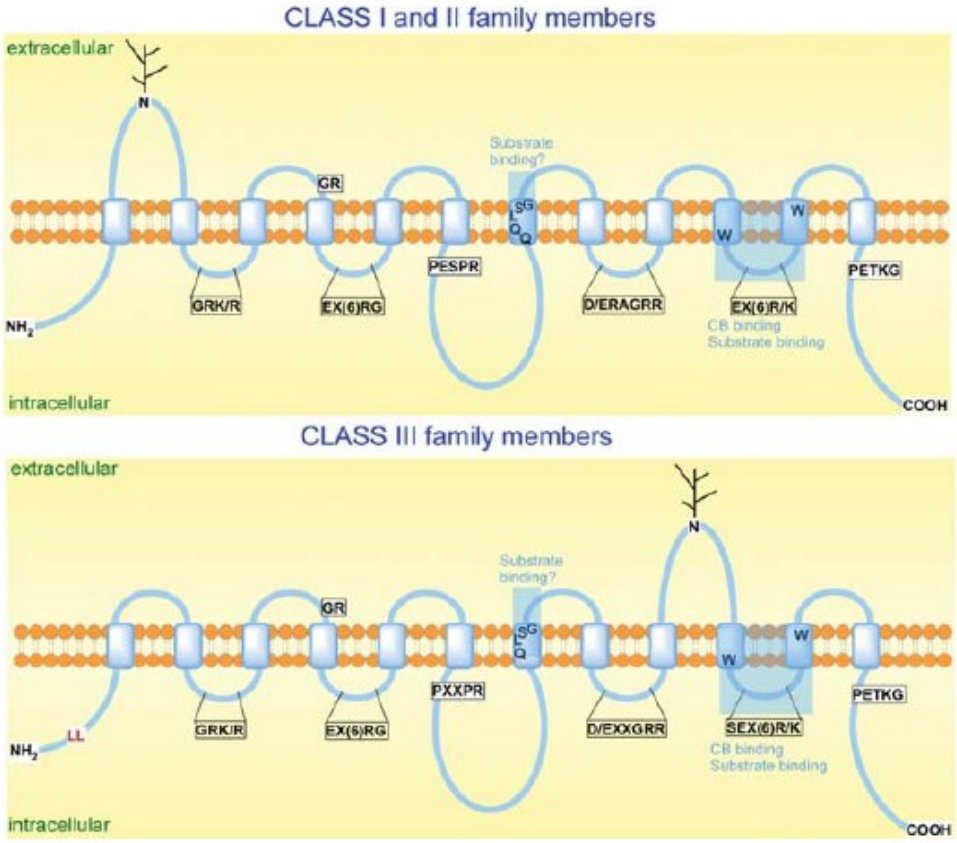

Figure 1. 5. Schematic models for class I and II (upper panel)and class III (lower panel) family members.

Specific features for the different classes are indicated such as the proposed substrate binding site, the N-linked glycosylation sites, conserved signature sequences, the tryptophan residues implicated in cytochalasin B (CB) binding (positions 338 and 412 in GLUT1) and the N-terminal dileucine signal present in class III members (except for GLUT10). Adapted from (90).

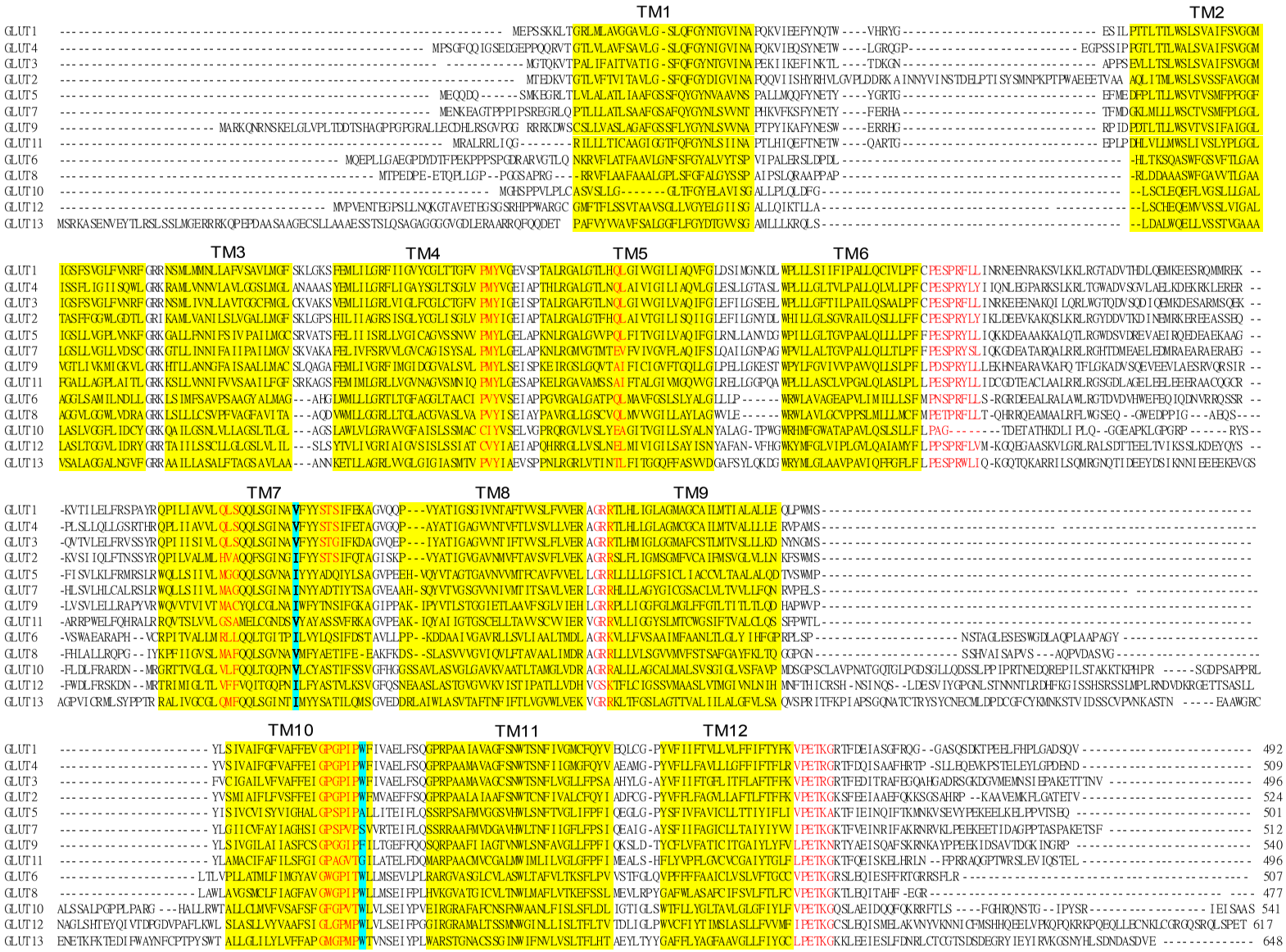
TM1
TM2
TM3
TM4
TM5
TM6
TM7
TM8
TM9
TM10
TM11
TM12
GLUT1
GLUT4
GLUT3
GLUT2
GLUT5
GLUT7
GLUT9
GLUT11
GLUT6
GLUT8
GLUT10
GLUT12
GLUT13

Figure 1. 6. Amino acid sequences alignments of human GLUT family proteins.

Transmembrane helices (Hs) are highlighted in yellow color based the new GLUT1 crystal structure. Highly conserved residues are red color. Residues highlighted in blue color are believed to be the cytochalasin B recognition/binding sites. Residues highlighted in blue color and bold fonts are believed to the critical hydrophobic residues responsible for substrate selectivities.

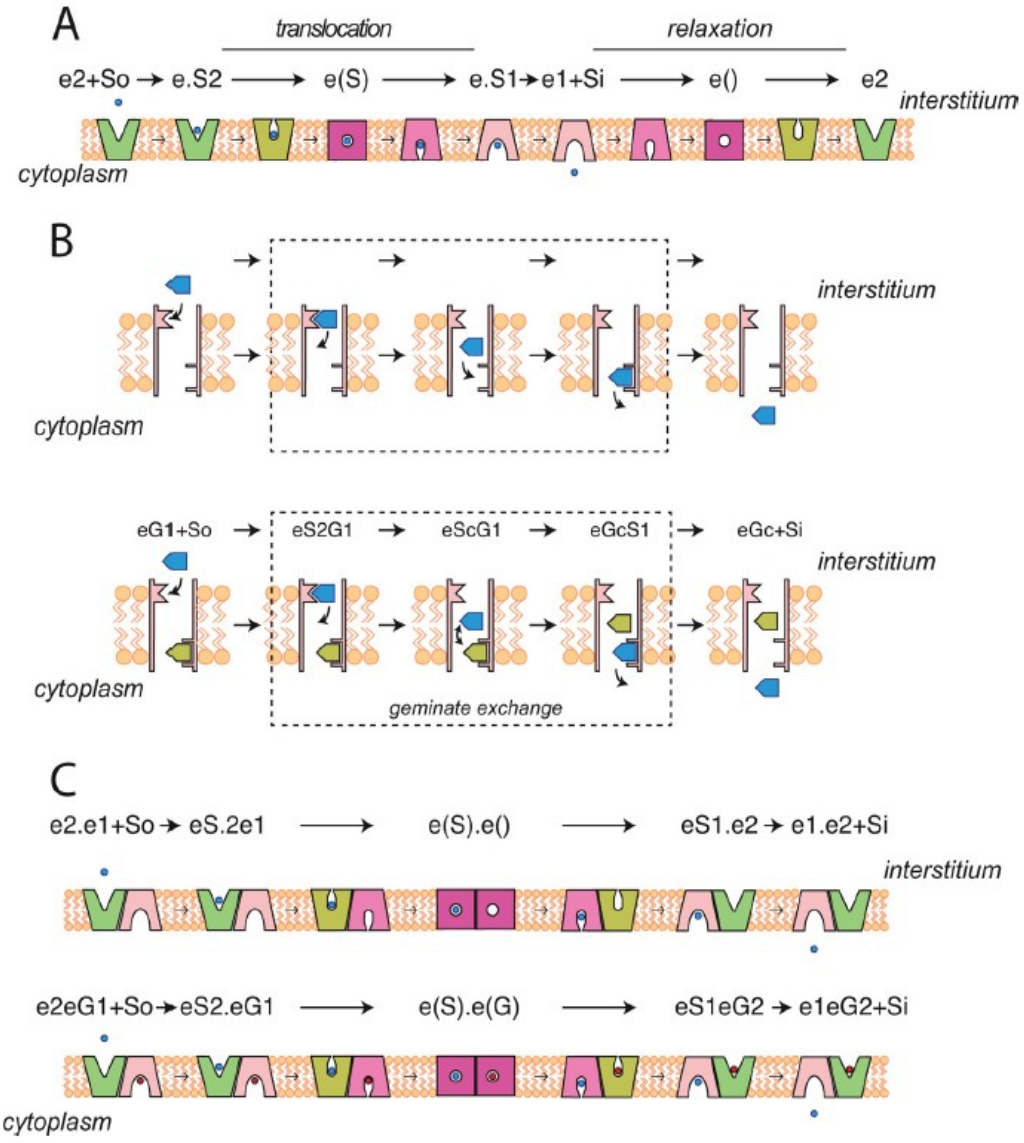

Figure 1. 7. Hypothetical hexose transport mechanism of GLUTs.

Panel A. simple carrier model of hexose transport. **Panel B.** The fixed sites hexose transport model. **Panel C.** A two-site hexose transport model. Adapted from (204).

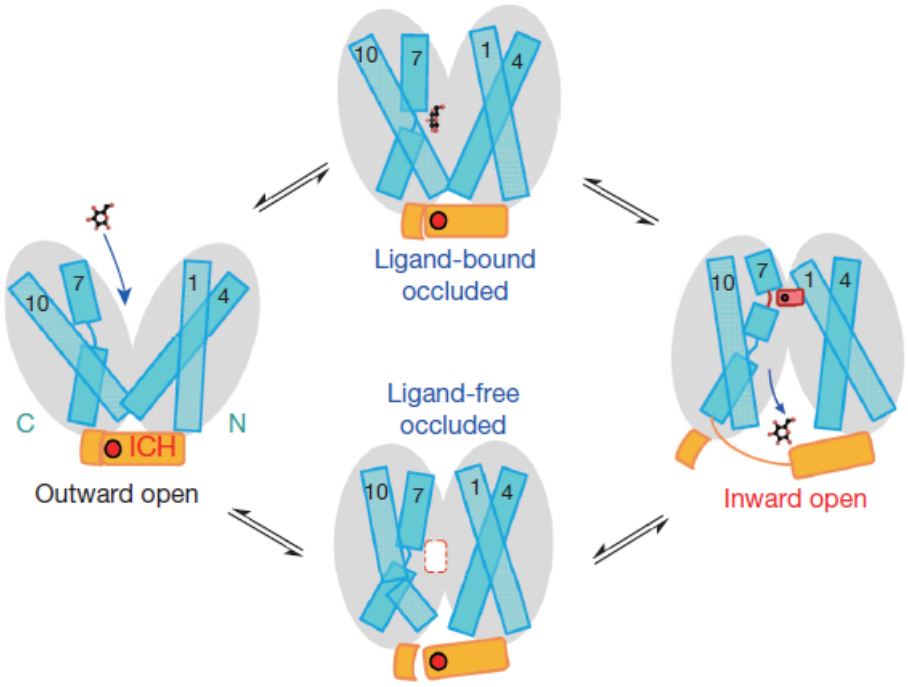

Figure 1. 8. Schematic hexose transport model of working GLUT1.

Model represents an alternating-access transport mechanism. Adapted from (170).

Chapter 2

Critical Roles of Two Hydrophobic Residues within Human Glucose Transporter 9 (hSLC2A9) in Substrate Selectivity and Urate Transport

(A version of this chapter has been published:
Long W, Panwar P, Witkowska K, Wong K, O'Neill D, Chen X, Lemieux, MJ, Cheeseman, CI. Critical Roles of Two Hydrophobic Residues within Human Glucose Transporter 9 (hSLC2A9) in Substrate Selectivity and Urate Transport. *J Biol Chem*. 2015;290(24):15292-15303.This work presented in this chapter represents a collaboration between the authors on the paper. WL performed all *in vitro* experiments and analysis herein. Computer modeling and analysis were done by PP).

2.1. Abstract

High blood urate levels (hyperuricemia) have been found to be a significant risk factor for cardiovascular diseases and inflammatory arthritis, such as hypertension and gout. Human glucose transporter 9 (hSLC2A9) is an essential protein that mainly regulates urate/hexose homeostasis in human kidney and liver. hSLC2A9 is a high affinity-low capacity hexose transporter and a high capacity urate transporter. Our previous studies identified a single hydrophobic residue in trans-membrane domain 7 of class II glucose transporters as a determinant of fructose transport. A mutation of isoleucine 335 to valine (I355V) in hSLC2A9 can reduce fructose transport while not affecting glucose fluxes. This current study demonstrates that the I335V mutant transports urate similarly to the wild type hSLC2A9; however, I335 is necessary for urate/fructose trans-acceleration exchange to occur. Furthermore, tryptophan 110 (W110) is a critical site for urate transport. Two structural models of the Class II glucose transporters, hSLC2A9 and hSLC2A5, based on the crystal structure of hSLC2A1 (GLUT1) reveals that I335 (or the homologous I296 in hSLC2A5) is a key component for protein conformational changes when the protein translocates substrates. The hSLC2A9 model also predicted that W110 is a crucial site that could directly interact with urate during transport. Together, these studies confirm that hSLC2A9 transports both urate and fructose, but it interacts with them in different ways. Therefore, this study advances our understanding of how hSLC2A9 mediates urate and fructose transport providing further information for

developing pharmacological agents to treat hyperuricemia and related diseases, such as gout, hypertension and diabetes.

2.2. Introduction

The membrane proteins making up the human facilitated glucose transporter family are encoded by the solute carrier gene family 2A (SLC2A). Many of these transport hexoses down their concentration gradient across mammalian cell membranes. Currently, fourteen hSLC2As have been identified and subdivided into three classes (142, 190, 192, 298), each associated with distinct substrate transport specificities. Many of these glucose transporter proteins are expressed specifically in different human tissues. For instance, the human glucose transporter 9 (hSLC2A9) is found primarily in the human kidney and liver (110, 111). Genome wide association studies suggest that nucleotide polymorphisms within hSLC2A9 are associated with uric acid (urate) handling and urate related diseases in humans, such as gout, diabetes, and hypertension (10, 12, 13, 17, 276, 299).

Initially, hSLC2A9 was shown to be a high affinity-low capacity glucose and fructose transporter; however, more recently studies have demonstrated that it is also a high capacity urate transporter, playing a key role in the handling of this important metabolite in humans. Detailed characterization of hSLC2A9 indicates that this transporter exhibits hexose/hexose trans-acceleration and hexose/urate exchange across the cell membrane (73, 300). That is, hexose on one side of the membrane can stimulate the unidirectional flow of hexose or urate

from the other side of the membrane. This trans-acceleration exchange behaviour provides confirmation that hexoses and urate share the same transporter despite the observation that there is little or no competition for transport between these substrates (73, 300). While trans-acceleration has been reported for a number of other members of this gene family, such as hSLC2A1, the exact mechanism for this interaction, particularly for hexoses and urate by hSLC2A9, remains unknown.

Extensive analysis has predicted that the SLC2As all have twelve trans-membrane domains (TMs) with both carboxyl and amino termini, and a long loop that connects H6 and H7, presenting to the cytosol (188). The recent report by Deng and associates providing the first crystal structure for SLC2A1 has now confirmed this topology (170). However, some features such as an intracellular helical bundle (ICH) domain formed by the intracellular loop and which apparently closes the inner vestibule when the protein is in the outward facing conformation appears to be novel. H7, long suspected to form part of the lining of the translocation pore with several key residues potentially involved in substrate binding and selectivity, is confirmed by this first SLC2A1 crystal structure.

We have previously proposed that residues in this pore lining helix, H7, play key roles in determining substrate specificity. We have also shown that a single hydrophobic residue in the H7 of several of the Class II glucose transporters, (hSLC2A5, 7, 9 and 11) and SLC2A2, markedly affects their ability to transport fructose, but not glucose (143). An early computer model of

hSLC2A7, based on the glycerol-3-phosphate transporter (GlpT), predicted that the isoleucine residue, I314, in H7 faces the aqueous pore and could potentially interact with a second hydrophobic residue, tryptophan (W89), on the other side of the pore in H2. This interaction was proposed to form a substrate selectivity filter, which determined the ability of fructose to access the translocation mechanism (144). Substitution of the equivalent isoleucine (I296) with a valine in hSLC2A5 abolished fructose transport while having no effect on glucose transport. Similarly, substitution of isoleucine 335 with valine (I335V) in hSLC2A9 also strongly decreased fructose transport with glucose transport remaining unaffected.

This current study examined the importance of the hydrophobic residues I335 and W110 of hSLC2A9 for urate transport and urate/hexose trans-acceleration exchange. For this, we constructed three point mutations of hSLC2A9: isoleucine 335 to valine (I335V) and tryptophan 110 to alanine (W110A) and phenylalanine (W110F). The impact of these mutations on hSLC2A9 transport characteristics was then assessed after expressing the proteins in *Xenopus* oocytes by the use of radiotracer flux measurements and electrophysiology. We found that the mutation I335V has urate transport kinetics similar to the wild type (WT) protein; whereas W110A has lower capacity and higher affinity for urate transport compared to WT hSLC2A9. Wild type and mutant transporters exhibited urate/urate trans-acceleration; however, fructose/ urate trans-acceleration was lost in both the I335V and W110A mutants; but retained in W110F mutant. Immunohistochemistry and biotinylation studies

indicated that all proteins are expressed at similar levels in the oocyte. This suggests that these functional differences between WT and mutant hSLC2A9 are due to structural changes in the protein, which is further discussed in light of a new structural model for hSLC2A9 based upon the crystal structure of hSLC2A1 (170).

These results demonstrate that I335 of hSLC2A9 is necessary for urate/fructose trans-acceleration exchange to occur. They also indicate that W110 of hSLC2A9 is critical for urate transport. Together they also confirmed that urate and fructose are both mediated by hSLC2A9, but that they interact with the transporter protein differently.

2.3. Experimental procedures

2.3.1. Plasmid construction -- Original hSLC2A9 was a gift from Kelle Moley (School of Medicine, Washington University, USA) and inserted into the pGEM-HE vector for oocyte expression. Site-directed mutagenesis was performed using the QuikChange II site-directed mutagenesis kit (Stratagene) to construct isoleucine 335 to valine (I335V), and tryptophan 110 to alanine (W110A) mutants of hSLC2A9 WT. The forward and reverse primers for the I335V mutant were 5’- GTG GCC TCA ATG CAG TTT GGT TCT ATA CCA ACA GC -3’ and 5’ - GCT GTT GGTATA GAA CCA AAC TGC ATT GAG GCC AC – 3’ (17); for the W110A mutant were 5'-CT CTG ACT TTG CTC GCG TCT GTG ACT GTG TCC-3' and 5' - GGA CAC AGT CAC AGA CGCGAG CAA AGT CAG AG - 3'; and for theW110F mutant were 5'- CCC AGA CAC TCT GAC TTT GCT CTT CTC TGT

GAC TGT GTC C -3' and 5'- GGA CAC AGT CAC AGA GAA GAG CAA AGT CAG AGT GTC TGG G -3' (Sigma Aldrich Canada). These plasmids were transformed into *Escherichia coli* DH5α competent cells for DNA propagation.

2.3.2.mRNA preparation and *Xenopus laevis* oocyte microinjection -- mRNA preparation and microinjection were performed as previously described (73, 300). In brief, plasmids containing hSLC2A9 WT and its I335V, W110A and W110F mutants were linearized with NheI and transcribed *in vitro* with T7 polymerase mMESSAGEmMACHINE^{TM} (Ambion). Individual adult female *X. laevis* oocytes were separated by collagenase and manually defoliculated before injection. Isolated oocytes were injected with 10-20 nL (20 ng) mutant plasmid mRNA and incubated in modified Barth's medium (MBM), 88 mM NaCl, 1mM KCl, 0.33 mM $Ca(NO_3)_2$, 0.41 mM $CaCl_2$, 0.82 mM $MgSO_4$, 2.4 mM $NaHCO_3$, 10 mM Hepes, 2.5 mM sodium pyruvate, 0.1 mg/ml penicillin and 0.05 mg/ml gentamycin sulfate, (pH 7.5) for 4 days at 16–18^{o}C prior to functional assays. All chemicals were obtained from Sigma-Aldrich unless otherwise stated. The same volume of water was injected into oocytes as a control. The concentration of mRNA was determined using a Nano Drop 1000 Spectrophotometer V3.7 (Thermo Fisher Scientific, USA).

2.3.3. Radiotracer flux experiments -- All radiotracer flux studies were conducted at room temperature (RT) 20-22^{o}C. ^{14}C labeled urate (Moravek) was used in flux and efflux experiments to test the urate handling ability of hSLC2A9 WT, I335V, W110A and W110F mutants. Radioactivity was measured with a

Beckman LS6500 liquid scintillation counter (Fullerton, CA, USA). Experiments were performed as previously described (13,17).

2.3.4. Urate kinetics --Urate transport was measured by incubating oocytes with 200 µL solution ranged from 100 µM to 5 mM urate. Oocytes were incubated for 20 min, which was determined as the linear portion of the urate uptake. The transport reaction was stopped by washing with ice cold MBM; then individual oocytes were placed into scintillation vials for uptake activity measurement. Uptake activity was corrected for non-specific activities measured from control water injected oocytes from the same batch for each experiment.

2.3.5. Trans-stimulation of urate uptake -- Oocytes were preloaded with substrates, D-fructose, urate or L-glucose with 1 hr incubation. Preloading was terminated by washing the oocytes with fresh MBM. Preloaded oocytes were then used to perform ^{14}C urate uptake experiments as described above.

2.3.6. Electrophysiology experiments --Experiments were conducted using the two-microelectrode voltage clamp (TEVC) technique with a GeneClamp 500B (Molecular Devices Inc. Sunnyvale, CA, USA). Sodium containing transport medium (STM), (100 mM NaCl, 2 mM KCl, 1 mM $CaCl_2$, 1 mM $MgCl_2$, 10 mM Hepes, pH 7.5 with Tris Base) was used to perfuse oocytes to obtain a base line current before adding experimental substrates. Urate-induced current (1 mM urate in standard STM) and urate kinetics analysis (with urate concentration ranging from 0.05 to 5 mM, added to STM) was performed using a Gap-free protocol. Individual oocytes were clamped at -30 mV and super-

perfused with different concentrations of urate for 30 seconds (range from 0.1 to 5 mM) followed by a 1 minute wash with urate free buffer in between. Data were collected at the peak of each urate-induced current (previous analysis had shown that using the plateau following the peak provided identical kinetics). Data were expressed in the form of urate-induced mean current ± SEM, where SEM stands for standard error of the mean. Current-voltage (I-V) curves were measured subjected to a RAMP protocol in which the voltage was changed from -120 to 60 mV for a 3 second period. I-V curves were RAMP at the peak of the urate-induced currents. A Digidata 1320A converter and pClamp8 (Axon Instruments, Union City, CA) were used to collect and analyze data. Then, we performed the Gap-free protocols to compare inward mean peak currents using either STM buffer or fructose containing STM buffer after oocytes were pre-incubated *in situ* with 1 mM urate for 1 minute. The trans-acceleration measured with TEVC assumed that the inward currents induced by washing the oocytes with STM are urate-induced. That is, these currents were induced when urate moved out of the oocyte (downward facing peak current value, see Fig. 2.4A and 4B).

2.3.7. Biotinylation -- Biotinylation and Western blot analyses were carried out to measure the protein expression level of each isoform based upon a previously published protocol (301) with modification. Oocytes were washed three times with PBS (pH 8.0); then, they were incubated in 2 mM Sulfo-NHS-LC-Biotin (Pierce) containing PBS buffer (pH 8.0) at room temperature for 30 minutes. The reaction was stopped by washing with quenching buffer (192 mM Glycine and 25 mM Tris-HCl in PBS, pH 7.5). Oocytes were then lysed with RIPA

buffer (150 mM NaCl, 1% Triton-X-100, 1% deoxycholic acid, 0.1% SDS, 1 mM EDTA, 10 mM Tris-HCl, pH 7.5). Lysates were incubated with streptadvidin (Pierce) at 4^{o}C overnight. On the next day, beads with bound protein were spun down gently at 3000 rpm. Biotinylated proteins were resuspended using SDS sample buffer and subjected to SDS-PAGE. Proteins from SDS-PAGE were transferred to nitrocellulose membranes and blocked with 3% milk in PBST (0.05% Tween 20 in PBS). After blocking, the membrane was probed with primary hSLC2A9 antibody (Cedarlane, Canada) and anti-rabbit secondary antibody (Abcam, Cambridge, MA, USA). Blots were developed into film through a film processor in a dark room. Protein quantification was done by measuring the band intensities on the film using ImageJ (http://imagej.nih.gov/ij/).

2.3.8. Immunohistochemistry--Immunohistochemistry was used to determine protein expression in *X. laevis oocyte* membranes. Oocytes were washed with Phosphate Buffer Saline (PBS; 137 mM NaCl, 2.78 mM, KCl, 4.3 mM Na_2HPO_4, 1.5 mM KH_2PO_4, pH 7.4), then fixed in 3% Paraformaldehyde (PFA) for 15 minutes at RT. After fixation, oocytes were washed with 50 mM NH_4Cl and permeabilized with 0.1% Triton. *X. laevis* oocytes were then blocked with 2% *Bovine Serum Albumin* (BSA) for 30 minutes followed by incubation with primary hSLC2A9 antibody in blocking buffer for 1 hour at room temperature at 22^{o}C (RT), and then with secondary antibody, Alexa 488 (Invitrogen, USA). After incubation, oocytes were mounted using Vectashield mounting medium (Vector Laboratories, Inc. Burlingame, CA USA) on slides with secure-seal spacers.

Protein expression was determined by Wave FX confocal microscopy (Quorum Technologies, ON, Canada) of the fluorescent secondary antibody.

2.3.9. Data analysis --Graphpad 5.0 was used to analyze all the data. Urate kinetic data was fitted using non-linear regression. Current-voltage (I-V) curves were graphed in X-Y plots. Trans-acceleration data was analyzed by One-way ANOVA for the flux studies and Student unpaired t-test in TEVC studies. Significant values were accepted when $p<0.05$. Biotinylation of protein expression level data was compared using arbitrary units of band intensity.

2.3.10. Homology modeling --The three-dimensional models of the human transporters SLC2A5 and SLC2A9 were built using the I-TASSER server, which is based on *ab initio*/threading methods (302) and choosing the crystal structure of human glucose transporter SLC2A1 (PDB ID 4PYP) as the preferred template. The sequence identity/similarity between SLC2A1 (or SLC2A5) and SLC2A9 are 28/49%(or 29/59%). The server generated 5 models with the best model for each target selected based on their C-scores (-1.2) implemented in I-TASSER. The score is calculated based on the significance of threading template alignments and the convergence parameters of the structure assembly simulations. The stereochemical quality of the model was assessed with Molprobity and it showed that 92% of the residues are in the most favourable regions of the Ramachandran plot for both molecular models (303). Sequence alignments were conducted with Clustal Omega (304) with figures created in ESPript 3.0 (305) and The PyMOL Molecular Graphics System, Version 1.5.0.4 Schrödinger, LLC.

2.4. Results

2.4.1. Urate kinetics

Flux studies. After determining that urate transport mediated by WT hSLC2A9 and its I335V, W110A and W110F mutants were similar at 0.1 mM substrate concentration, the kinetics for both mutants were then fully characterized. As shown in Figures 1A and 1B, the data indicate that the Michaelis-Menten like kinetics for urate are similar for both the WT and the I335V mutant. WT hSLC2A9 has an average V_{MAX} of 981.9±136.5 pmol/oocyte/20 min with a K_M of 4.5±11.6 mM; I335V has a V_{MAX} of 937.7±278.1 pmol/oocyte/20 min, K_M of 6.6±3.1 mM;W110A has an average V_{MAX} of 108.5±11.1 pmol/oocyte/20 min, K_M of 0.3±0.1 mM; and W110F has an average V_{MAX} of 355.6±61.9 pmol/oocyte/20min, K_M of 1.7±0.7 mM. This indicates that urate transport by the I335V mutant is very similar to the WT. The W110A mutant, on the other hand, has higher affinity and lower transport capacity compared to WT. W110F show a intermediate V_{MAX} and K_M between W110A and WT hSLC2A9.

Two-Electrode Voltage Clamp Experiments (TEVC). Because urate transport by WT hSLC2A9 is electrogenic (73, 300) we also used the TEVC method to further investigate how hSLC2A9 and its mutants transport urate. A representative trace from the actual recording obtained with WT hSLC2A9 is shown in Figure 2A. We clamped a single oocyte at a holding potential of -30 mV, then perfused the oocyte with different concentrations of urate followed by a 1 minute wash with STM. We then measured the mean induced outward current Data were collected at the peak of each urate-induced current. Fig. 2.2B shows

that urate transport by hSLC2A9 WT and its mutants displayed classical Michaelis-Menten kinetics. This confirms that all these proteins have only a single binding site for urate. Also, we can conclude that hSLC2A9 WT and I335V transport urate in the same way because they have very similar kinetic constants, Fig. 2.2C; (WT: V_{MAX}=433.4±21.5 nA, K_M=1.9 ±0.2 mM, I335V: V_{MAX}=451.0±26.5 nA, K_M=2.2±0.3 mM). However, the W110A and W110F mutations shift the urate kinetic curve to the right with a significantly smaller V_{MAX} (115.0±5.8 nA and 158.9±14.5 nA), and K_M (0.7±0.1 mM and 1.0±0.3 mM), suggesting that this tryptophan residue may play a key role in substrate preselection or binding.

2.4.2. I-V curve using TEVC -- In addition, we further investigated the protein function using current-voltage (I-V) curves as shown in Fig. 2.2D using a RAMP protocol. I-V curves were subjected to a RAMP protocol at the peak of the urate-induced currents. The voltage was progressively changed from -120 to 60 mV within a 3 second time period. Current recordings were filtered and current values at 20 different voltages from -120 to 60 mV were shown. As indicated in **Fig. 2.2C**, urate transport showed a quasi-linear relationship with the membrane potential in the range from -120 mV to 60 mV, indicating that urate transport is driven, but not gated by the voltage. The I-V curves of WT and I335V are similar; however, the I-V curve of W110A shows that urate-induced current is smaller than WT similar to the urate kinetics analysis, and the curve of W110F indicates the urate-induced current is in between those recorded for WT and W110A. Overall, this suggests that the ability of SLC2A9 to bind and translocate urate is driven by the membrane potential.

2.4.3. Urate/ hexose trans-stimulation

Isotopic flux studies. hSLC2A9 was originally reported to be a high affinity - low capacity hexose transporter and subsequently a high capacity urate transporter. It was also noted that hexoses can trans-accelerate urate uptake into oocytes (73, 300). Thus, we further examined the effect of trans-stimulation of urate transport by hexoses mediated by hSLC2A9 and its I335V, W110A and W110F mutants. **Fig. 2.3A** shows urate flux activities comparing the experimental condictions, D-Fructose or urate, to the control condition, non-transported L-glucose. **Fig. 2.3B** shows the normalized percentage of the trans-stimulation effect of both fructose and urate relative to the control, L-glucose. These results indicate that urate trans-stimulates urate uptake in all cases (One-way ANOVA, $p<0.05$) and that fructose trans-stimulated urate uptake mediated by WT and W110F hSLC2A9 (One-way ANOVA, $p<0.05$) but not by the I335V or W110A mutants (One-way ANOVA, $p> 0.05$, $n \geqslant 4$).

TEVC studies. **Fig. 2.4A** and **4B** show representative traces of urate-induced current mediated by hSLC2A9 WT, I335V, W110A, and W110F expressing oocytes using the Gap-free protocol in which the oocytes were clamped at -30 mV and incubated with 1 mM urate for 1 minute. These traces clearly indicate that the inward current increases in the presence of extracellular fructose in oocytes expressing WT and W110F but not in those expressing I335V and W110A. **Fig. 2.4C** is a bar graph showing the peak mean inward currents. Again, results showed that increased inward currents were observed in WT and W110F expressing oocytes when extracellular fructose was present (**Fig. 2.4A** and **4B**, n

⩾18, unpaired t-test, $p<0.05$). In contrast, no stimulation by fructose was seen in I335V and W110A expressing oocytes (n⩾18, unpaired t-test, $p>0.05$).

2.4.4. Qualitative and quantitative protein expression -- Qualitative analysis of hSLC2A9 and its I335V, W110A and W110F mutant protein expression in the plasma membranes of *X. laevis* oocytes was determined using immunohistochemistry as shown in **Fig. 2.5A**. hSLC2A9 WT, I335V, W110A and W110F proteins were expressed in the oocyte membrane, whereas water injected oocytes showed no detectable protein expression (n=3). Membrane proteins of all variants were also detected by biotinylation indicated in **Fig. 2.5B**. Indicated in **Fig. 2.5C**, protein expression levels were almost identical in both hSLC2A9 WT and the I335V mutant. Although the total expression protein levels seem slightly less in W110A and W110F compared to the WT, these differences are not statistically significant. The membrane protein expression levels are all proportional to the their total protein levels. (n⩾6, One-way ANOVA, $p>0.05$).

2.4.5. Structural analysis of SLC2A9 using homology modeling-- To provide structural insight into these critical residues, a model of the human SLC2A9 transporter was generated based on the human glucose transporter SLC2A1 (PDB ID 4PYP) (170). The accuracy of homology model is dependent on the template sequence identity (>30%) or the quality of the alignment between the target and template. Fortunately for membrane proteins, even low levels of template sequence identity, accurate model prediction is possible. The membrane environment imposes topological constrains on the relative

orientations of helices, which limit structural diversity available to families of membrane proteins. SLC2A1 and SLC2A9 share 28% sequence identity and a high degree of similarity, 49%. Phylogenetic comparison reveal three classes within all glucose tranporters , with hSLC2A1, a class 1 GLUT, and hSLC2A9, a class II GLUT, having similar predicted topologies (90). Due to such high homology the template treading alignment score was remarkably high as indicated by the normalized Z-score of 3.4. Alignments with a normalized Z-score > 1 reflects a confident alignment and most likely have the same fold as the query protein. Furthermore, I-TASSER confidence score (C-score) for the derived SLC2A9 model is also in the higher range (1.2). I-TASSER defined as Iterative Threading Assembly Refinement and is a hierarchical method for protein structure and function prediction. Confidence values higher than 1 indicatethat the overall derived structural homology model is likely accurate, that is, that deviation between derived homology model and the template 3D structure is low (302).

The SLC2A9 model has 12 transmembrane helices and represents the inward facing conformation (**Fig. 2.6A**). **Fig. 2.6B** and **6C** show both views from intracellular face and extracellular face of the model. These 12 helices segments are organized into two structural repeats, H1-6 and H7-12, related by a pseudo two-fold inversion axis parallel to the membrane bilayer, yielding a 6+6 inverted repeat fold. The transmembrane helices 1, 2, 4, 5, 7, 8, 10, 11 line the central transport cavity and 3, 6, 9, and 12 form the outer helices as seen in **Figure 2.6A**. Furthermore, we see evidence of an intracellular helical bundle (ICH) on the

cytoplasmic face of the transporter (**Figs. 2.6A**). Crystal structures of SLC2A1, XylE (171) and GlcP (172) suggest that all of the MFS transporters have an ICH located at the cytoplasmic face that is thought to affect the conformational change between inward- and outward-facing conformations (167).

A comparison of the SLC2A9 model with the SLC2A1 structure indicates an excellent structural agreement with an r.m.s.d. of 0.49 Å over 442 C-alpha atoms excluding variable N and C terminals. A central amphipathic pore 30 Å deep is formed by two interior pairs of symmetry-related helices — H1 and H4, and H7 and H10 — that are surrounded by an outer ring of helices, H2, H5, H8 and H11. A higher r.m.s.d. of 0.32 Å is obtained when the pore region of SLC2A9 is aligned with those in SLC2A1, which underlies functional conservation. Both H7 and H10 are discontinuous helices having a non helical hinge-region. This structural element plays a significant role in conformational changes during substrate transport. Main structural features of SLC2A9 and SLC2A1 are very similar, however the size of this hinge region in SLC2A9 different than SLC2A1 - smaller for H7 and larger for H10. These subtle differences can account for isoform specific transport properties. **Fig.2.6D** shows that in SLC2A9, I335 is located in H7 and faces away from the binding and translocation pore, in contrast to our earlier hypothesis (18). This residue interacts with two residues in helix 10 to form an intricate hydrophobic patch. Conversion of this residue to valine disrupts these interactions (**Fig. 2.6E**). Since substitution of this residue in SLC2A5 has also been shown to affect fructose and urate transport (143), SLC2A5 was also modeled based on SLC2A1, with models being made of the

equivalent isoleucine (Ile) to valine (Val) mutations (**Fig. 2.6F and 6G**). The SLC2A5 shares 41.7% sequence identity and 56.1 similarity with SLC2A1 (105), resulting in a model with an r.m.s.d. of 0.81 Å. As with SLC2A9, a mutation of Ile to Val disrupts important hydrophobic linkages of H7 with helices at the outer edge of the transporter.

Structural analysis of the W110 residue indicates it is located on H2, and the indole ring of the residue faces towards the substrate recognition and translocation pore. We compared side chain orientations of key residues in all 5 top scoring models. I335 side chain position was nearly identical in all the models; however, W110 adopted multiple orientations within the pore (**Fig. 2.7**). The kinetic data suggest that this residue may be involved in substrate binding, as urate transport is greatly reduced when this residue is mutated to alanine.

2.5. Discussion

2.5.1. Hydrophobic residues are well known determinants in protein structure-function relationships. Residues such as isoleucine, valine, leucine, and phenylalanine, are often clustered within active sites (173). For example, SLC2A1 has a leucine (L279) within the most conserved motif ‘QLS’ in GLUTs adjacent to the postulated ‘bottle-neck’ region of the substrate transport pathway (141) and valine165 is also predicted to be located near the exofacial surface of the substrate binding site (174). Subsequently, Manolescu *et al.* proposed that an isoleucine in H7 is a critical determinant of substrate selection in class 2 hSLC2As (91). They found that substituting an isoleucine for valine at the

equivalent position within these proteins significantly reduces or abolishes fructose transport, while not affecting glucose fluxes (143). Dietvorst *et al.*. also demonstrated that isoleucine 374 in H7 of Snf3 is essential for fructose sensing in yeast *Saccharomyces cerevisiae,* but does not affect their glucose sensing (306). Given that hSLC2A9 also transports urate, this study was designed to examine the effect of this I-V substitution on urate transport and the trans-stimulation behaviour between hexoses and the organic anion. In addition, our earlier prediction that isoleucine or valine might form a hydrophobic interaction across the translocation pore with a tryptophan in H2 led us to also investigate the role of this residue (W110).

The electrogenic property of urate transport by hSLC2A9 allows further characterization of urate fluxes by measuring the urate-induced current. The representative trace from the Gap-free protocol of WT hSLC2A9 expressing oocytes shows a typical urate-induced current trace, in which a fast occurrence of outward current is followed by a slow decline to a plateau (**Fig. 2.2A**). This observation was previously reported in both Bibert *et al.'s* and our studies (300, 307). We propose that there must be a rapid accumulation of the entered urate in the proximity of the inner face of the oocyte surface membrane. Previous studies have reported that this phenomenon corresponds to the presence of a so-called “unstirred layer” due to the slower urate diffusion away from the membrane than the rate of urate entry (180). This leads to a decreased chemical gradient/driving force for urate entry, thereby resulting in a decreasing current from its peak value. In fact, this reduced current at the plateau must be the net result of two opposing

currents: influx of extracellular urate and efflux of urate from the unstirred layer, which represents a steady state condition of the unstirred layer. However, upon extracellular urate withdrawal, only the latter is present, corresponding to the observed undershooting currents, which quickly vanished, likely due to exhaustion of the urate within the cytoplasmic unstirred layer. Thus, the concept of the presence of an accumulated urate proximal to the inner face of the surface membrane is in agreement with the time course of these events.

The urate kinetics and current-voltage (I-V) curves determined by TEVC matched the isotopic flux confirming that both WT hSLC2A9 and the I335V mutant transport urate similarly (**Fig. 2.1 and 2.2**). However, it is not so easy to do a direct comparison of the transport properties from these two methods due to the different conditions achieved using the two techniques. In the flux study, the oocyte membrane potential was not clamped; thus, entry of negatively charged urate into an oocyte should have quickly hyperpolarized the membrane potential, from an initial value of around -30 mV to a value of -50 mV or so, depending on the magnitude of the influx (14). The hyperpolarized voltage, representing a reduced driving force, thus decreased urate entry. This effect would increase as the urate concentration employed rose. In contrast, the oocyte membrane potential was held constant at -30 mV, by a gap-free protocol during a TEVC experiment; hence, the chemical gradient becomes the dominant driving force for urate transport into the oocytes. Thus, the urate entry rate for a given concentration will differ between the two protocols. Nevertheless, one conclusion we could draw from the I-V curve experiments is that the more the membrane

potential is depolarized, the higher the urate influx. (**Fig. 2.2D**) This confirms our previous suggestion that the membrane potential is a driving force for hSLC2A9 to bind and translocate urate.

2.5.2. The role of isoleucine 335

Our flux trans-acceleration measurements indicate that both intracellular fructose and urate are capable of stimulating urate uptake into WT hSLC2A9 expressing oocytes. This could be explained by the Simple Carrier Model theory in which reorientation of an empty carrier from one side of the membrane to the other is the rate limiting step (308, 309). That is, when a substrate is presented on the *trans* side of the membrane it will be energetically more favourable for the substrate-protein complex to reorient from the *trans* side to the *cis* side. A more recent study on another MFS protein, the lactose permease, LacY, also demonstrated that the empty protein is the rate limiting step for sugar binding and transport. Smirnova *et al.*. found that sugar binding is energetically favourable for increasing the open probability of LacY to the periplasm (204). We observed a similar phenomenon in our trans-acceleration experiments in which both preloaded fructose and urate (*trans*) simulate ^{14}C urate hSLC2A9 mediated transport into (*cis*) the oocytes. Our data also suggest that I335 of hSLC2A9 is necessary for urate/fructose trans-acceleration to occur during transport (**Fig. 2.3**). Fructose/urate stimulation was lost in the I335V mutant, while the urate/urate exchange remained unchanged. The reduction of fructose transport activity in the I335V mutant could thus lower the energy for the mutant transporter to reorient from the intracellular to extracellular side. Consequently,

the trans-accelerating effect of fructose was lost. These data provide additional evidence for a role of I335 in fructose permeation in a class II hSLC2A protein, but that I335 is not involved in urate transport in hSLC2A9 (**Fig. 2.1.A**). Urate kinetics and urate/urate trans-acceleration were unaffected in I335V compared to the WT hSLC2A9, which supports our previous conclusion that fructose and urate share the same transporter but they interact with the translocation pathway quite differently.

Until now, hSLC2A9 is the only Class II glucose transporter in which trans-acceleration behaviour has been reported. Other members of Class I, like hSLC2A1 and 3 but not hSLC2A2 and 4, have also been characterized for their ability to exchange hexoses in both oocyte and mammalian cell studies (194, 203, 206, 310). Through the construction of chimæras between hSLC2A1 and 4, Vollers and Carruthers found that H6 of hSLC2A1 contains residues necessary for trans-acceleration with glucose-glucose exchange (206). In the TEVC trans-stimulation study, we used the Gap-free protocol to detect urate efflux elicited inward currents by perfusing oocytes with fructose and fructose-free buffer. After preloading the oocytes with urate, we observed that extracellular fructose increased the urate elicited inward current with WT hSLC2A9, but not with the I335V mutant (**Fig. 2.4**). Thus, our study has shown that I335 in H7 is an essential residue for fructose to accelerate urate movement in the opposite direction. This confirms that I335 plays an important role in the ability of hSLC2A9 to transport fructose (143, 144).

2.5.3. Structural modelling of hSLC2A9

An early computer model of hSLC2A7 based on the GlpT structure (310) was constructed and used to reveal the important hydrophobic residues in GLUTs. Manolescu *et al.* suggested, that the isoleucine in the equivalent position (I314) appeared to be located on H7 within the extracellular vestibule facing the translocation pore. Consequently, they suggested that a hydrophobic residue at that site could either interact directly with substrates as they entered the pore or there could be a hydrophobic interaction across the pore with W89 on H2 (144).

However, our revised model of hSL2A9 based upon the recent crystal structure of human SLC2A1 indicates that this residue is not oriented towards the central pore. Instead, it appears to interact with residues on the adjacent TM 10 via an intricate hydrophobic network (**Fig. 2.6D**). Notably, our new hSLC9A model provides a higher degree of accuracy, given that both SLC2A1 and SLC2A9 are in the same transporter classification, from the same species, resulting in a considerable increase in sequence similarity with SLC2A1 compared to GlpT. The single amino acid change in SLC2A9, I335V, decreased fructose transport, but not glucose. A structural model for the mutant SLC2A9-I335V was also generated, in which we observed an apparent loss of the hydrophobic contacts observed with isoleucine in the identical position (**Fig. 2.6E**). The structural model strongly suggests that via its hydrophobic network, I335 affects the rigid body movement of one of the two six-helix bundles, and subsequently the orientation of helix 7 in the translocation pore of the transporter. The alternating access model developed for MFS transporters proposes that the

two six-helix bundles form the translocation pore and moving through an occluded state to provide access of the substrate binding pocket to one side of the membrane or the other (206). This central isoleucine residue may promote a more rigid coupling of helix 7 to the other members of its helical bundle altering how it faces the translocation pore and subsequently influencing its ability to bind fructose. In the I335V mutant this interaction appears to be weakened changing the orientation of H7 and hence the protein then loses its ability to bind fructose.

A molecular model of SLC2A5 was also generated based on the SLC2A1 crystal structure to gain insight into how this residue influences substrate specificity among other family members. In the SLC2A5 model, this isoleucine promotes a more complex interaction with the surrounding helices 9, 10 and 12 – essentially linking helix 7 to its half of the transporter (**Fig. 2.6F**). Similarly, when we modeled the same substitution in SLC2A5 the hydrophobic network was again lost (**Fig. 2.6G**). Together these observations suggest that this hydrophobic residue plays a crucial role in altering the different conformational states in the alternating access model and subsequently substrate specificity.

2.5.4. The role of tryptophan 110

Our new model also rules out an interaction of W110 with I335 but suggests that W110 has a role in regulating substrate transport. As mentioned above, earlier modeling studies of hSLC2A7 suggested that W85 in H2 (equivalent to W110 in hSLC2A9) might form a hydrophobic interaction with I314 across the pore in H7 serving as a pre-selection site in regulating fructose transport through hSLC2A7 (144). Our new model indicates interactions of W110

in the central pore, and substitutions lead to altered transport further suggesting a role in substrate pre-selection. However, at this stage it is unclear whether these observed effects are due to direct interaction with substrates or structural changes.

Such pre-selection mechanisms have also been observed for other transporters, early crystal structures of LacY and SGLT1 showed that the indole ring of tryptophan/tyrosine is a common feature of sugar-binding proteins, where the primary hydrophobic interaction occurs between sugar and the sugar binding sites (311, 312).

In the glucose transporter 1 (SLC2A1), tryptophans in H10 and H11 are known to be responsible for glucose transport activity and substrate binding (313, 314). Also, a docking study indicated that W65 formed a direct interaction with the C6 of glucose (160). In addition, a tryptophan residue mutation had been identified in another urate transporter, hSLC22A12, as a major cause in hypouricemia in Japanese patients (315). These observations support the view that W110 in hSLC2A9 could also be interacting with urate and/or fructose directly. Indeed when mutated to alanine (W110A) urate transport was affected substantially (Fig. 2.2.1.A). The K_M for urate uptake was reduced indicating an increased affinity for the substrate while at the same time the V_{MAX} was very significantly reduced. However, despite these changes in urate kinetics the urate/urate exchange was still present (**Fig. 2.3**).

The effect on urate transport could therefore result from a loss of a direct interaction between W110 and the substrate or be a consequence of an altered structure of the protein. In the latter case, the time spent in the occluded state during the conformational change between the outward and inward facing states could be affected. W110A, has very similar K_M in both TEVC and flux studies, suggesting that varying the intracellular membrane potential did not affect how W110A handles urate transport. We were also interested in determining whether urate and fructose transport would still be maintained when W110 is mutated into another aromatic residue. Therefore, we constructed a third mutant of hSLC2A9, tryptophan 110 into phenylalanine (W110F). We observed that W110F partially reduced urate transport with a lower V_{MAX} and smaller K_M compare to WT; whereas these values are higher when compared to W110A (**Fig. 2.1**). This indicated that W110F has higher capacity and lower affinity for urate when compared to W110A. In addition, the trans-stimulation experiment data demonstrated that both urate/urate and urate/fructose exchange were maintained in W110F. This indicated that the aromatic ring structure is not only important for urate transport, but also fructose transport at this W110 position of hSLC2A9 (**Fig. 2.3 and 2.4**).

These data support our hypothesis that either these electronic rich aromatic rings are forming direct interactions with the charged substrates during transport, or they are involved in maintaining protein structure by interacting with other residues in the protein. With a partially altered the ring structure, W110F maintains the primary hydrophobic interaction with the substrates; thus, it is still

able to transport both urate and fructose. In contrast, W110A has no aromatic ring in the residue; hence, it was not able to sense changes in the ionic environment and influence the urate/fructose transport properties. All these data imply that the bulky side chain of tryptophan is essential for urate transport in hSLC2A9.

Additional analysis of structural models generated using I-TASSER indicated a considerable degree of flexibility for the W110 residue in the pore region (**Fig. 2.7**) again suggesting that it may play a role in substrate binding, selectivity or occlusion. Transition of SLC2A9 from an outward facing to an inward facing conformation through an occluded state is possibly associated with conformational changes in the inner pore region, which might involve the repositioning of the W110 side chain**. Fig. 2.7** suggests that the indole ring of tryptophan could act as a lid between the protein's central cavity and the extracellular face, which could serve as a 'thin gating element' similar to that proposed for other sugar transporters, like vSGLT (316). MFS transporters are known to have several mechanisms for substrate occlusion and permeation. Common denominators in all these structures include an extracellular facing "thin gate" that plays a role in providing access to the primary substrate binding site. We propose W110 could play such a role in controlling access to the primary binding site and could be one of the residues forming a 'thin gate'. In addition, it could also serve as a closure to prevent urate escaping from the binding site before the protein changed from an outward to an inward conformation avoiding

a futile cycle. However, several crystal structures are needed to determine the precise nature of the role of W110.

Although many studies indicate that hSLC2A9 is primarily a urate transporter, its ability to transport hexoses should not be ignored. Our studies have demonstrated hSLC2A9 cannot only transport both hexoses and urate, but can also exchange the two different types of substrate. There is an obvious implication in that hSLC2A9 could serve as an excellent candidate in regulating both blood sugar and urate in humans. For example, Emmerson pointed out that when fructose is given orally it causes an increase in urate excretion in the urine of children (317). hSLC2A9 is expressed in both the proximal convoluted tubule and collecting duct in human kidney nephrons, sites where both sugars and urate are handled (20, 318–320). Therefore, understanding the mechanism of how hSLC2A9 can exchange hexoses and urate in the human kidney will be valuable for developing new treatments for patients with hyperuricemia or hyperglycemia.

In summary, this study has further demonstrated that the hydrophobic residues, isoleucine 335 and tryptophan 110, of hSLC2A9 are important residues influencing both hexose and urate transport. Future studies of hSLC2A9 substrate selectivity and specificity will provide an even better understanding of urate transport and its regulation and hence the causation of hyperuricemia. A series of crystal structures is needed to determine the exact roles of both residues within hSLC2A9. Furthermore, understanding the hSLC2A9 binding sites for urate and hexoses could help to provide a pharmacological basis for

effective treatment of hyperuricemia and other related diseases, such as gout, hypertension and diabetes.

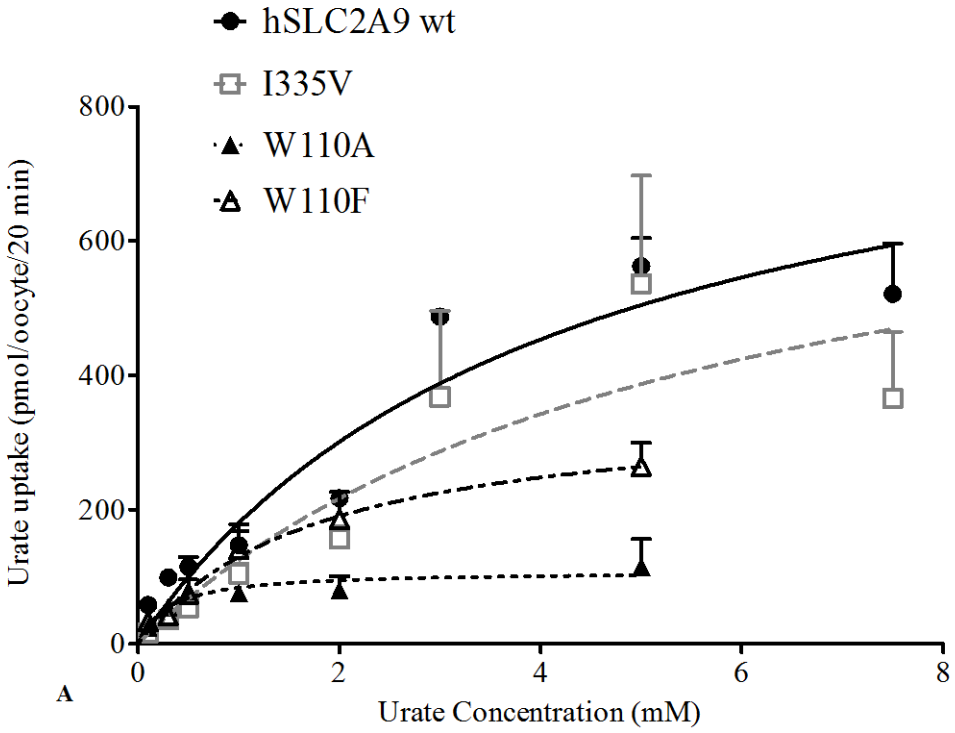

A

	hSLC2A9 wt	I335V	W110A	W110F
$K_{M\ (mM)}$	4.5	6.6	0.3	1.7
SEM	11.6	3.1	0.1	0.7
V_{MAX} (pmol/oocyte/20min)	981.9	937.7	108.5	355.6
SEM	136.5	278.1	11.1	61.9

B

Figure 2. 1. ^{14}C Urate kinetic measurements in oocytes expressing hSLC2A9.

Panel A. Michaelis-Menten curves of ^{14}C urate kinetics of hSLC2A9 WT (●) and its mutants I335V (□), W110A (▲), and W110F (Δ). Urate uptake was measured by incubating 12 protein expressing oocytes in 200 µL urate solution ranged from 100 µM to 5 mM for 20 minutes. Uptake activity was corrected for non-specific transport measured in control water injected oocytes from the same batch of oocytes. **Panel B.** ^{14}C urate kinetic constants of the 3 isoforms (n =4).

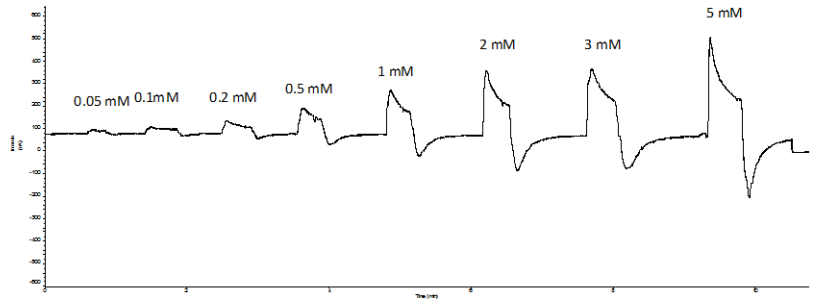

A

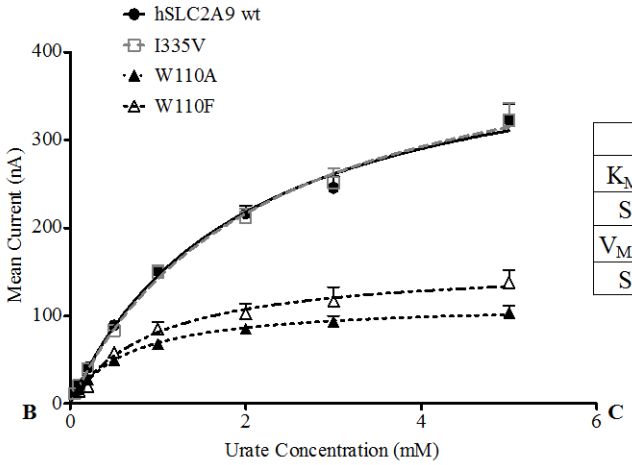

B C

	hSLC2A9 wt	I335V	W110A	W110F
$K_{M\ (mM)}$	1.97	2.2	0.7	1
SEM	0.2	0.3	0.1	0.3
$V_{MAX\ (nA)}$	433.4	451	115	158.9
SEM	21.5	26.5	5.8	14.5

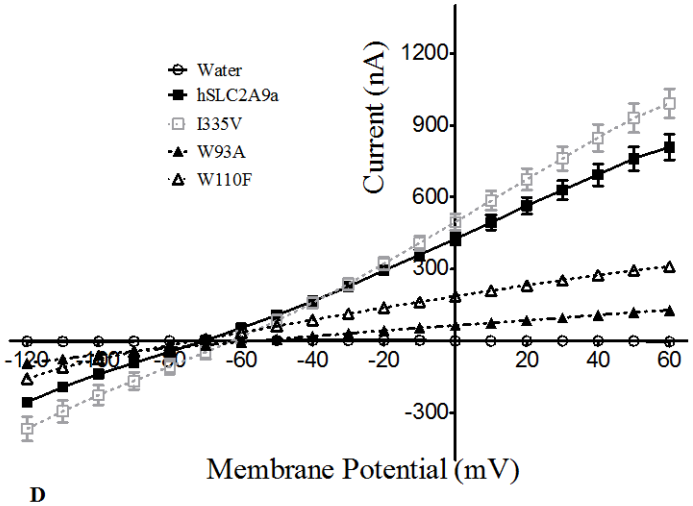

D

Figure 2. 2. Urate-induced currents in oocytes measured with Two Micro-Electrode Voltage Clamp (TEVC).

Panel A provides a representative trace from the Gap-free protocol of WT hSLC2A9 expressed oocytes. Single oocytes were clamped at -30 mV and super-perfused with different concentrations of urate (range from 0.1 to 5 mM) followed by a 1 minute wash with urate free buffer in between**. Panel B.** Michaelis-Menten curves of urate kinetics of hSLC2A9 WT (■) and its mutants I335V (□), W110A (▲), and W110F (Δ). Points represent the mean of urate-induced outward current for each concentration. **Panel C.** Urate kinetic constants of the WT and mutant isoforms (n >15 oocytes from 3 frogs). **Panel D.** Current-Voltage curve of 1 mM urate-induced current obtained from RAMP protocol for control, WT hSLC2A9 (■), the I335V (□), W110A (▲) and W110F (Δ) mutant expressing oocytes. The oocytes were clamped initially at -30 mV followed by voltage change instantly from -120 to 60 mV for a 3 seconds period. (n >15 oocytes from 3 frogs).

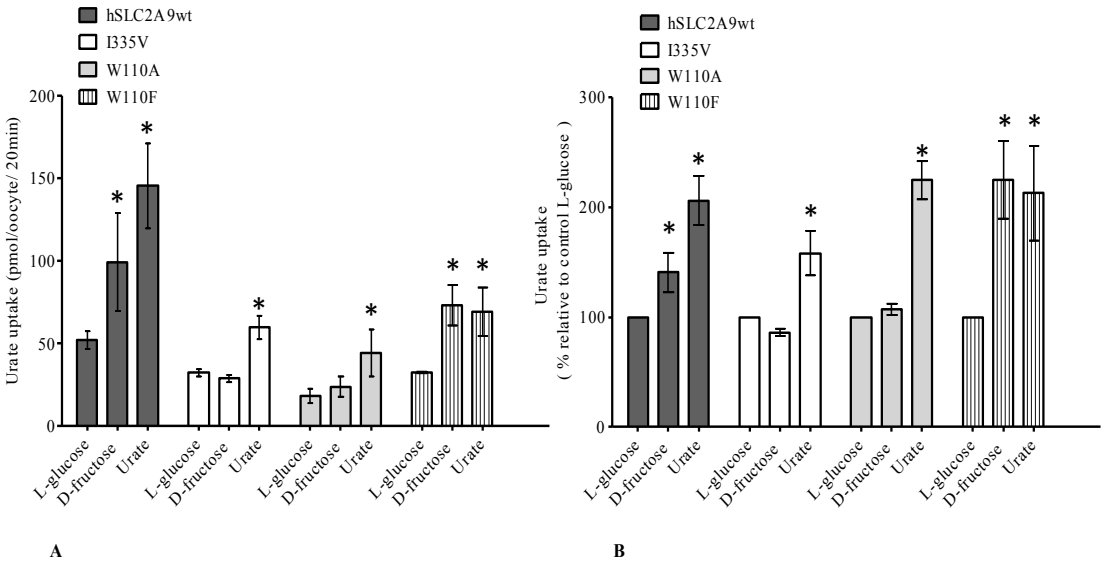

Figure 2. 3. Trans-acceleration studies for urate uptake into oocytes preloaded with urate or fructose.

Panel A. Trans-acceleration experiments of urate flux in the presence of intracellular substrates mediated by hSLC2A9 WT (dark grey), I335V mutant (white), W110A mutant (light grey), and W110F (straight line) expressing oocytes. Oocytes were preloaded with intracellular substrates, (L-glucose, urate or D-fructose) by preincubation for 1 hour. Preloaded oocytes were then washed with fresh MBM prior to performing ^{14}C urate uptake experiments. **Panel B.** Bar graphs represent the percentage of each condition relative to control experiments (L-glucose), (n>3, One-way ANOVA, * $p<0.05$).

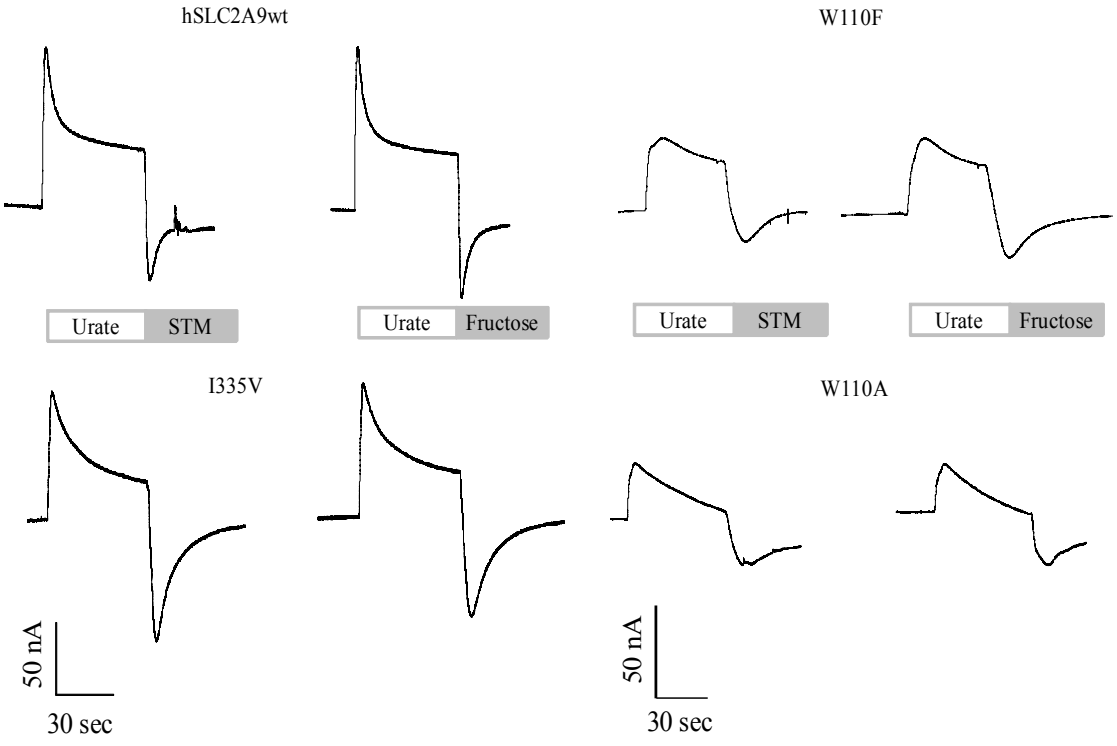
hSLC2A9wt
W110F
Urate
STM
Urate
Fructose
Urate
STM
Urate
Fructose
I335V
W110A
50 nA
30 sec
50 nA
30 sec

A B

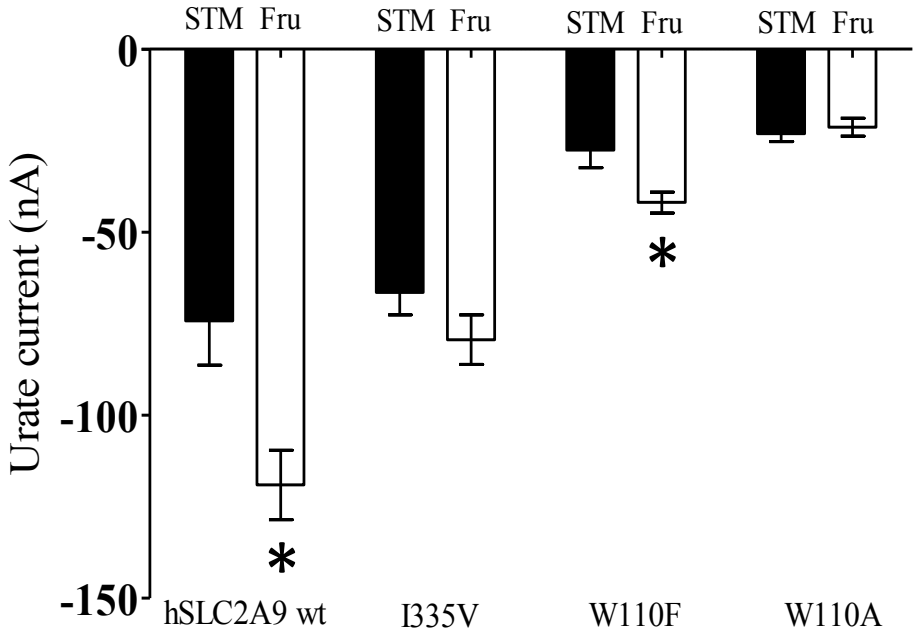
STM Fru
STM Fru
STM Fru
STM Fru
0
-50
-100
-150
Urate current (nA)
*
*
hSLC2A9 wt
I335V
W110F
W110A

C

Figure 2. 4. Trans-acceleration studies of urate-induced currents mediated by hSLC2A9 measured with TEVC.

Panels A and **B** are representative current traces in a single oocyte expressing hSLC2A9 WT (upper traces), the I335V (lower traces), W110F (upper traces), and W110A (lower traces) mutants. All traces indicate one minute of urate preloading followed by washing with either substrate free STM buffer (left) or 50 mM D-fructose STM buffer (right). Oocytes were clamped at -30 mV and traces were recorded under the Gap-free protocol. **Panel C**. Mean urate-induced inward currents were collected at the peak of the inward currents. hSLC2A9 WT, I335V , W110F, and W110A. Urate pre-loading oocytes were washed with either standard transport medium (STM, dark) or 50mM fructose containing STM (Fru, white). ($n \geqslant 15$ oocytes from 3 frogs, unpaired t-test, * $p<0.05$)

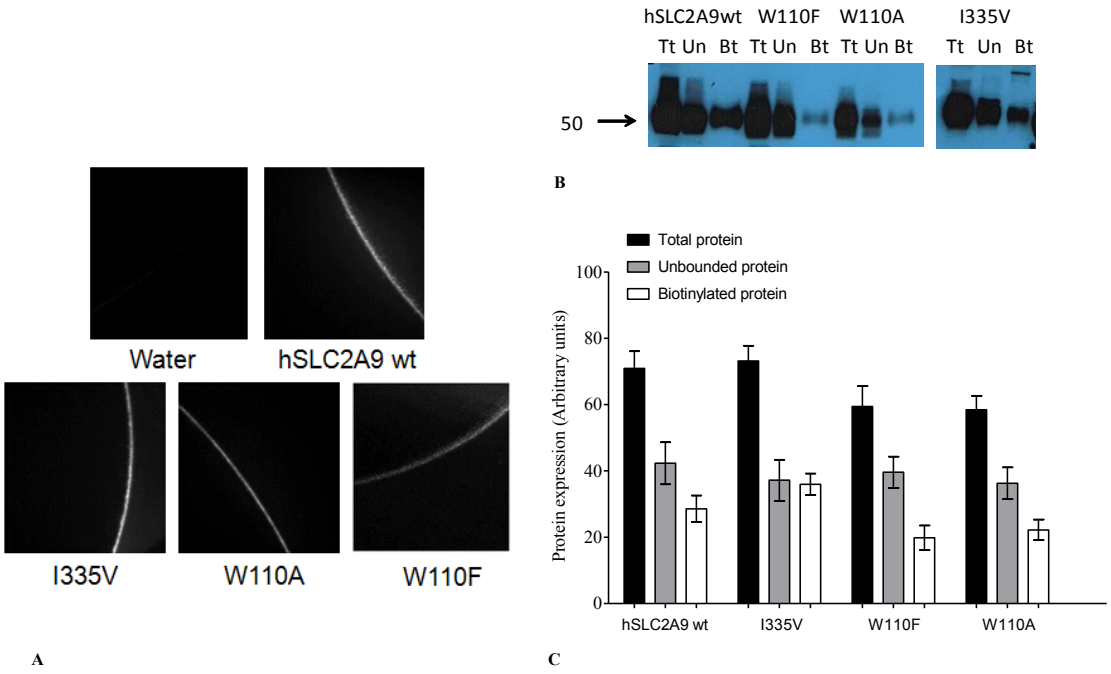

Figure 2. 5. Qualitative and quantitative determination of WT and mutant hSLC2A9 protein expression.

Panel A. Representative pictures of immunohistochemistry of water injected, hSLC2A9 WT, I335V， W110A, and W110F mutant expressing oocytes. **Panel B**. Representative Western Blot analysis of protein expression of water injected, hSLC2A9 WT, I335V, W110F and W110A expressing oocytes. Tt: total protein; Un: Unbound protein; Bt: biotinylated protein. **Panel C**. Quantitative analysis of protein expression. Data was calculated from band intensity using a formula Biotinylated protein = Total protein - Unbound protein. Protein expression levels shown as bar graphs with arbitrary units for Total protein (dark), Unbound protein (grey) and biotinylated protein (white) (n=3, One-way ANOVA among the three biotinylated proteins, $p>0.05$).

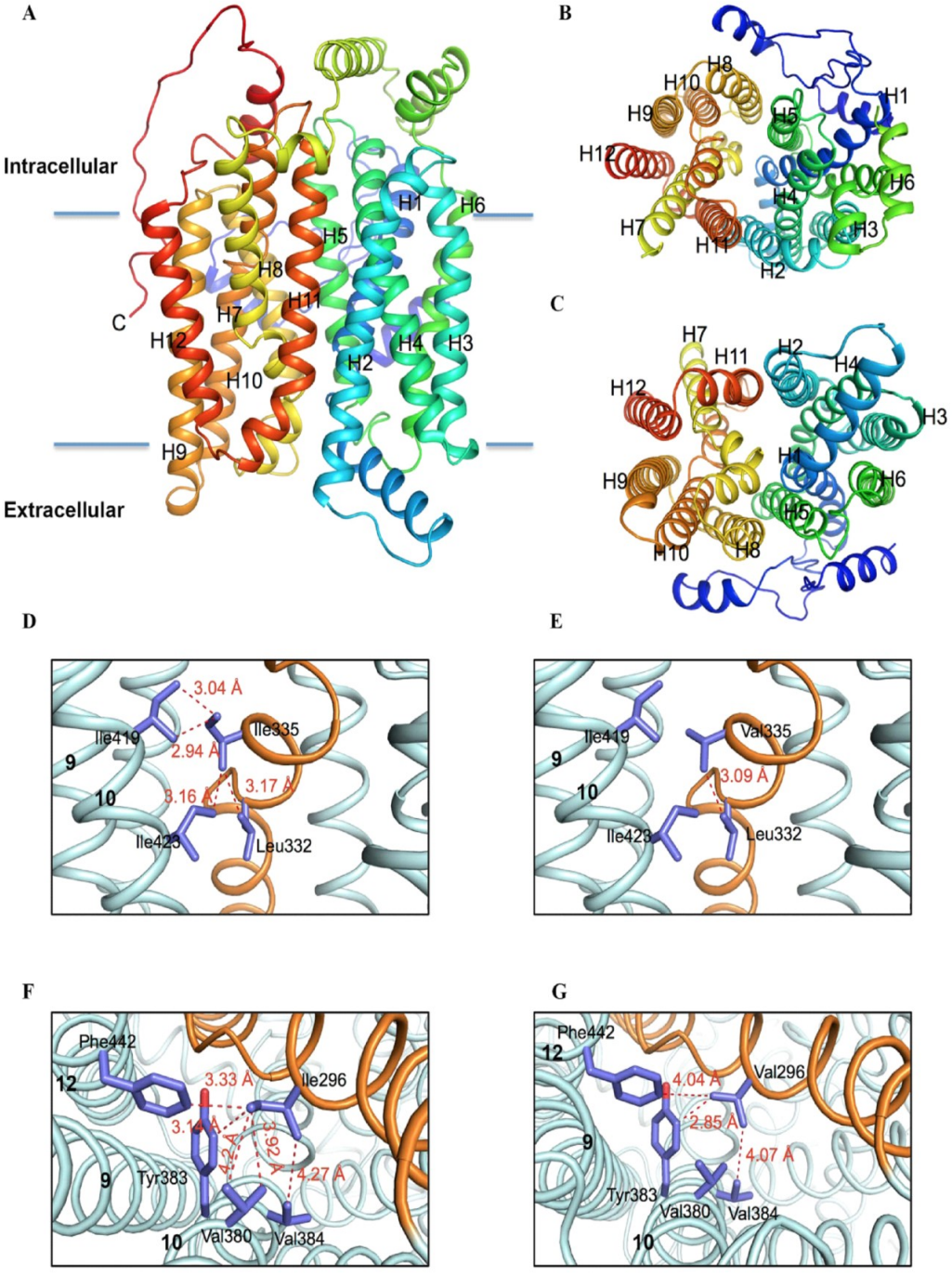
A
Intracellular
Extracellular
C
H1
H2
H3
H4
H5
H6
H7
H8
H9
H10
H11
H12
B
C
D
3.04 Å
2.94 Å
3.16 Å
3.17 Å
Ile419
Ile335
Ile423
Leu332
9
10
E
Ile419
Val335
3.09 Å
Ile423
Leu332
F
Phe442
3.33 Å
3.14 Å
4.2 Å
3.92 Å
4.27 Å
Ile296
Tyr383
Val380
Val384
12
G
Phe442
4.04 Å
2.85 Å
4.07 Å
Val296
Tyr383
Val380
Val384

Figure 2. 6. Molecular model of the human SLC2A9 & SLC2A5 transporters comparing possible hydrophobic interactions.

Panel A. Cartoon representation of the molecular homology model of the hSLC2A9a based on the SLC2A1 crystal structure (4PYP.pdb). The twelve transmembrane helices are labeled. **Panel B.** and **C**. Views from the intracellular face and extracellular face are shown. The intracellular face contains the conserved intracellular helical bundle. **Panel D**. Potential interactions of I335 indicate a hydrophobic network with residues within TM 10, thus linking the critical H7 (coloured in orange) to one half of the transporter. **Panel E**. Structural model of the mutant SLC2A9 I335V was generated that demonstrates this intricate linkage to helix 10 is disrupted when I335 is converted to Val. **Panel F**. In SLC2A5 Ile296, equivalent of Ile335 in SLC2A9, forms an even more extensive hydrophobic cluster with neighbouring residues at H10 and H12**,** **Panel G**. Structural model of the mutant SLC2A5 I296V, highlights the loss of the hydrophobic network, which subsequently leads to alteration in substrate specificity.

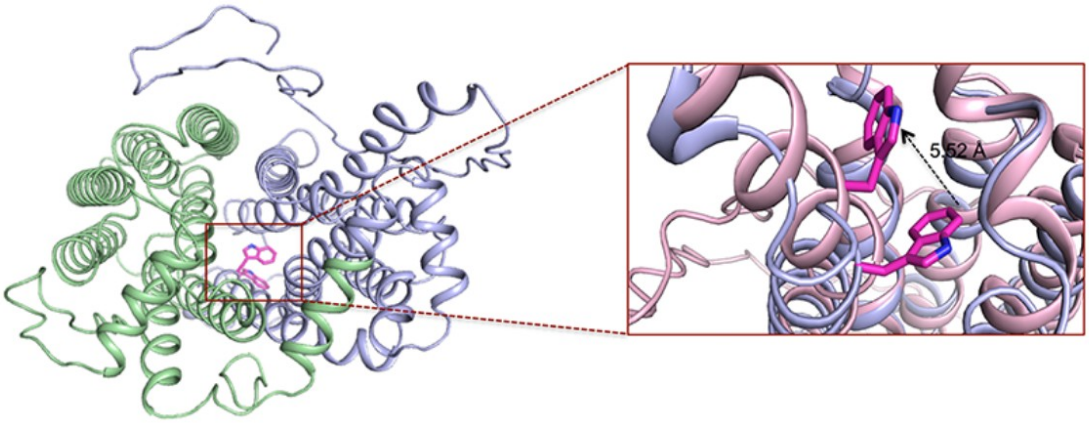

Figure 2. 7. Analysis of Tryptophan 110 orientation within the translocation pore of hSLC2A9.

A cartoon representation of the extracellular face of two SLC2A9 homology models, with the two halves of 6 helical bundles colored in green and purple, indicate that the W110 residue is located within the substrate translocation pore of the transporter. Furthermore, it was noted among the molecular models generated, W110 was observed in different orientations within the pore suggesting a possible role of W110 side chain movements during the transport cycle.

Chapter 3

An Approach to the Identification of Urate Binding Site of Human Glucose Transporter 9 (hSLC2A9). critical roles of cysteine residues, transmembrane helix 7 (H7) and a plausible urate binding site in hSLC2A9

(A version of this chapter has been prepared for publication:
Wentong Long, Pankaj Panwar, Kenneth Wong, Debbie O'Neill, Xing-Zhen Chen, M. Joanne Lemieux, Chris I. Cheeseman.
This work presented in this chapter represents a collaboration between the authors on the paper. WTL performed all *in vitro* experiments and analysis herein. Computer modeling, substrate docking and analysis were done by PP.)

3.1. Abstract

Human urate (uric acid) homeostasis is critically important as even very small deviations from the normal plasma concentrations can lead to either chronic disease or acute metabolic disturbances. Recent studies have focused on one urate transporter, the human glucose transporter 9 (hSLC2A9), which is believed to be important in human urate homeostasis. Our recent report showed that W110 and I335 have an important role in regulating substrate transport by hSLC2A9; however, these two residues do not appear to be part of the urate binding site in hSLC2A9. Thus, the objective of this present study tries to further explore the residues involved in binding urate within the translocation pore of hSLC2A9 using a computer model of hSLC2A9b for *in silico* substrate docking studies, followed by functional studies of mutated residues. The hSLC2A9b computer model predicted three amino acids, Y42, Y298 and N429, forming the possible binding site(s). Functional studies indicated that urate transport was strongly reduced by N429H without affecting fructose transport. Our results also indicated that C181 and C398 are important for urate translocation while C297 and C451 are not. Mutation of either C301 or C459 also decreased urate transport significantly. Together with the computer model analysis, we propose that 1) C181 is the residue with which pCMBS reacts; and 2) C301 and C459 could plausibly have an internal disulfide linkage, which is also critical for protein conformation and urate transport. Analysis of the chimæric proteins, hSLC2A9$_{(7)5}$ (H7 of hSLC2A9b is replaced by the one from hSLC2A5) , hSLC2A5$_{(7)9}$ (H7 of hSLC2A5 is replaced by the one from hSLC2A9), and the double mutants

G297C/S301C in hSLC2A9$_{(7)5}$, and triple mutant T171C/A388C/S441C in hSLC2A5$_{(7)9}$ indicate that H7 and the cysteine residues are necessary for urate transport in hSLC2A9b. However, they are not sufficient alone to allow hSLC2A5$_{(7)9}$ to gain urate transport. Together with the docking analysis, these results allow us to postulate that N429 is a key residue for urate binding.

3.2. Introduction

The human glucose transporter 9 (encoded by hSLC2A9) is an essential urate/fructose transporter found mainly in human kidney and liver, where urate homeostasis is achieved (110, 308, 321, 322). Human SLC2A9 belongs to the 14-member glucose transporter family, in the subdivision Class II, the fructose transporters. Human SLC2A9 has the highest sequence similarity with hSLC2A5, having 29% identity and 59% similarity (90, 105, 145). Radiolabelled urate/fructose flux studies demonstrated that urate transport does not compete with fructose transport mediated by hSLC2A9 (73). In addition, a hydrophobic residue isoleucine335 (I335) in the transmembrane helix 7 (H7) of hSLC2A9 influences only fructose but not urate transport was reported recently (145). Together, these suggested that hSLC2A9 transport urate and fructose through different pathways. A genome wide association study indicated that hSLC2A9 is associated with high serum urate level, which might cause disease like gout and hypertension (73). Many single nucleotide polymophism studies illustrated that hSLC2A9 is associated with abnormal serum urate level in gout patients (74, 75, 77, 79, 276, 322, 323). Therefore, understanding how hSLC2A9 transports urate

will allow researchers to develop better methods to handle abnormal urate levels in human patients.

Human SLC2A9 has two splice variants: full length and truncated amino (N-) terminus isoforms (300, 324, 325). Previous studies exposed that both isoforms function similarly, and difference in the N-termini affect only the protein localization. Full length hSLC2A9 was found on the basolateral membrane; whereas the truncated N-terminus hSLC2A9 was located on the apical membrane on the polarized epithelial cells (266). We used the N-terminus truncated hSLC2A9 as our protein of interest, which we named it as hSLC2A9b, in the current study. This is because the N-terminus truncated hSLC2A9 differs from the full length hSLC2A9 (hSLC2A9a) in 29 amino acids on the N-terminus, and hSLC2A9b has almost the same functional activity as hSLC2A9a when expressed in *Xenopus* oocytes. Moreover, we generated the full length hSLC2A9 computer model based on the hSLC2A1 crystal structure in our previous study; this study we created a hSLC2A9b model, also based on the hSLC2A1 crystal structure, to further explore the structure function relationship in hSLC2A9. We believed that understanding the relationship between the protein structure and substrate transport function of hSLC2A9b will allow us to comprehend how hSLC2A9 translocate urate, and to develop more specific pharmaceutical agents to treat abnormal urate condition in human.

Structure and function studies have been the major foci on the glucose transporters (hSLC2A) ever since the glucose transporter 1 (hSLC2A1) was

discovered. Seatter and his colleagues pointed out that a conserved QLS site is found in H7 in the glucose transporters hSLC2A1, 3, and 4, but not the fructose transporters hSLC2A2, 5, and 7 (141). Through cysteine scanning mutagenesis of hSLC2A1, Mueckler *et al.* (159, 163) discovered that residues like Gln282, Gln283, Ile287, Ala289, and Phe291 are within the aqueous environment of the substrate transporting pore. Mueckler *et al.* also suggested that Gln282 and Gln283 in H7 are the two essential sites for glucose binding because they form hydrogen bonds with the C1 position of glucose during transport process (144). Later, Manolescu *et al.* located a single hydrophobic residue, isoleucine/valine in H7 that is responsible for transport selectivity of fructose in class I and II hSLC2As (143, 144). Long *et al.* demonstrated that substitution of this isoleucine into valine in hSLC2A9 only affects fructose but not urate transport (145). Together with the hSLC2A9 computer model, they proposed that this isoleucine in H7 was involved in regulating the rigid body movement of one of the two six-helix bundles; thus, it affects the orientation of H7 in the translocation pore of the transporter. The new hSLC2A1 crystal structure implied that H7 plays a significant role in both protein structural regulation and substrate binding (170). The three potential glucose binding residues, Q282, Q283 and N288, were observed within the substrate bound crystal structure, and these residues correspond to the ones from the structure function studies proposed by Mueckler *et al.* (150, 158). However, only Q282/283 were shown to face the aqueous environment but not N288. All these suggest that H7 is necessary for substrate translocation in hSLC2As.

Although some early studies revealed that cysteine residues in glucose transporters might be important for hexose translocation in hSLC2A1 (175, 176, 326, 327), Due *et al.* (177) demonstrated that cysteine residues were not required for transport of 3-O-methylglucose. Until now, only a single cysteine residue, C429, on the exofacial side of the transporter was identified to be responsible for the inhibitory effect by the thiol-group-reactive reagent, p-Chloromercuribenzene sulfonic acid (pCMBS) (177). Thus far, no one has ever looked into the importance of cysteine residues in urate transport in hSLC2A9. Our hSLC2A9b model predicted that six out of eight cysteines, located within the transmembrane helix regions in hSLC2A9b, might be important for urate transport. Moreover, we discovered that pCMBS inhibited urate transport mediated by hSLC2A9b during both ^{14}C urate flux and two micro-electrode voltage clamp studies. These predictions allowed us to hypothesize that hSLC2A9 could have naturally occurring cysteine residue(s), which is facing the aqueous pore. This (these) cysteine residues could also be able to affect the accessibility of urate to the transporter during the transport process. We substituted five cysteine residues (C181, C297, C301, C398, C451) with the equivalent residues in hSLC2A5, one cysteine residue, C459, with leucine in hSLC2A11, and a double mutant C181T/C398A. Both functional results and computer model suggested that C297 and C451 are not required for urate transport; whereas both C181 and C398 are involved in urate translocation, and only C181 reacts with pCMBS. Mutation of either C301 and C459 decreased urate transport significantly. Our hSLC2A9b model illustrated that these two

residues are in close proximity between transmembrane helix 7 and 12; thus, we proposed that these two residues could plausibly have a disulfide interaction, which is critical for protein conformation in maintaining the tertiary structure for urate transport mediated by hSLC2A9.

In addition, we constructed a chimæric protein by replacing the H7 of the hSLC2A9b with that from hSLC2A5, and vice versa, to further examine the role of H7 in urate transport in hSLC2A9b. Experimental data of these chimæric proteins, and the double mutants G297C/S301C in $hSLC2A9_{(7)5}$, and triple mutant T171C/A388C/S441C in $hSLC2A5_{(7)9}$ divulged that H7 and the cysteine residues are necessary for urate transport in hSLC2A9b; however, they are not sufficient enough to allow $hSLC2A5_{(7)9}$ to gain urate transport.

The hSLC2A9b computer model was constructed based on the hSLC2A1 crystal structure. We also used this model to perform a urate docking study, which predicted that Y42, Y298, and N429 are the three possible binding sites for urate. We mutated two hSLC2A9 residues into the corresponding residues (Y298Q and N429H) that from hSLC2A5, and results indicated that urate transport was strongly reduced mediated by N429H without affecting fructose transport. Together with the docking analysis, these results permitted us to postulate that N429 is a possible urate binding site.

This study provides strong evidence that urate and fructose are translocated by hSLC2A9b through different pathways. All mutations constructed in this study do not affect fructose transport but have moderate to significant

influences on urate transport. With the novelty of the possible binding site and accessibility inhibition by pCMBS in hSLC2A9, we are one step closer to help scientists to develop more specific pharmaceutical agents for treating urate related diseases.

3.3. Experimental procedures

3.3.1. Plasmid construction – We received the original human wild type (WT) hSLC2A9b plasmid as a gift from Kelle Moley (School of Medicine, Washington University, USA), and we constructed it into pGEM-HE vector for oocyte expression. Site-directed mutagenesis was performed using the QuikChange II site-directed mutagenesis kit (Stratagene) to generate the point mutations (C181T, C297G, C301S, C398A, C451S, C459L of hSLC2A9b), double/triple mutations (C181T/C398A of hSLC2A9b, G297C/S301C of $hSLC29_{(7)5}$, and T171C/A388C/S441C of $hSLC2A5_{(7)9}$), and chimæra mutation $hSLC2A9_{(7)5}$ of the wild type hSLC2A9b and $hSLC2A5_{(7)9}$ of hSLC2A5. Fast cloning protocol was used in chimæra protein primer design (328). All primers are shown in **Table A.1**, **A.2** and **A.3**. The consequential plasmids were transformed *into Escherichia coli DH5α* competent cell for DNA propagation. DNA plasmids were sequenced by Macrogen (Maryland, USA) to ensure accuracy of the construction (**Fig. A.3**).

3.3.2. mRNA preparation & *Xenopus laevis* oocyte micro injection – mRNA preparation and microinjection were performed as previously described (145, 300). In short, wild type and mutant plasmids were lineraized

with *NheI* and transcribed *in vitro* with T7 polymerase mMESSAGE mMACHINETM (Ambion). *Xenopus laevis* oocytes were treated by collagenased and defoliculated procedures before injection (300). Then, oocytes were injected with 10-20 nL (20 ng) mutant plasmid mRNA and incubated in modified Barth's medium (MBM, 88 mM NaCl, 1 mM KCl, 0.33 mM $Ca(NO_3)_2$, 0.41 mM $CaCl_2$, 0.82 mM $MgSO_4$, 2.4 mM $NaHCO_3$, 10 mM Hepes, 2.5 mM sodium pyruvate, 0.1 mg/ml penicillin and 0.05 mg/ml gentamycin sulfate, pH 7.5) for 4 to 5 days at 16–18 °C prior to functional assays. All chemicals were obtained from Sigma-Aldrich (Oakville, Ontario, Canada) unless otherwise stated. Same amount of water was injected into oocytes (control) for control experiments. NanoDrop 1000 Spectrophotometer V3.7 (Thermo Fisher Scientific, USA) was used to determine the concentration of mRNA of all isoforms.

3.3.3 Radiotracer flux – Radiotracer flux studies were conducted at room temperature (RT) at 20-22^{o}C . ^{14}C labeled urate (8-^{14}C urate) (Moravek) and ^{14}C fructose [^{14}C-(U)] was used in flux studies. As previously described (73, 145), urate transport was measured by incubating oocytes with 200 µL urate solution ranging from (50 µM to 5 mM). Oocytes were incubated for 20 min, which was within the the linear range of urate uptake. Transport reaction was stopped by washed with ice cold MBM; then individual oocytes were placed into scintillation vial for quantitation of radioactivity by liquid scintillation counting. All radioactivities were measured by Beckman LS6500 liquid scintillation counter (Fullerton, CA, USA). Uptake activity was corrected by non-specific activities measured from control water injected oocytes. Prism5.0 software was used to

analyze the urate kinetics mediated by hSLC2A9b and all mutants mutant by non-linear regression analysis.

3.3.4. Electrophysiology experiments – Electrophysiology experiments were carried out by two-microelectrode voltage clamp (TEVC) technique with GeneClamp 500B (Molecular Devices Inc. Sunnyvale, CA, USA) (145). Sodium containing transport medium (STM, 100 mM NaCl, 2 mM KCl, 1 mM $CaCl_2$, 1 mM $MgCl_2$, 10 mM Hepes, pH 7.5 with Tris Base) was used to perfuse oocytes to obtain a current base line before adding experimental substrates. Urate-induced current (1 mM urate in STM) and urate kinetic analysis (urate concentration range from 0.05 mM to 5 mM in STM) was performed by using GAP-Free protocol (145). Data were expressed as urate-induced mean peak current. Current-voltage (I-V) curve were performed by RAMP protocol, in which voltage changed instantly from -120 to 60 mV for a 3-second period. Degidata 1320A converter and pClamp8 (Axon Instruments, Union City, CA) were used to attain and analyze data.

3.3.5. p-Chloromercuribenzene sulfonic acid (pCMBS) experiments – ^{14}C urate flux was used to screen the inhibition effect of pCMBS on WT hSLC2A9b and its cysteine mutants. Experiments were performed as previously described with modifications (154, 156). Briefly, oocytes expressing WT or mutant hSLC2A9b were incubated in of 100 μM pCMBS, or MBM for control, for one minute followed by three times washes with RT MBM. Both pCMBS treated oocytes and control oocytes were subjected to the 20 min

^{14}C urate flux assay to determine the amount of radioactivity oocytes had taken up.

Furthermore, we used the TEVC to reveal more properties of the pCMBS effect on WT hSLC2A9b and C181T. In the TEVC study, protein injected oocytes were perfused with 1mM urate followed by 1min STM wash; then pCMBS (range from 10 μM to 500 μM) was directly added to the oocyte holding chamber (extracellular solution) and incubate for 1 min. After that, pCMBS was washed out and continued being washed for 1 min to ensure all the pCMBS was clear. Finally, oocytes were perfused with 1mM urate containing STM buffer again to obtain the urate-induced current. Peak values of the urate-induced currents, before and after pCMBS treatments, were collected for comparison and IC_{50} calculation, which IC_{50} is the concentration of pCMBS that inhibits 50% of the urate-induced currents. Additional experiments were performed to distinguish whether urate will protect the pCMBS inhibition effect. Experiments are as follows: protein oocytes were perfused with 1 mM urate, when the urate-induced current reached its plateau, 100 μM pCMBS in 1 mM urate were adminstrated directly to the oocyte holding chamber and incubated for 1 min. Both urate and pCMBS were washed away by STM after incubation and continued for 1 min to ensure all urate and pCMBS were cleared out. Finally, oocytes were perfused again with 1 mM urate containing STM buffer to obtain urate-induced current. The peaks of the urate-induced currents were collected for data comparison.

3.3.6. Immunohistochemistry – Immunohistochemistry was used to determine relative protein levels at the *X. laevis* oocyte membrane. Oocytes were washed with Phosphate Buffer Saline (PBS; 137 mM NaCl, 2.78 mM KCl, 4.3 mM Na_2HPO_4, 1.5 mM KH_2PO_4, pH 7.4), then fixed in 3% paraformaldehyde (PFA) in PBS for 15 minutes at RT. After fixation, oocytes were washed with 50 mM NH_4Cl and permealbized with 0.1% Triton X-100. Oocytes were then blocked with 2% bovine serum albumin (BSA) for 30 minutes followed by incubation with primary hSLC2A9 anitibody (Cedarlane, Canada) in blocking buffer for 1 hour at RT, and then secondary antibody, rabbit anti goat conjugated to Alexa 488 (Invitrogen, USA). After incubation, oocytes were mounted using Vectashield mounting medium (Vector Laboratories, Inc. Burlingame, CA USA) on slides with secure-seal spacers. Protein expression was determined by Wave FX confocal microscopy (Quorum Technologies, ON, Canada) of the fluorescent secondary antibody.

3.3.7. Biotinylation – Protein expression was analysed using cell surface biotinylation followed by Western blot of each isoform based on a previously published protocol with modifications (145). Oocytes were washed three times with PBS (pH 8.0); then, they were incubated in 2 mM Sulfo-NHS-LC-Biotin (Pierce) in PBS at room temperature for 30 minutes. The reaction was stopped by washing with quenching buffer (192 mM Glycine and 25 mM Tris-HCl in PBS, pH 7.5). Oocytes were then lysed with RIPA buffer (150 mM NaCl, 1% Triton-X-100, 1% deoxycholic acid, 0.1% SDS, 1 mM EDTA, 10 mM Tris-HCl, pH 7.5).

Lysates were incubated with streptavidin agarose (Pierce) at 4^{o}C overnight. On the next day, beads with bounded protein were centrifuged at 3000 rpm. Biotinylated proteins were resuspended using SDS sample buffer and subjected to SDS-PAGE. Proteins from SDS-PAGE were transferred to nitrocellulose membranes and blocked with 3% skim milk in PBST (0.05% Tween 20 in PBS). After blocking, the membrane was probed with primary hSLC2A9 antibody (Cedarlane, Canada) and anti-rabbit secondary antibody (Abcam, Cambridge, MA, USA). Relative protein levels were determined measuring the band intensities using ImageJ (http://imagej.nih.gov/ij/).

3.3.8. Data analysis – Protein amino acid sequence alignments were performed using Clustal OMEGA (http://www.ebi.ac.uk/Tools/msa/clustalo/). Graphpad 5.0 was used to analyze all the data. Urate kinetic data were fitted using non-linear regression. Current-voltage (I-V) curves were graphed using X-Y plots. Fructose flux studies, pCMBS inhibition experiment and protein expression data were analyzed by One-way ANOVA for the flux studies and Student unpaired t-test in TEVC studies. Values were considered significant when $p<0.05$. Cell surface biotinylation of protein was detected by Western blot and the protein band intensity was analyzed by ImageJ. Data were expressed as percentage of biotinylation protein to the total expressing protein (designated as 100%) .

3.4. Results

3.4.1. Search of cysteine residues in hSLC2As sequences and in hSLC2A9b homology computer model

Multiple amino acid sequence alignments showed that the Class I glucose transporters (hSLC2A1-4) have only four to six cysteine residues in their entire sequences (**Fig. A.2**), and not all of these cysteines are present in the transmembrane helices (Hs). Class II glucose transporters, on the other hand, have more than six cysteine residues, and many of these cysteines are present in the TMs. hSLC2A9b, for example, has eight cysteines in its amino acid sequence, and they all distribute to various location within transmembrane helices.

Our hSLC2A9b computer model was constructed based on the crystal structure of hSLC2A1 (**Fig. 3.1A**). This model shows very similar features as the full length hSLC2A9 model, which we recently reported. This model predicts six cysteine residues might be involved in urate transport and that C181 and C398 locate close to the aqueous pore of the protein transporter (**Fig. 3.1B**). C297 and C301 in H7 are facing away from the aqueous pore; however, these two cysteines are facing another two cysteine residues, C451 and C459 in H12. In particular, the model predicted that C301 and C459 are very close to each other (**Fig. 3.1C**).

3.4.2. Roles of cysteine residues in hSLC2A9

Shown in **Fig. 3.2E**, ^{14}C fructose flux experiments were performed as control experiments to ensure that all cysteine mutants are functional and all isoforms transported fructose similarly to WT hSLC2A9b (One-way ANOVA, * $p<0.05$).

Urate kinetics - Flux studies. Urate transport kinetics for both WT hSLC2A9b and its cysteine mutants were fully characterized. Showing in **Fig. 3.2A**, both wild type hSLC2A9 and its mutants exhibited Michaelis-Menten type kinetics for urate transport. However, urate transport activities varied among the cysteine mutants. **Fig. 3.2A & 2B**. point out that urate transport kinetics are similar among WT, C297G and C451S; whereas higher urate affinity and lower urate carrying capacity (lower K_M and V_{MAX} values) were seen in C181T, C398A, and double mutant C181T/C398A comparing to WT. On the other hand, urate transport activities were dramatically reduced in C301S and C459L. Signified in the **Fig. 3.3.1B**, the V_{MAX} values of both C301S and C459L are 50 to 20-times lower compared to WT, respectively; this indicated that both mutants have much lower urate carrying capacity compared to WT. The K_M values of both C301S and C459L are 10-times and 5-times lower than WT, respectively; this indicate that both mutants have very high affinity for urate binding compared to WT. (WT hSLC2A9b has an average V_{MAX} of 1122.0 ± 388.5 pmol/oocyte/20 min with a K_M of 6.6 ± 3.7 mM; C181T has a V_{MAX} of 244.5 ± 53.3 pmol/oocyte/20 min, K_M of 5.2 ± 1.9 mM; C297G has an average V_{MAX} of 493.6 ± 70.4 pmol/oocyte/20 min, K_M of 2.0 ± 0.6 mM; and C301S has an average V_{MAX} of 21.1 ± 5.7 pmol/oocyte/20 min,

K_M of 0.7 ± 0.5 mM; C398A has an average V_{MAX} of 178.8 ± 22.9 pmol/oocyte/20 min, K_M of 1.5 ± 0.5 mM; C451S has an average V_{MAX} of 457.8 ± 78.6 pmol/oocyte/20 min, K_M of 1.5 ± 0.6 mM; C459L has an average V_{MAX} of 43.1 ± 7.8 pmol/oocyte/20 min, K_M of 1.3 ± 0.6 mM; C181T/C3998A has an average V_{MAX} of 219.9 ± 21.1 pmol/oocyte/20 min, K_M of 1.7 ± 0.4 mM).

Two-Electrode Voltage Clamp Experiments (TEVC) - Due to urate transport mediated by hSLC2A9 is electrogenic (73, 145, 300), in addition to the flux studies, we used the Two-Electrode Voltage Clamp (TEVC) method to further examine the abilities of urate transport by hSLC2A9 and its cysteine mutants. We clamped a single oocyte at a holding potential of -30 mV, then perfused the oocyte with different concentrations of urate followed by one-minute wash with STM. We then measured the mean of the induced outward current. Data were collected at the peak of each urate-induced current. Shown in **Fig. 3.2C and 2D**, urate kinetics are similar in both TEVC and flux studies. Again, urate transport kinetics are similar among WT hSLC2A9, C297G and C451S. On the contrary, higher urate affinity and lower urate carrying capacity (lower K_M and V_{MAX} values) were seen in C181T, C398A, and double mutant C181T/C398A compared to WT. Interestingly, urate-induced currents were dramatically reduced in both C301S and C459L. However, only C301S had more than 10 times lower K_M and almost 50 times lower V_{MAX} compared to WT; whereas C459L has similar K_M but very low V_{MAX} (400 times reduced) compared to WT. Therefore, C301S has very low urate capacity and very high urate affinty during the transport; whereas the urate affinity of C459L is similar to WT but the urate capacity is very low in the C459L

when compared to WT. (WT hSLC2A9b has an average V_{MAX} of 425.63.0 ± 57.0 nA with a K_M of 3.0 ± 0.8 mM; C181T has a V_{MAX} of 191.7 ± 16.7 nA, K_M of 2.0 ± 0.4 mM; C297G has an average V_{MAX} of 311.4 ± 38.6 nA in, K_M of 2.0 ± 0.6 mM; and C301S has an average V_{MAX} of 11.2 ± 0.8 nA, K_M of 0.2 ± 0.1 mM; C398A has an average V_{MAX} of 143.4 ± 9.0 nA, K_M of 1.2 ± 0.2 mM; C451S has an average V_{MAX} of 313.1 ± 29.0 nA, K_M of 1.1 ± 0.3 mM; C459L has an average V_{MAX} of 1.6 ± 1.0 nA, K_M of 1.2 ± 2.4 mM; C181T/C3998A has an average V_{MAX} of 222.2 ± 12.4 nA, K_M of 2.6 ± 0.3 mM).

3.4.3. Inhibition effect of p-Chloromercuribenzenesulfonic acid (pCMBS) on hSLC2A9b

For the first time, we discovered that urate transport mediated by hSLC2A9 is inhibited by a compound known as p-Chloromercuribenzenesulfonic acid (pCMBS). This pCMBS is a sulfhydryl reagent, and it will react with the sulfhydryl group of the cysteine residues, when it is facing the aqueous environment of the protein transporter. Illustrated in **Fig. 3.3A**, we screen the inhibition effect of pCMBS on all the cysteine mutants on hSLC2A9b in both flux and TEVC studies, only C181T and the double mutant C181T/C398A become insensitive to the pCMBS inhibition; all other cysteine mutants showed similar activities as WT hSLC2A9 (unpaired t-test, * $p<0.05$). After, this dose dependent inhibition of hSLC2A9b and C181T by pCMBS was dtermined. **Fig. 3.3B & 3C** demonstrate an inhibition curve that urate-induced current reduces as the concentration of pCMBS increased, and the urate-induced current by WT hSLC2A9b was abolished completely after incubate with 500 μM pCMBS. The

IC_{50} of hSLC2A9b equals 52.5 μM, which reveals that only 52.5 μM pCMBS can inhibit 50% of the urate transport activity of hSLC2A9. On the other hand, the IC_{50} of C181T equals 110.2 μM, which indicates that it requires twice the concentration of pCMBS to inhibit 50% of the urate-induced current. Two representative traces shown in **Fig. 3.3D and 3E** are from single hSLC2A9b protein expressing (upper) and water injected (lower) oocyte clamping at -30 mV. Both protein expressing oocyte and the water injected control oocytes were perfused with 1 mM urate followed by 1 min 100 μM pCMBS incubation in either presence (**Fig. 3.3D**) or absence (**Fig. 3.3E**) of urate. This first peak of the traces was induced by perfusing the oocyte with 1 mM urate before pCMBS treatment; the second peak was obtained also by perfused the same oocyte with 1 mM urate after pCMBS incubation. These results illustrated that urate-induced currents were significantly larger when there was urate present during the pCMBS incubation. Experimental data is shown in **Fig. 3.3F** that urate-induced currents have a higher percentage of recovery after incubation with both urate and pCMBS when compared to the one incubated with only pCMBS. This is true for both WT hSLC2A9b and C181T mutant (One-way ANOVA, * $p<0.05$). Consquently, these experiments disclosed that the pCMBS inhibition effect is protected by the presence of urate; thus, we postulated that urate is competing with pCMBS at the same substrate access site.

3.4.4. Urate/fructose transport in hSLC2A9$_{(7)5}$ chimæric proteins

We tested our hypothesis by replacing the transmembrane helix 7 of hSLC2A9 with that from hSLC2A5. This is because hSLC2A9 has the highest

homology sequence similarity with hSLC2A5 among all glucose transporters. In addition, both transporters are fructose transporters. Therefore, fructose uptake can serve as an internal control experiment to ensure that our chimæric protein construction is functionally suitable for further investigation.

^{14}C Fructose flux experiments were performed as control experiments to ensure the chimæric protein and its double cysteine mutants are functional.All three isoforms transported fructose with similar uptake activities (**Fig. 3.4A**) (One-way ANOVA, * $p<0.05$). Both the ^{14}C urate flux study (**Fig. 3.4B & 4C**) and TEVC study (**Fig. 3.4D & 4E**) showed that urate transport activities were completely eradicated in $hSLC2A9_{(7)5}$ chimæric protein. Urate kinetics mediated by the chimæric protein $hSLC2A9_{(7)5}$ has very low V_{max} and K_M compared to the hSLC2A9b. In the flux study, WT has a V_{MAX} of 1122.0 ± 388.5 pmol/oocyte/20 min with a K_M of 6.6 $\pm$ 3.7 mM; $hSLC2A9_{(7)5}$ had a V_{MAX} of 11.0 $\pm$ 0.9 pmol/oocyte/20 min with a K_M of 1.1 $\pm$ 0.3 mM. In the TEVC study, $hSLC2A9_{(7)5}$ has an average V_{MAX} of 14.4 $\pm$ 1.4 nA with a K_M of 1.1 ± 0.3 mM. These results allowed us to conclude that chimæra protein $hSLC2A9_{(7)5}$ has extremely high affinity and low capacity during urate transport compared to WT.

Nevertheless, we mutated two cysteine residues back to the $hSLC2A9_{(7)5}$ chimæra in H7, G297C and S301C. We would like to see whether these two cysteines will allow us to gain the urate transport function back. we performed a ^{14}C fructose flux study to ensure $hSLC2A9_{(7)5}$ G297C/S301C is functional (**Figure 3.A**) (One-way ANOVA, * $p<0.05$). Both ^{14}C urate flux study (**Fig. 3.4B & 4C**) and

TEVC study (**Fig. 3.4D & 4E**) showed that urate transport activities were partially recovered after we mutated the two cysteine residues back to the chimæra. hSCL2A9$_{(7)5}$ G297C/S301C has a V_{MAX} of 419.2 ± 95.7 pmol/oocyte/20 min, K_M of 2.3 ± 1.1 mM. In the TEVC study, hSCL2A9$_{(7)5}$ G297C/S301C has a V_{MAX} of 90.6 ± 21.1 nA, K_M of 5.2 ± 1.9 mM.This indicated that the two cysteine residues are essential in H7 of hSLC2A9, but not sufficient to bring back the full urate transport activity.

3.4.5. Urate/fructose transport in hSLC2A5$_{(7)9}$ chimæric proteins

We substituted transmembrane helix 7 of hSLC2A5 with that from hSLC2A9b, and we mutated three amino acid residues in hSLC2A5 into cysteines, in which these residues are corresponding to the similar position as three important cysteine residues in hSLC2A9b. ^{14}C fructose flux studies showed that all hSLC2A5 isoforms transport fructose indistinguishably (**Fig. 3.5A**) (One-way ANOVA, * $p<0.05$). However, when we perform the time course of urate uptake mediated by hSLC2A5 and its chimæra hSLC2A5$_{(7)9}$ and chimæra mutant hSLC2A5$_{(7)9}$ T171C/A388C/S441C, none of them showed significant urate uptake compare to hSLC2A9b (**Fig. 3.5B**). Consequently, we concluded that the H7 alone is insufficient to turn hSLC2A5 into a urate transport. Together with the important corresponding cysteine residues from hSLC2A9b, the hSLC2A5$_{(7)9}$ T171C/A388C/S441C was still unable to gain urate transport activity.

3.4.6. Urate docking and the possible binding sites

The urate docking study predicted three possible amino acids that could responsible for the urate binding site (s) in hSLC2A9b (**Fig. 3.6**). Two out of

these three are different from the corresponding residues in hSLC2A5, they are Y298 and N429. We mutate these two residues into the residues corresponding to those from hSLC2A5, Y298Q and N429H. Both ^{14}C urate flux and TEVC studies indicated that Y298Q transport urate similarly as hSLC2A9b, whereas N429H has a low V_{MAX} and very low K_M value compared to WT hSLC2A9b (**Fig. 3.7A, 7B, 7C, & 7D**). This specified that N429H has a very high affinity and low capacity for urate. Additionally, we examined the protein function using current-voltage (I-V) curves, which was subected to a RAMP protocol. I-V curves were RAMP at the peak of the urate-induced currents (**Fig. 3.7E**). Similar to our findings in full length hSLC2A9, urate transport mediated by hSLC2A9b showed a quasi-linear relationship with the membrane potential in the voltage range from -120 to 60 mV, indicating that urate transport is driven by the membrane voltage (**Fig. 3.7E**). The I-V curves of WT hSLC2A9b and Y298Q are similar; however, the I-V curve of N429H indicates that urate-induced current is significantly smaller than WT similar to the urate kinetics analysis. Furthermore, both Y298Q and N429H have comparable fructose transport activities to WT hSLC2A9b (**Fig. 3.7F**) (One-way ANOVA, * $p<0.05$).

3.4.7. Determination of protein expression level of hSLC2A9b, hSLC2A5, and their mutants in *Xenopus* oocytes

Protein express level of all isoforms, WT hSLC2A9b, its cysteine mutants and chimæric protein, and WT hSLC2A5 and its chimæric protein and cysteine mutants, were confirmed by immunohistochemistry and biotinylation. As indicated in the confocal imagines in **Fig. 3.8A, 3.8B** and **3.8C**, all protein expressed on

the oocyte membranes; whereas water injected oocytes showed no detectable expressing protein (n=3). Moreover, biotinylation and Western blot were applied to quantitatively detect the membrane expressing proteins. Shown in **Fig. 3.8D**, protein expression levels are comparable in all hSLC2A9b isoforms, WT, its cysteine mutants and chimæric protein $hSLC2A9_{(7)5}$ and $hSLC2A9_{(7)5}$ G297C/S301C. The membrane protein expression levels are all proportional to their total protein levels. (n≥3, One-way ANOVA, p >0.05). On the other hand, biotinylated protein of hSLC2A5 and its $hSLC2A5_{(7)9}$ and cysteine mutant $hSLC2A9_{(7)5}$ T171C/A388C/S441C showed very thin bands on the Western blot membrane, and total protein and unbound protein were clearly indicated on the membrane comparing to the biotinylated protein..

3.5. Discussion

3.5.1. Roles of the cysteine residues

This is a novel study that we are the first group examining the critical roles of the cysteine residues in glucose transporter 9 (hSLC2A9). Since hSLC2A1 has very few cysteinine residues present in its transmembrane helices, cysteine mutagenesis scanning was well known in screening the aqueous pore facing residues in hSLC2A1 (144, 149, 159). Through multiple sequence alignments (**Fig. A.2**), we noticed that Class I glucose transporters (hSLC2A1, 2, 3 & 4) have no more than six cysteine residues in their sequences (175). hSLC2A1 has only four cysteine present in TMs, whereas, hSLC2A4 has no cysteine in any of the TMs. Though Wellner *et al.* (329) reported that mutation of all the cysteine residues in the C-terminal half of hSLC2A1 caused a moderate reduction in 2-

deox-d-glucose uptake, Due *et al.* (177) demonstrated that cysteine-less hSLC2A1 transports 3-o-methylglucose similarly to WT hSLC2A1. Conversely, Class II glucose transporters have more than eight cysteines in their sequences, and most of the cysteines presented in the TMs. hSLC2A9b, for example, has eight cysteines and all eight of them present in TMs. Our new hSLC2A9b computer model predicted that six of these cysteine might be important in substrate translocation.

Functional studies showed that C297 and C451 were not required for urate transport in hSLC2A9b. However, C181T, C398A and the double mutants C181T/C398A have reduced urate transport activities compared to WT. This disclosed that C181 and C398 are functionally important. However, the urate transport activity behaves like the two single mutants indicating that these two cysteines do not have direct interaction between each other. Furthermore, C181T was the only cysteine mutant found responsible for the pCMBS inhibition effect. It became insensitive to pCMBS when we mutated this cysteine 181 into threonine, suggesting that C181 has a SH- group, which can react with the thiol-group-reactive reagent, facing the aqueous environment of the transport pore of the protein. This is also validated by our computer model (**Fig. 3.1B**). Cysteine residues in other transporters, like equilibrative nucleoside transporter (ENT) and concentrative nucleoside transporter (CNT) proteins, were also reported in the transport channel (330–332). For instance, a single cysteine, C140, was located within the substrate translocation channel in rat ENT2, where it reacted with pCMBS (330). Moreover, cysteines in human ENT1 were reported responsible

for inhibitor binding and substrate transport function. Although C398 was also predicted as a cysteine residue within the aqueous surroundings, functional study supported that its SH- group is not facing the aqueous pore; instead, it is actually facing away from the pore towards other side chains (**Fig. 3.1B**).

Either C301S or C459L mutant lost most of the urate transport ability with very low urate carrying capacity and high affinity. Cysteine is well known to maintain protein structures and conformations by forming disulfide bridges (333–335). The hSLC2A9b computer model recommended that these two cysteines are very close to each other between H7 and H12, suggesting a plausible disulfide interaction could form between them. Hence, this tight interaction was lost when one of these two cysteines was mutated to the other amino acid; thus, changes the TMs orientations and protein conformation. Another possible explanation is that the difulside interaction helps to bring in other residues close to each other, such as the hydrophobic residues, within the membrane to tightly hold the helices of the protein in a proper conformation; therefore, the protein can function properly (168, 196, 333). In parallel to this assumption, our previous study pointed out that a hydrophobic residue, isoleucine 335 in H7 in hSLC2A9, was forming hydrophobic interactions with other hydrophobic residues on the other side of the TMs, resulting in a protein rigid body; hence, it allows to the protein to translocate both urate and fructose (145). However, future study with purified hSLC2A9 protein is needed to determine the formation of the disulfide bridges between the two cysteine residues, C301 and C459.

3.5.2. Roles of H7 in urate transport in hSLC2A9

More interestingly, we constructed two chimæra proteins, hSLC2A9$_{(7)5}$ and hSLC2A5$_{(7)9}$, to examine the role of the H7 of hSLC2A9b in urate transport. Our results pointed out that replacement H7 of hSLC2A9b with that from hSLC2A5 cause a substantial loss of urate transport in the chimæric protein hSLC2A9$_{(7)5}$. This enlightened us that H7 is necessary for urate transport. However, substitution of H7 of hSLC2A5 with that from hSLC2A9b did not allow the chimæric protein hSLC2A5$_{(7)9}$ to gain any urate transport. This explained that H7 alone is not sufficient to bring urate transport into other glucose transporter, like hSLC2A5. Other TMs must be involved in urate transport in hSLC2A9b.

With the substitution of cysteine residues back to the H7 in chimæric protein, the hSLC2A9$_{(7)5}$ was able to recover partial but not all urate transport. This provides further support that cysteines in H7 are essential for the protein to transport urate. However, other residues are also important for full recovery of the transport activity. Besides, when we replaced the residues,T171/A388/S441, in the hSLC2A5$_{(7)9}$ protein into corresponding cysteine from hSLC2A9b, the chimæric protein, together with the three cysteine residues still did not gain any urate function. All these guided us to conclude that both H7 and cysteine residues are critical in urate transport in hSLC2A9b; yet, they are not sufficient to bring urate transport into hSLC2A5, and other helices and residues must be also crucial in regulating protein structur and urate binding. Therefore, these other helices and residues are also important in regulating the urate transport in hSLC2A9.

3.5.3. Asparagine 429 (N429) as part of the possilbe binding site

Our substrate docking study predicted that three amino residues, Y42, Y298, N429, are involved in urate binding in hSLC2A9b. Our functional data stated that Y298Q transport urate similarly as WT hSLC2A9b, whereas N429H had a strongly reduced urate transport compared to the WT. Together with the urate docking study, we postulate that N429 is the one (one of) the long-sought residue(s) for urate binding. Another hSLC2A9 computer model based on XylE suggested another asparagine, N433 (N462 in full length hSLC2A9), as the possible binding site for urate (168). This N433 is very close to the one (N429) we predicted with our model. This further confirms that asparagine is important for urate transport in hSLC2A9. However, additional experiments are need to determine whether both asparagines are equally important or only the one we predicted is more crucial.

In summary, this study illustrated three critical cysteine residues (C181, C301 and C459) and a plausible binding site (N429) of hSLC2A9b are crucial in urate transport accessibility, protein regulation and substrate binding. Despite some mutants of hSLC2A9b lost urate transport activities, all mutants can transport fructose. This result provided additional evidence to our previous studies that urate and fructose were transported through different pathways by hSLC2A9. The inability to bring urate transport into the hSLC2A5 with both H7 and the cysteine residues from hSLC2A9b leads us to a future question: What is/are other TM(s) or residue(s) might also be essential for urate transport by hSLC2A9? Also, we noticed that, from the multiple sequence alignments (**Fig.**

A.2), the Class II glucose transporters have many cysteines presenting in their TMs, hSLC2A11 has 16 cysteine and 12 of them are within its TMs. It will be very interesting to further explore what are the actual substrates mediated by these transporters, and what are the roles of the cysteines involved in these substrates transport process. Future crystallization of hSLC2A9 is also needed to further unveil the structure function relationship between the transport substrates and the protein transporter. With further comprehensive knowledge of substrate binding sites and protein structure of hSLC2A9, we could advance our research in providing a pharmacological basis for effective drugs/treatments of unusual serum urate level and other related diseases, such as gout, hypertension and diabetes.

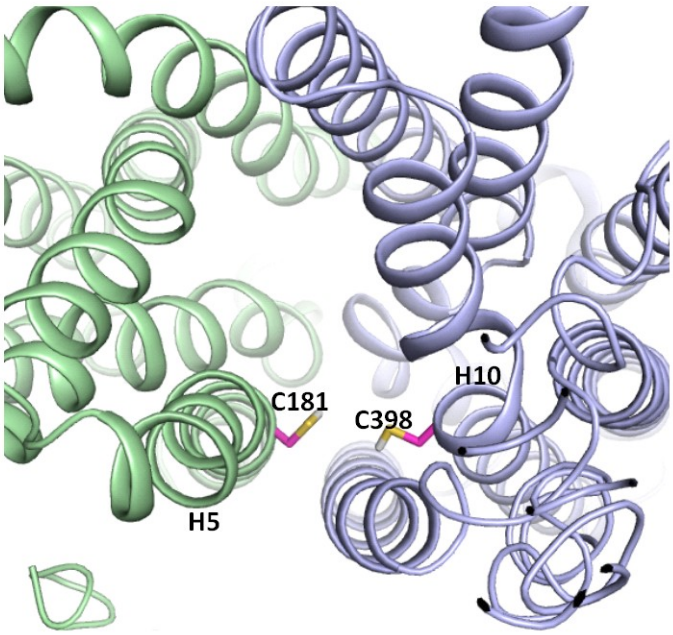

A

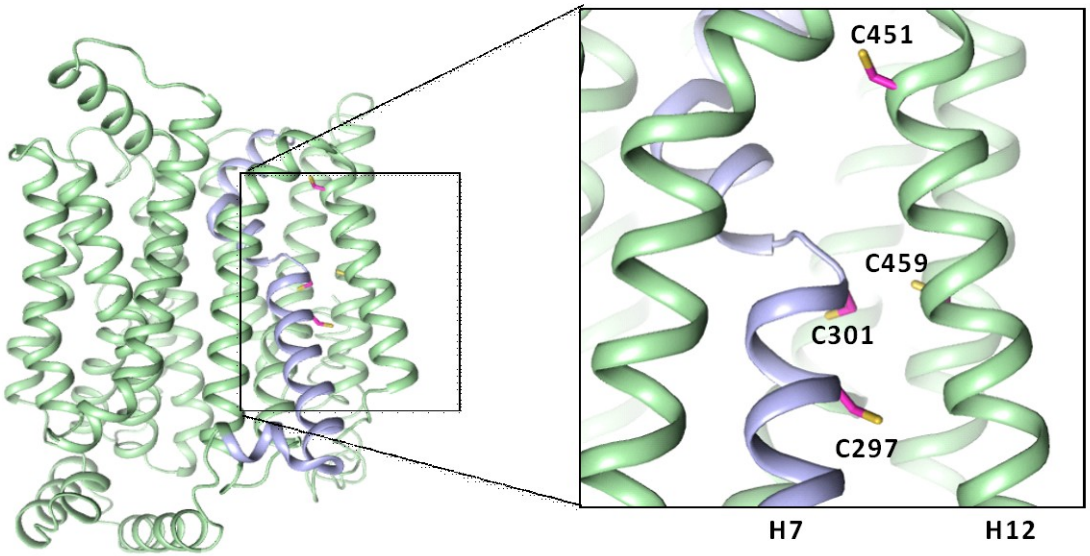

B

Figure 3.1. Molecular model of the human SLC2A9b with predicted locations of cysteine residues.

Panel A. View from the intracellular side of the inward faicing comformation hSLC2A9b. Transmembrane helix 5 and 10 were labelled to indicated two predicted cysteines, C181 and C398, located within the aqueous translocation pore. **Panels B.** Side views of hSLC2A9b. The intracellular face contains the conserved intracellular helical bundle. Predicted cysteine residues C297, C301 in H7, C451 and C459 in H12 were labelled. Potential interactions of C301 to C459. Cartoon representation of the molecular homology model from the extracellular face of the hSLC2A9b based on the human SLC2A1 crystal structure (4PYP.pdb).

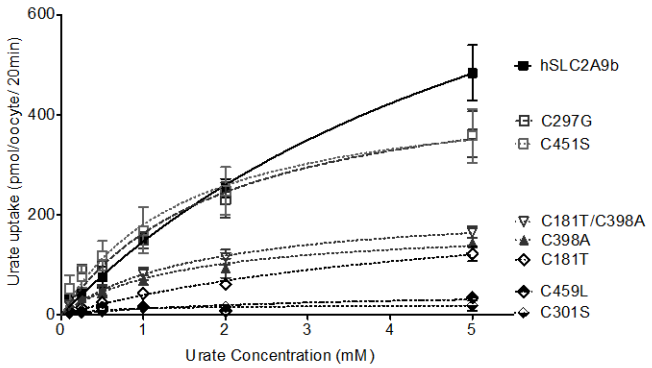

A

B

	hSLC2A9b	C181T	C297G	C301S	C398A	C451S	C459L	C181T/C398A
$K_{M\ (mM)}$	6.6	5.2	2.0	0.7	1.5	1.5	1.3	1.7
SEM	3.7	1.9	0.6	0.5	0.5	0.6	0.6	0.4
V_{MAX} (pmol/oocyte/20 min)	1122.0	244.5	493.6	21.1	178.8	457.8	43.1	219.9
SEM	388.0	53.3	70.4	5.7	22.9	78.6	7.8	21.1

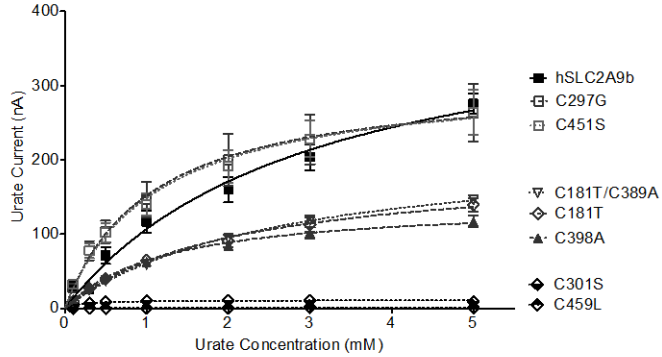

C

D

	hSLC2A9b	C181T	C297G	C301S	C398A	C451S	C459L	C181T/C389A
$K_{M\ (mM)}$	3.0	2.0	1.0	0.2	1.2	1.1	1.2	2.6
SEM	0.8	0.4	0.4	0.1	0.2	0.3	2.4	0.3
$V_{MAX\ (nA)}$	425.6	191.7	311.4	11.2	143.4	313.1	1.6	222.2
SEM	57.0	16.7	38.6	0.8	9.0	29.0	1.0	12.4

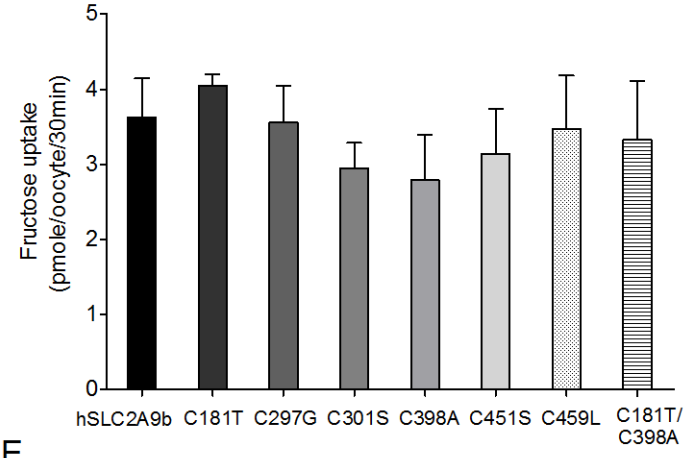

E

Figure 3. 2. Urate and fructose transport mediated by WT hSLC2A9b and its cysteine mutants.

Panel A. Michaelis-Menten curves of ^{14}C urate kinetics of hSLC2A9 WT (■) and its mutants C297G (□), C451S (□), C181T (◊), C398A (▲), double mutant C181T/C398A (▽), C301S (◆), and C459L (◆). Urate uptake was measured by incubating protein expressing oocytes in 200 µL urate solution ranged from 100 µM to 5 mM for 20 minutes. Uptake activity was corrected for non-specific transport measured in control water injected oocytes from the same batch of oocytes. **Panel B.** ^{14}C urate kinetic constants of the 3 isoforms (n ≥3). **Panel C.** Michaelis-Menten curves of urate-induced currents of WT hSLC2A9b and its cysteine mutants. Currents were measured by Two Micro-electrode Voltage Clamp (TEVC). Data were collected at the peak of each urate-induced current. Points represent the mean of urate-induced peak outward current for each urate concentration. **Panel D.** Urate-induced current kinetic constants of the WT and cysteine mutants (n ≥15 oocytes from 3 frogs). **Panel E.** ^{14}C fructose uptake mediated by WT hSLC2A9b and its cysteine mutants. Urate uptake was measured by incubating protein expressing oocytes in 200 µL 100 µM fructose solution for 20 minutes. Bar graphs represent fructose uptake activities, which were corrected for non-specific transport measured in control water injected oocytes from the same batch of oocytes (n≥3, One-way ANOVA, * $p<0.05$).

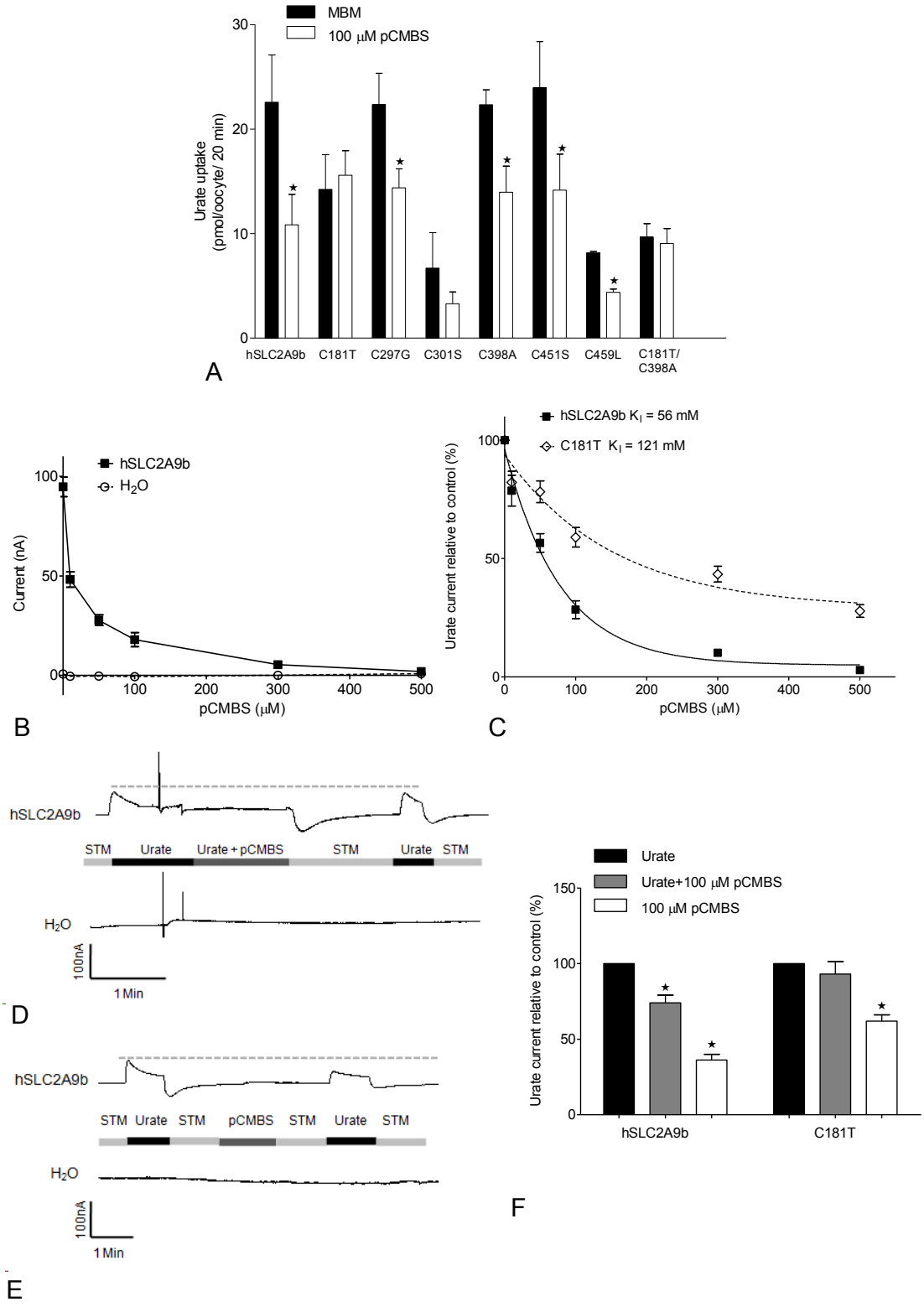
MBM
100 μM pCMBS
Urate uptake (pmol/oocyte/ 20 min)
hSLC2A9b
C181T
C297G
C301S
C398A
C451S
C459L
C181T/ C398A
A
hSLC2A9b
H2O
Current (nA)
pCMBS (μM)
B
hSLC2A9b KI = 56 mM
C181T KI = 121 mM
Urate current relative to control (%)
pCMBS (μM)
C
hSLC2A9b
STM
Urate
Urate + pCMBS
STM
Urate
STM
H2O
100nA
1 Min
D
hSLC2A9b
STM
Urate
STM
pCMBS
STM
Urate
STM
H2O
100nA
1 Min
E
Urate
Urate+100 μM pCMBS
100 μM pCMBS
Urate current relative to control (%)
hSLC2A9b
C181T
F

Figure 3. 3. pCMBS inhibition experiments.

Panel A. pCMBS screening in ^{14}C urate uptake mediated by WT hSLC2A9b and its cysteine mutants. Bar graphs represent 100 µM urate uptake activities before (dark) and after (white) 100 µM pCMBS treatments to the protein expressing oocytes. Data was corrected for non-specific transport measured in control water injected oocytes from the same batch of oocytes (n≥3, unpaired t-test, * $p<0.05$). **Panel B.** pCMBS inhibition curves of urate-induced currents of WT hSLC2A9b (■) expressing and control water injected (○) oocytes (n ≥15 oocytes from 3 frogs). **Panel C.** pCMBS inhibition curves of urate-induced current of WT hSLC2A9b (■) and C181T (◊) protein expressing oocytes. Data were corrected with control currents that before the pCMBS treatments. IC_{50} is the pCMBS concentration that required to inhibit 50% of the urate-induced current (n ≥15 oocytes from 3 frogs). **Panel D.** Representative trace of urate protecting pCMBS inhibition. Urate-induced current was elicited by perfused either the WT hSLC2A9b (upper trace) or water injected (lower trace) oocyte with 1 mM urate (first urate-induced peak) followed by 1 min 100 µM pCMBS incubation; oocyte then was washed with STM for at least 1 min to remove both extracellular pCMBS and urate; finally, oocyte was perfused with 1 mM urate again (second urate-induced peak). **Panel E.** Representative trace of unpaired control experiments for urate protecting pCMBS inhibition. Urate-induced current was elicited by perfused either the WT hSLC2A9b (upper trace) or water injected (lower trace) oocyte with 1 mM urate (first urate-induced peak) followed by 1 min washed with STM to remove urate; oocyte was then incubated in 100 µM pCMBS for 1 min. Finally, oocytes were washed by STM and perfused with 1 mM urate again (second urate-induced peak). **Panel F.** Urate protecting pCMBS inhibition experiments of WT hSLC2A9b and C181T. Bar graphs are data corrected to control (first peak of urate-induced current before pCMBS treatment) current with dark is the control current, grey is the current after oocyte was incubate in both 1 mM urate and 100 µM pCMBS, and white is the current after oocyte was incubate in only 100 µM pCMBS (n ≥15 oocytes from 3 frogs, One-way ANOVA, * $p<0.05$).

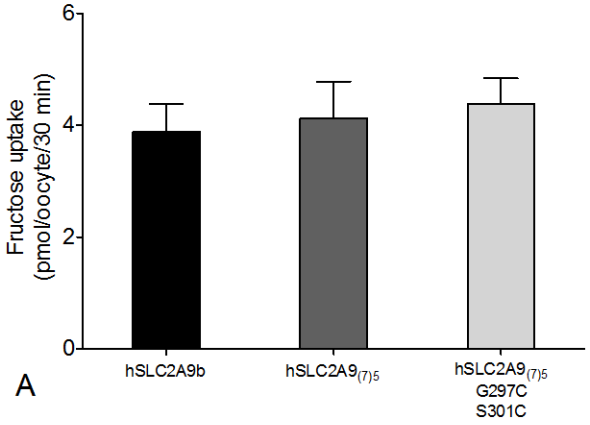

A

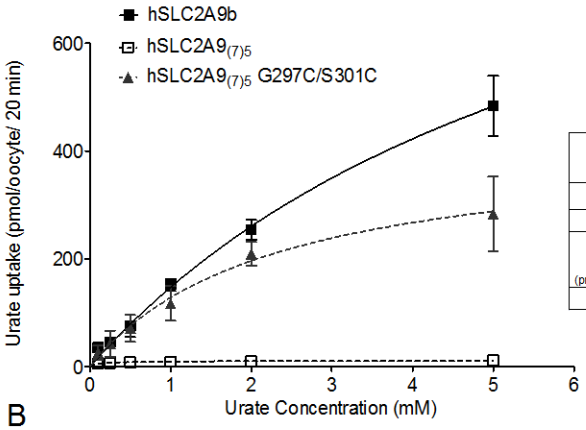

B

	hSLC2A9b	hSLC2A9$_{(7)5}$	hSLC2A9$_{(7)5}$ G297C/S301C
$K_{M\ (mM)}$	6.6	0.1	2.3
SEM	3.7	0.1	1.1
V_{MAX} (pmol/oocyte/20 min)	1122.0	11.0	419.2
SEM	388.0	0.9	95.7

C

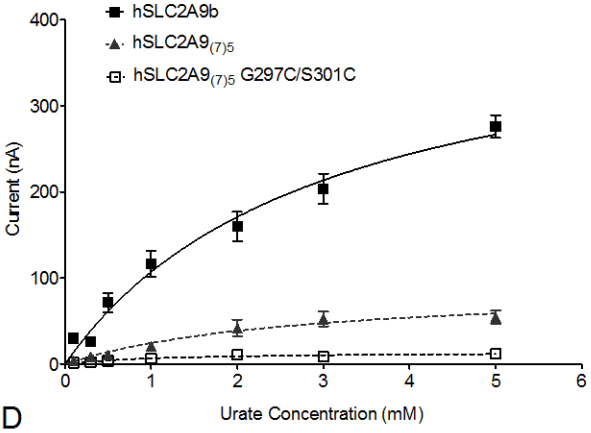

D

	hSLC2A9b	hSLC2A9$_{(7)5}$	hSLC2A9$_{(7)5}$ G297C/S301C
$K_{M\ (mM)}$	3.0	1.1	2.6
SEM	0.8	0.3	1.2
$V_{MAX\ (nA)}$	425.6	14.4	90.6
SEM	57.0	1.4	21.1

E

Figure 3. 4. Fructose and urate transport mediated by WT hSLC2A9b, its chimæra hSLC2A9$_{(7)5}$ and hSLC2A9$_{(7)5}$ G297C/S301C.

Panel A. ^{14}C fructose uptake mediated by WT hSLC2A9b and its chimæric mutants. Urate uptake was measured by incubating protein expressing oocytes in 200 µL 100 µM fructose solution for 20 minutes. Bar graphs represent fructose uptake activities, which were corrected for non-specific transport measured in control water injected oocytes from the same batch of oocytes (n≥3, One-way ANOVA, * $p<0.05$). Panel B. Michaelis-Menten curves of ^{14}C urate kinetics of hSLC2A9 WT (■), its chimæric hSLC2A9$_{(7)5}$ (□) , and hSLC2A9$_{(7)5}$ G297C/S301C (▲). Urate uptake was measured by incubating protein expressing oocytes in 200 µL urate solution ranged from 100 µM to 5 mM for 20 minutes. Uptake activity was corrected for non-specific transport measured in control water injected oocytes from the same batch of oocytes. **Panel C.** ^{14}C urate kinetic constants of the 3 isoforms (n ≥3). **Panel D.** Michaelis-Menten curves of urate-induced currents of WT hSLC2A9b and its chimæric mutants. Currents were measured by Two Micro-electrode Voltage Clamp (TEVC). Data were collected at the peak of each urate-induced current. Points represent the mean of urate-induced peak outward current for each urate concentration. **Panel E.** Urate-induced current kinetic constants of the WT and its chimæric mutants (n ≥15 oocytes from 3 frogs).

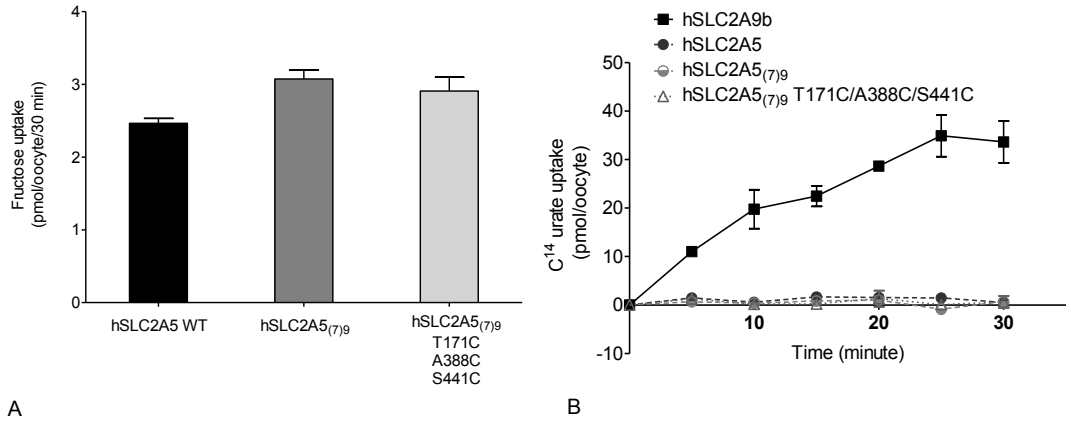

Figure 3. 5. Fructose and urate transport mediated by WT hSLC2A5, its chimæra hSLC2A5(7)9 and hSLC2A5(7)9 T171C/A388C/S441C.

Panel A. ^{14}C fructose uptake mediated by WT hSLC2A5 and its chimæric mutants. Urate uptake was measured by incubating protein expressing oocytes in 200 µL 100 µM fructose solution for 20 minutes. Bar graphs represent fructose uptake activities, which were corrected for non-specific transport measured in control water injected oocytes from the same batch of oocytes (n≥3, One-way ANOVA, * $p<0.05$). Panel B. ^{14}C urate uptake time course experiment of hSLC2A9b, WT (■), WT hSLC2A5 (●), $hSLC2A5_{(7)9}$ (◒) and $hSLC2A5_{(7)9}$ T171C/A388C/S441C (Δ). Urate uptake was measured by incubating protein expressing oocytes in 200 µL 100 µM urate solution incubated from 5 min up to 30 minutes. Uptake activity was corrected for non-specific transport measured in control water injected oocytes from the same batch of oocytes.

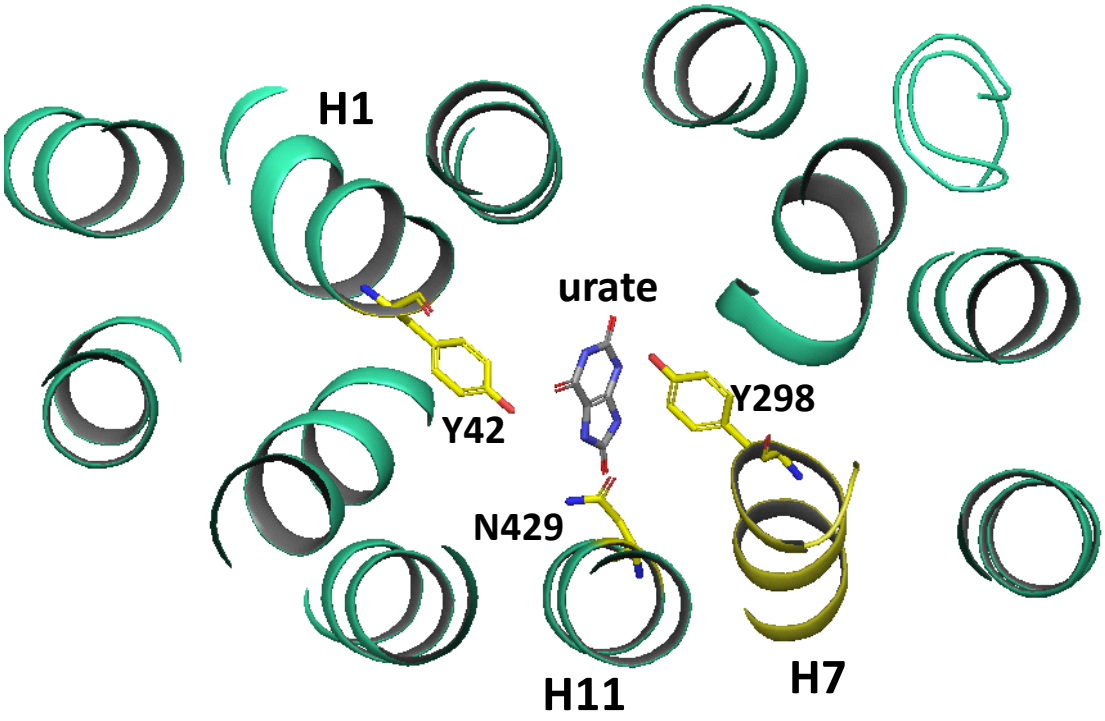

Figure 3. 6. Docking study of urate molecule to human glucose transporter 9 (hSLC2A9) with the predicted three binding sites of urate.

Tyrosine 42 (N42) is on H1, tyrosine is on H7, and asparagine 429 is on H11.

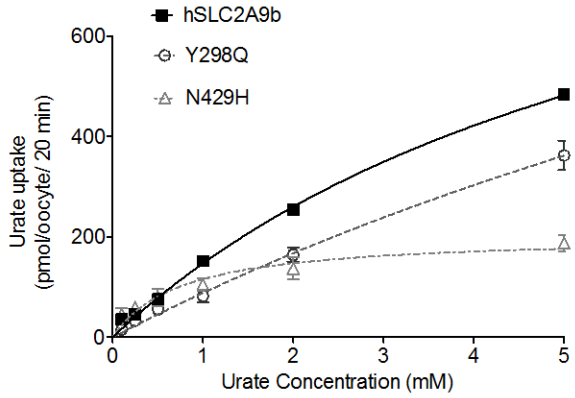

A

	hSLC2A9b	Y298Q	N429H
$K_{M\ (mM)}$	6.6	11.1	0.4
SEM	3.7	6.4	0.1
V_{MAX} (pmol/oocyte/20 min)	1122.0	969.9	217.5
SEM	388.0	414.4	11.3

B

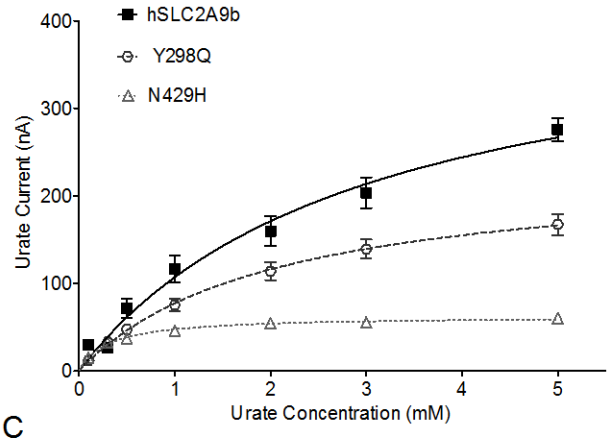

C

	hSLC2A9b	Y298Q	N429H
$K_{M\ (mM)}$	3	2	0.3
SEM	0.8	0.4	0.06
$V_{MAX\ (nA)}$	425.6	233.7	62.58
SEM	57	20.8	2.99

D

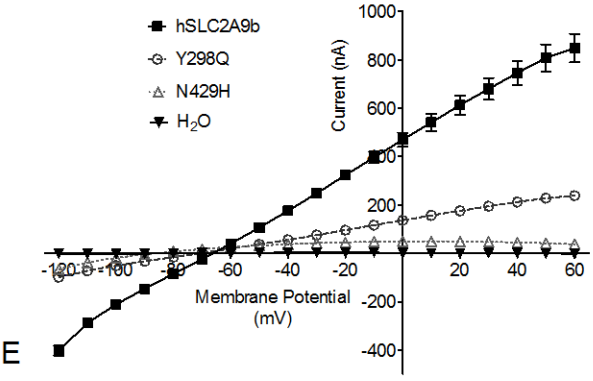

E

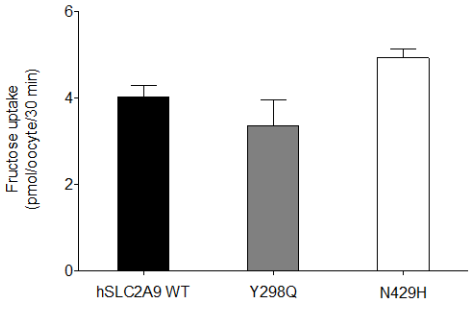

F

Figure 3. 7. Urate and fructose transport mediated by WT hSLC2A9b and its Y298Q and N429H mutants.

Panel A. Michaelis-Menten curves of ^{14}C urate kinetics of hSLC2A9 WT (■), Y298Q (○) and N429H (Δ). Urate uptake was measured by incubating protein expressing oocytes in 200 µL urate solution ranged from 100 µM to 5 mM for 20 minutes. Uptake activity was corrected for non-specific transport measured in control water injected oocytes from the same batch of oocytes. **Panel B.** ^{14}C urate kinetic constants of the 3 isoforms (n ≥3). **Panel C.** Michaelis-Menten curves of urate-induced currents of WT hSLC2A9b, Y298Q and N429H mutants. Currents were measured by Two Micro-electrode Voltage Clamp (TEVC). Data were collected at the peak of each urate-induced current. Points represent the mean of urate-induced peak outward current for each urate concentration. **Panel D.** Urate-induced current kinetic constants of the WT and two mutants (n ≥15 oocytes from 3 frogs). **Panel E.** Current-Voltage curve of 1 mM urate-induced current obtained from RAMP protocol for control (▼), WT hSLC2A9 (■),Y298Q (○) and N429H (△) mutant expressing oocytes. The oocytes were clamped initially at -30 mV followed by voltage change instantly from -120 to 60 mV for a 3 second period. I-V curves were subjected to RAMP protocol at the peak of the urate-induced currents. (n ≥15 oocytes from 3 frogs). **Panel F.** ^{14}C fructose uptake mediated by WT hSLC2A9b and its mutants. Urate uptake was measured by incubating protein expressing oocytes in 200 µL 100 µM fructose solution for 20 minutes. Bar graphs represent fructose uptake activities, which were corrected for non-specific transport measured in control water injected oocytes from the same batch of oocytes (n≥3, One-way ANOVA, * $p<0.05$).

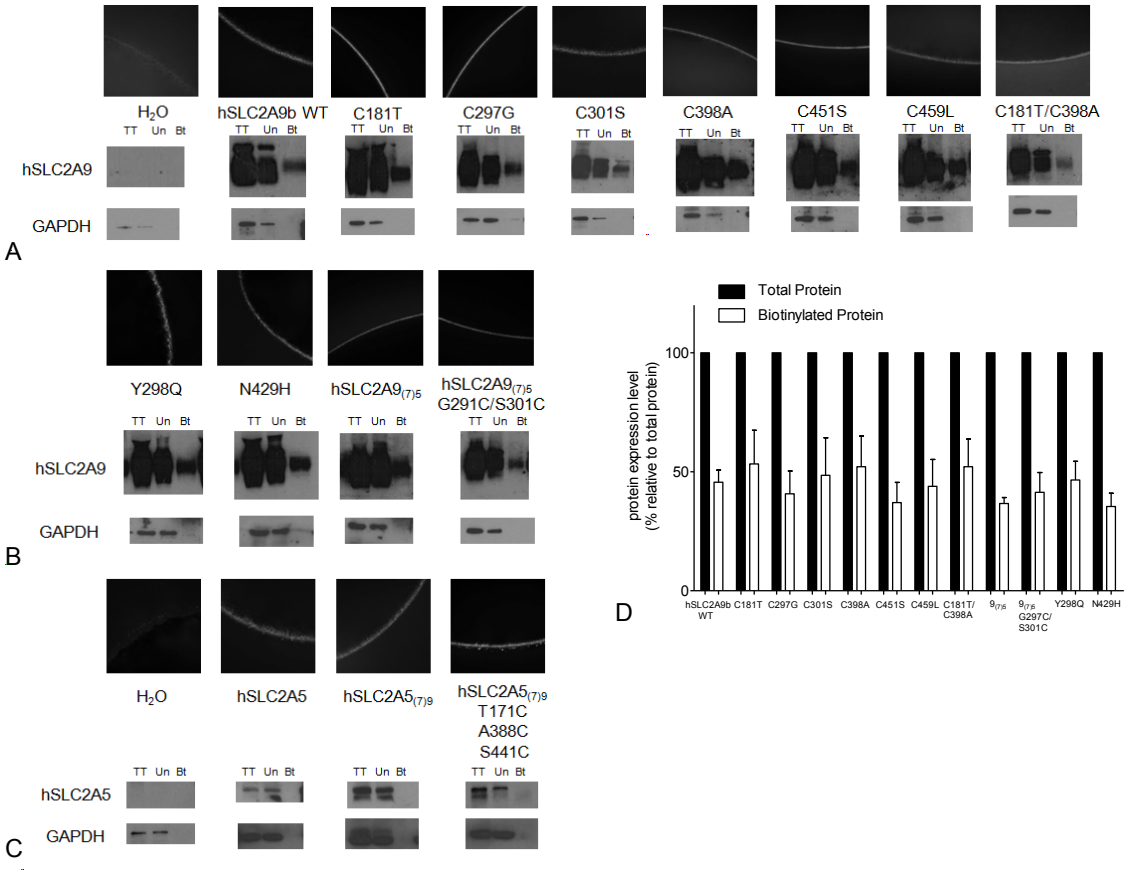

Figure 3. 8. Qualitative and quantitative determination of WT and mutant hSLC2A9 protein expression.

Panel A. Representative pictures of immunohistochemistry and Western blot analysis of protein expression of water injected, WT hSLC2A9b and its cysteine mutants expressing oocytes. Tt: total protein; Un: Unbound protein; Bt: biotinylated protein. **Panel B**. Representative pictures of immunohistochemistry and Western blot analysis of protein expression of Y298Q, N429H and chimæra $hSLC2A9_{(7)5}$, and $hSLC2A9_{(7)5}$ G297C/S301C mutants expressing oocytes. **Panel C.** Representative pictures of immunohistochemistry and Western blot analysis of protein expression of water injected, WT hSLC2A5, chimæric protein $hSLC2A5_{(7)9}$ and $hSLC2A5_{(7)9}$ T171C/A388C/S441C expressing oocytes. Total (black), Unbound (grey), and biotinylated (white) proteins of all isoforms. **Panel D.** Quantitative analysis of protein expression of all hSLC2A9 isoforms. Data were calculated from band intensities obtained from Image J and use a formula: % Biotinylated protein = (Total protein - Unbound protein)/Total protein x 100%. Protein expression levels shown as bar graphs with arbitrary units. ($n \geq 3$, One-way ANOVA, * $p<0.05$).

Chapter 4

Conclusions and Future Direction

Researchers have put significant efforts into the study of glucose transporters for more than half a century. The search for the substrate binding site is still the hottest topic in today's research field, in which scientists are hoping to develop the specific reagents to block or activate the glucose transporter protein. Hence, these reagents will become the possible treatments to heal the GLUT-related diseases, like diabetes, hypertention and gout. The first crystal structure of GLUT1 will certainly lead to a better understanding of how these GLUTs proteins interact with their substrates. Although major genetic mutations are rare in human diseases, their patterns of expression can change significantly in some medical complications, like cancer or heart disease. Therefore, new focus of developing the profiles of these polymorphic GLUTs has been expanded, and these profiles, hopefully, can be used as diagnostic tools or cures for such medical circumstances.

The current thesis demonstrates part of the structure function relationship of urate transport through examining different isoforms of hSLC2A9. In Chapter 2, the roles of two different hydrophobic residues, I335 and W110 of hSLC2A9, were explored. We summarized that isoleucine 335 (I335) is a critical hydrophobic residues in transmembrane helix 7 (H7) that holds the "rigid body" by forming hydrophobic interaction with other residues on the other TMs. Mutation of I335 into valine affected the trans-acceleration between urate and fructose transport; however, it did not affect urate transport directly. Tryptophan 110 (W110), on the other hand, was proposed as a "thin gate" that the electronic rich aromatic ring can directly interact with the transported substrate, urate in this

study, influencing the substrate translocation by the hSCL2A9 protein. Substitution of W110 into phenylalanine, with the aromatic ring maintaining, partially affect urate transport; whereas substitution of W110 into alanine, lacking the aromatic ring, reduced urate transport significantly. Therefore, it is concluded that the bulky side chain in position is critical for urate transport in hSLC2A9.

In Chapter 3, the roles of six cysteine residues in hSLC2A9 were determined. Cysteine 297 and 451 were demonstrated as not required for urate transport by hSLC2A9. Cysteine 181 and 398 were shown to be important for urate transport; in particular, C181 was found as the site responsible for binding pCMBS, which inhibit urate transport in hSLC2A9. Cysteine 301 and 459 were illustrated as necessary for urate transport in the protein that both of them were structurally critical; and a plausible disulfide interaction might form to create a core center to hold other residues, like the hydrophobic residues shown in Chapter 2, close to each other. Hence, all these amino acid communications hold the rigid body of the protein, allowing an appropriate conformation for urate transport in hSLC2A9.

Functional studies of the transmembrane helix 7 (H7) chimæric protein of both hSLC2A9 ($hSLC2A9_{(7)5}$) and hSLC2A5 ($hSLC2A5_{(7)9}$) permitted us to conclude that H7 is necessary for urate transport in hSLC2A9. Nonetheless, the H7 of hSLC2A9 alone is not sufficient to convey urate transport by hSLC2A5, suggesting other TMs and residues are also important in hSLC2A9 for urate transport. The partial recovery of urate transport by $hSLC2A9_{(7)5}$ G297C/S301C

also gave us an impression that H7 is structurally important for urate transport other than contain the critical binding site in it. Our results further displayed that both chimæric proteins transport fructose similarly as their wild type protein, signifying that both hSLC2A9 and hSLC2A5 H7s contain the required residues for fructose transport. Although the docking study on the hSLC2A9 computer model confirmed the urate binding sites are possibly located on the H1, H7, and also H11, the functional data suggested that N429 is the possible urate binding site in H11.

It is also worth to mention that hSLC2A9 transports urate ten times faster than it transports fructose (**Fig. 3.2, 3.4 and 3.**7), however, fructose was able to trans-accelerate the urate transport from extracellular space into the intracellular side of the oocytes (**Fig. 2.3**). This indicated that the rate to hSLC2A9 transport fructose must be faster than the empty hSLC2A9 protein to allow the substrates trans-acceleration to occur. Therefore, these observations further confirms that the hypothesis of the empty carrier as the rate limited step is valid.

Overall, this thesis shines light on the structure-function relationship in urate transport mediated by the hSLC2A9 protein. The results clearly demonstrated that the structure of the hSLC2A9 strongly affects its urate transport function. Moreover, according to the docking study, we postulate a animo acid, N429, that is necessary for urate translocating during transport mediated by hSLC2A9, and it could be an important part of the urate binding site.

One thing I need to point out that all the functional studies were based on the heterologous *Xenopus* oocyte expression system. So far, functional study of hSLC2A9 has not yet being confirmed in mammalian cell system. During my thesis study, I also found it is difficult to identify a common cell line with relatively low expression of hSLC2A9. I screened the SCL2A9 expression level in Madin-Darby canine kidney epithelial cells (MDCK), human embryonic cell line 293 (HEK293), and the rat pancreas insulin secreting beta cell line (INS 1). All three cell lines have high expression level of SLC2A9 (**Fig. A.4**). Future search of suitable cell line is necessary to validate the function of SLC2A9 in mammalian cell lines.

In terms of animal studies, DeBosch *et al.* (277) generated intestine specific and SLC2A9 knockout mice. These enterocyte-specific SLC2A9 knockout mice demonstrated several characteristic metabolic sydromes, like hyperuricemia, hyperuricosuria, and spontaneous hypertension. However, these mice have normal kidney phenotype. Preitner *et al.* (336, 337), on the other hand, created both systematic and liver specific SLC2A9 inactivated mice. The systematic SLC2A9 inactivated mice developed moderate metabolic sydrome with abnormal renal tissues during early stage of growth; whereas the liver specific SLC2A9 inactivated mice developed severe hyperuricemia and hyperuricosuria with normal organ structures. More recent studies have shown that there is link among fructose, urate and diabetic nephropathy, a vascular complication in diabetes (338). Studies also showed that lowering fructose

metabolism could reduce urate production, hence mitigated the development of tubulointestinal injury in mice (338, 339).

Although these three types of knockout mice indicate SLC2A9 is important for maintaining urate homeostasis in mice, other researchers might argue that rodents might not be the appropriate model for study, because rodents do not have urate as their final metabolite. Therefore, it would be ideal to search an experimental model that has urate as its final metabolite for the study of SLC2A9.

Finally, careful consideration needs to be given to the future development of therapeutics for urate related diseases based on hSLC2A9 because it is expresseed in many regions in the human body. Finally, it may provide reasonable evidence in the future to develop inhibitors or activity modulators for hSLC2A9 based on a detailed knowledge of its binding sites and how substrate transport is mediated.

Appendix

Appendix. A. Figures and Tables.

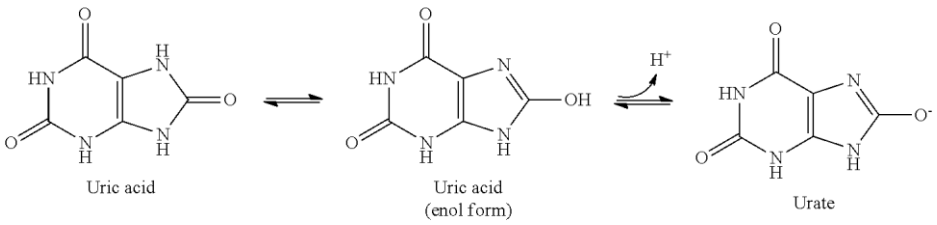

Figure A. 1. Urate and its urate anion.

http://www.google.com/patents/US20130296345

Table A. 1. Primers of cysteine, Y298Q, and N429H mutants of hSLC2A9b.

hSLC2A9b C128V	Forward	5' GCATTGCTGATGGCCGTCTCGCTCCAGGC 3'
	Reverse	5' GCCTGGAGCGAGACGGCCATCAGCAATGC 3'
hSLC2A9b C181T	Forward	5' GGCAGGTGACTGCCATCTTTATCACTATTGGCGTG 3'
	Reverse	5' CACGCCAATAGTGATAAAGATGGCAGTCACCTGCC 3'
hSLC2A9b C301S	Forward	5' CTGCTACCAGCTCTCGGGCCTCAATGCAATTTG 3'
	Reverse	5' CAAATTGCATTGAGGCCCGAGAGCTGGTAGCAG 3'
hSLC2A9b C297G	Forward	5' GTCACCATGGCGGCCTACCAGCTCTGTGGC 3'
	Reverse	5' GCCACAGAGCTGGTAGGCCGCCATGGTGAC 3'
hSLC2A9b C398A	Forward	5' CATCGCCTCTTTCGCCAGTGGGCCAGGTGG 3'
	Reverse	5' CCACCTGGCCCACTGGCGAAAGAGGCGATG 3'
hSLC2A9b C451S	Forward	5' GTCTGGACACCTACAGCTTCCTAGTCTTTGC 3'
	Reverse	5' GCAAAGACTAGGAAGCTGTAGGTGTCCAGAC 3'
hSLC2A9b C459L	Forward	5' GTCTTTGCTACAATTCTGATCACAGGTGCTATCTACC 3'
	Reverse	5' GGTAGATAGCACCTGTGATCAGAATTGTAGCAAAGAC 3'
hSLC2A9b Y298Q	Forward	5'GTCACCATGGCCTGCCAGCAGCTCTGTGGCCTCAATG 3'
	Reverse	5' CATTGAGGCCACAGAGCTGCTGGCAGGCCATGGTGAC 3'
hSLC2A9b N492H	Forward	5' GCAGGCACCGTCCACTGGCTCTCCAAC 3'
	Reverse	5' GTTGGAGAGCCAGTGGACGGTGCCTGC 3'

Table A. 2. Primers of chimæra protein construction, and primers of cysteine mutation in H7 of hSLC2A9$_{(7)5}$.

hSLC2A9$_{(7)5}$	Forward	5' CATGGGCGGCCAGCAGCTGTCGGGCGTCAACGCTATCTACTATACCAACAGCATCTTTGG 3'
	Reverse	5' CTGCTGGCCGCCCATGAGGACGATGATGGACAGCAGCTGCCAGCGGACGTAGGGAGCTCTCAGCAG 3'
hSLC2A9$_{(7)5}$ S301C	Forward	5' CAGCAGCTGTGCGGCGTCAACGCTATC 3'
	Reverse	5' GATAGCGTTGACGCCGCACAGCTGCTG 3'
hSLC2A9$_{(7)5}$ G297C	Forward	5' CATCGTCCTCATGGGCTGCCAGCAGCTGTC 3'
	Reverse	5' GACAGCTGCTGGCAGCCCATGAGGACGATG 3'

Table A. 3. Primers of chimæra protein construction of WT hSLC2A5, and cysteine mutation in hSLC2A5$_{(7)9}$.

hSLC2A5$_{(7)9}$	Forward	5' CCATGGCCTGCTACCAGCTCTGTGGCCTCAATGCAATTTGGTTCTATTACGCGGACCAGATCTACCTGAGC 3'
	Reverse	5' GAGCTGGTAGCAGGCCATGGTGACAATCACGGTGACCACCTGCCAGCGCAGCGAGCGCATCCGGAACAGC 3'
hSLC2A5$_{(7)9}$ T171C	Forward	5' CCAGCTCTTCATCTGCGTTGGCATCCTTGTGG 3'
	Reverse	5' CCACAAGGATGCCAACGCAGATGAAGAGCTGG 3'
hSLC2A5$_{(7)9}$ A388C	Forward	5' GCCTACGTCATAGGACATTGTCTCGGGCCCAG 3'
	Reverse	5' CTGGGCCCGAGACAATGTCCTATGACGTAGGC 3'
hSLC2A5$_{(7)9}$ S441C	Forward	5' CTCGGCCCGTACTGCTTCATTGTCTTCGCCG 3'
	Reverse	5' CGGCGAAGACAATGAAGCAGTACGGGCCGAG 3'

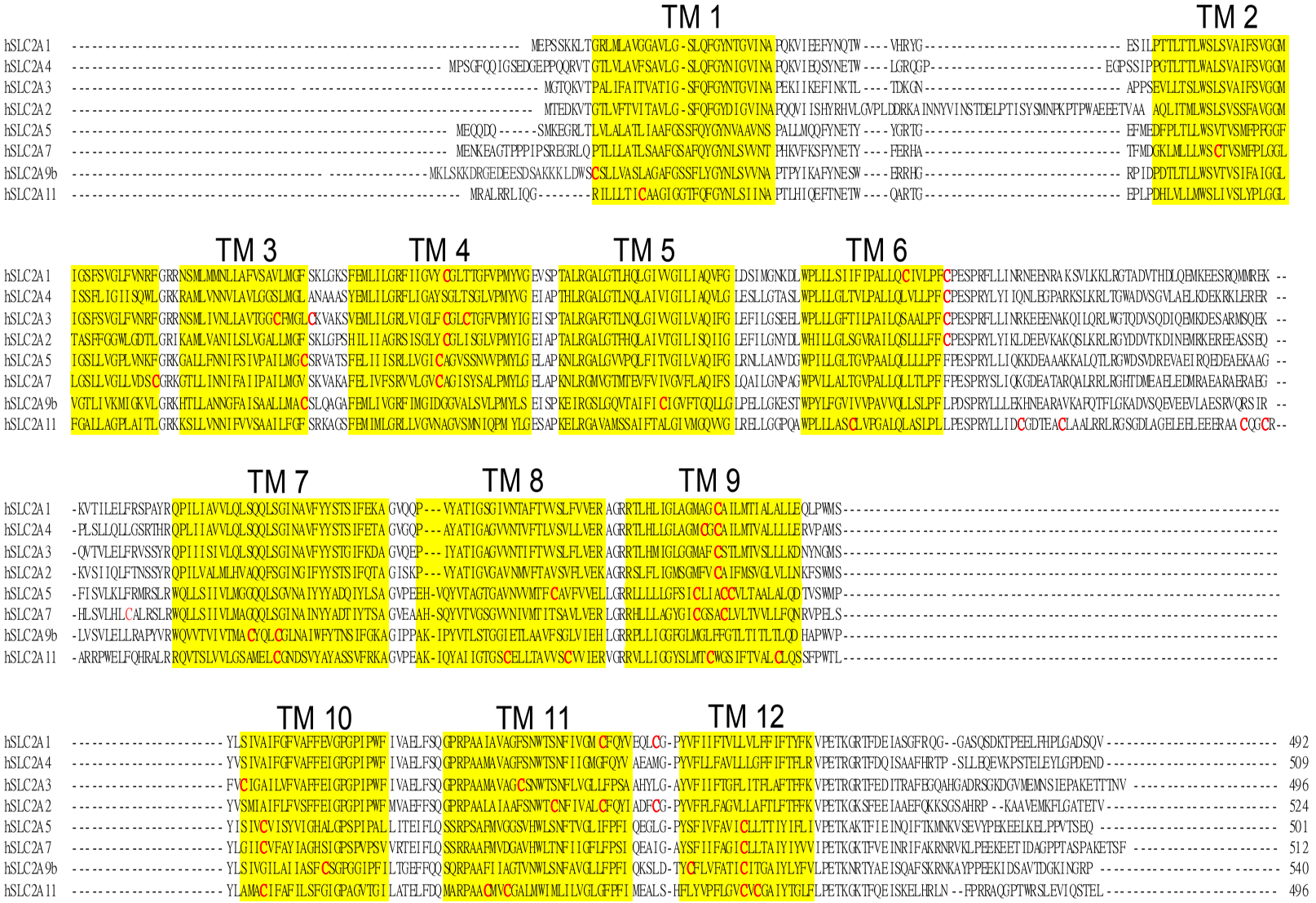
TM 1
TM 2
TM 3
TM 4
TM 5
TM 6
TM 7
TM 8
TM 9
TM 10
TM 11
TM 12
hSLC2A1
hSLC2A4
hSLC2A3
hSLC2A2
hSLC2A5
hSLC2A7
hSLC2A9b
hSLC2A11

Figure A. 2. Multi-amino acid sequences alignments of Class I and II glucose transporter family proteins.

Transmembrane helices (Hs) are highlighted in yellow color based the new GLUT1 crystal structure. Cysteine residues are highlighted in red color. Protein amino acid sequences alignments were performed by Clustal OMEGA (http://www.ebi.ac.uk/Tools/msa/clustalo/).

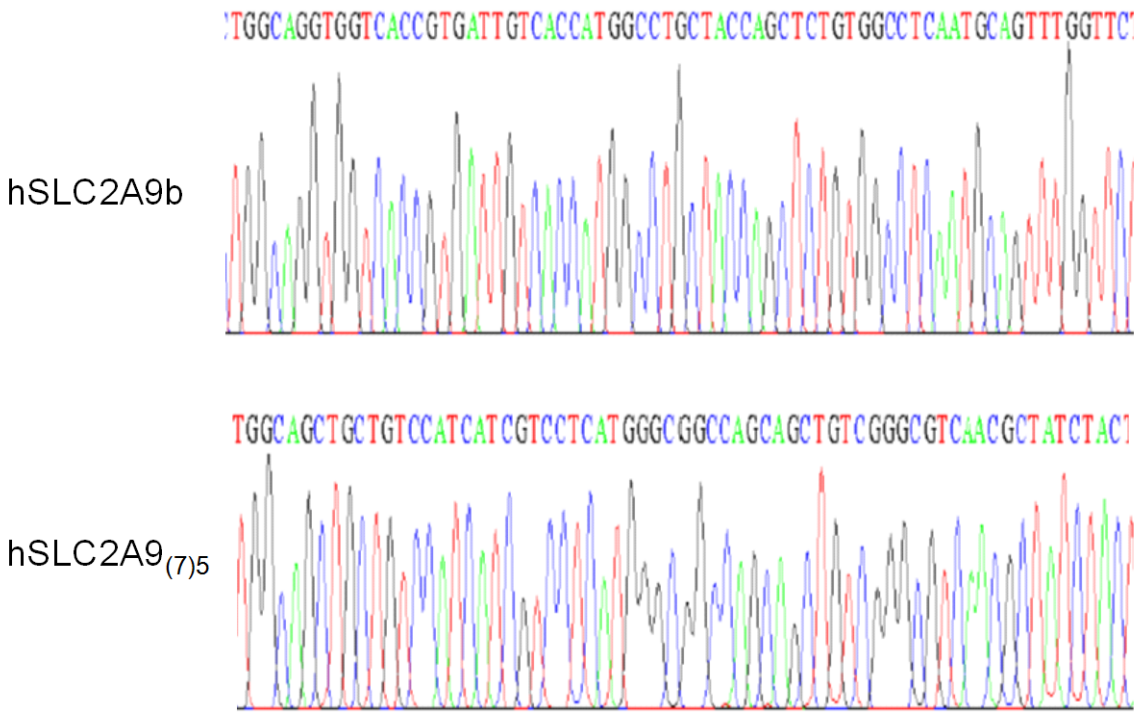

Figure A. 3. Representative DNA sequencing result of wild type hSLC2A9b and chimæra hSLC2A9$_{(7)5}$.

DNA sequencing result is performed by Macrogen USA. (Maryland, USA)

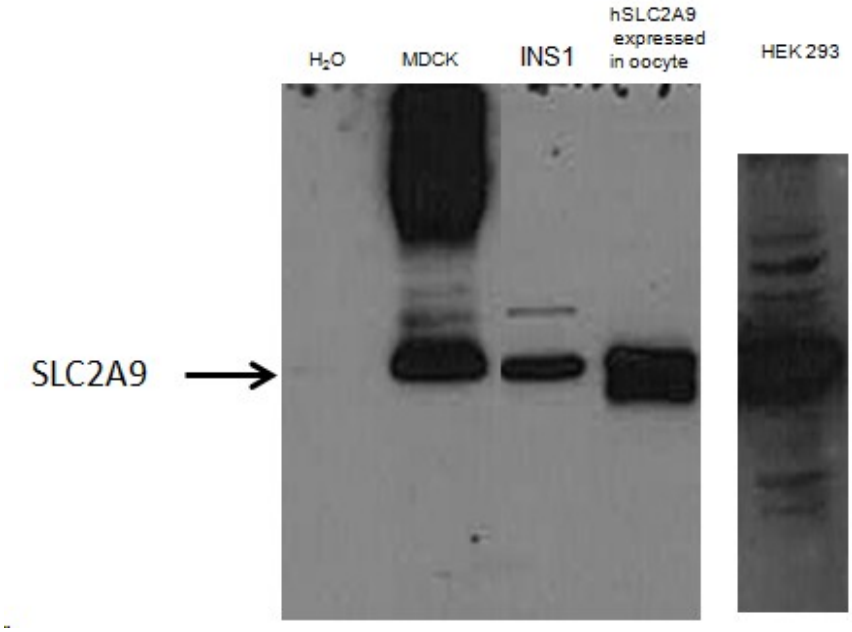

Figure A. 4. Representative picture of Western blot analysis of hSLC2A9 expression level in various cell lines.

From left to right: Madin-Darby canine kidney epithelial cell lines (MDCK), rat pancreas insulin secreting beta cell (INS1) and *Xenopus* oocytes with overexpressed hSLC2A9 protein.

Apppendix B. Additional experiments.

Besides of the experiments discussed in previous chapters, we also tried to explore some other directions of how uratetransport is mediated by hSLC2A9. Although these data are not yet published, they still contribute important information on the relationship of the structure and function of hSLC2A9.

Appendix. B1. Benzbromarone is a well known uricosuric drug, a xanthine oxidase inhibitor, for treating gout. Few studies claimed that benzbromarone has potent inhibition effect on urate influx mediated by hSLC2A9. For instance, our lab reported that benzbromarone inhibited urate uptake during the radioisotope flux measurement with a K_i equals to 27 μM (K_i is the concentration value of benzbromarone that reduced 50% of urate transport activity). Later, Bibert *et al.* showed that 500 μM benzbromarone reduced 90% of urate transport by hSLC2A9.

This present study uses the electrophysiology measurement to further reveal the benzbromarone inhibitory property. To our surprise, instead of affecting the urate-induced current, benzbromarone application to the unclamped oocyte decreased the oocyte membrane potential directly. This reduction was seen in both hSLC2A9 expressing oocytes and the control water injected oocytes (Fig. B1). We also observed that the membrane potential decreased as the benzbromarone incubation time increase, and it will return to the base membrane potential as the drug withdraw from the incubation bath. The diminution magnitude of the membrane potential is similar in both hSLC2A9 and water injected oocyte.

These data allowed us to conclude that the benzbromarone inhibits urate transport by decreasing the membrane potential. We know that hSLC2A9 transport urate anion in a electrogenic manner, i.e., besides of the chemical gradient, urate is also transported down its electrical gradients. Consequently,

when the membrane potential is more negative inside the oocytes, the electrical potential is not favorable for urate to move into the oocytes, thus less urate was taken up in those radiolabelled flux measurements.

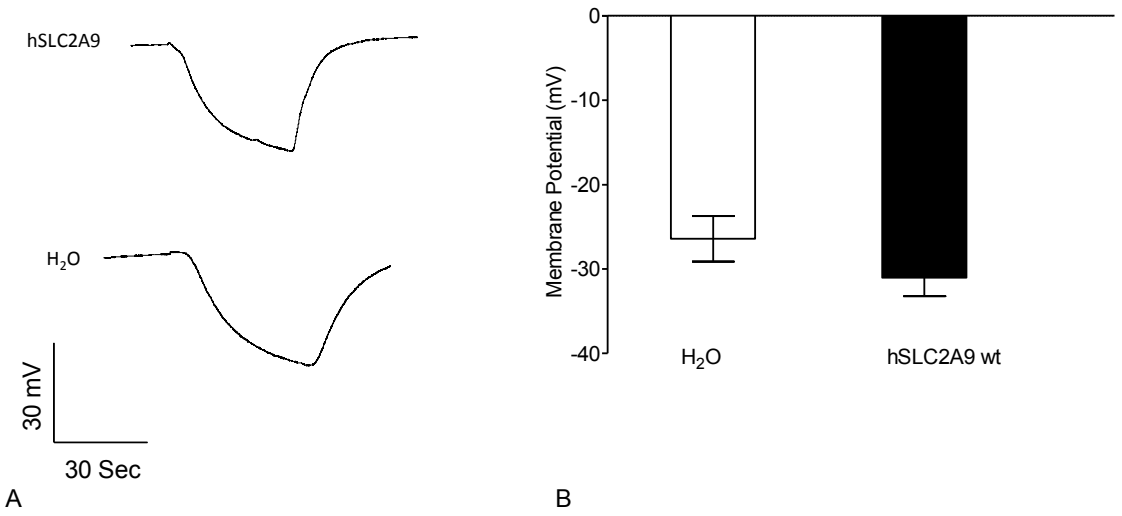

Figure B. 1. Benzbromarone inhibition experiments.

Panel A. Representative traces of membrane potential of a hSLC2A9 (upper) and a control water injected (lower) ooctyes. Both oocytes were not clamp. 500 μM of benzbromarone was used to perfused the oocytes when base line became stable after probing with two electrodes. **Panel B.** Changes of membrane potential of the hSLC2A9 expressing oocytes and water injected oocytes. Bar graphs indicate the shift of membrane potential after the benzbromarone application. Student un-paired t-tests were performed as the statistical analysis. Significant level is defined when $p<0.05$ (n=4).

Appendix. B2. Cysteine 128. Besides of all the cysteines discussed in Chapter 3, we examine the additional one, C128. Unlike the other cysteines, this C128 residue located at the edge of the transmembrane helix 3 on the exofacial side of hSLC2A9b.

Methods please referr to Chapter 2.3. Experimental procedures.

Results. Substituted C128 into valine, a corresponding residue in hSLC2A5, caused loss in urate transport capacity and increase urate binding affinity. Showing in **Fig. B2A-2D.,** both V_{MAX} and K_M of C128V are smaller compared to wild type. The urate transport kinetics curve of C128V is similar to the ones of C181T, C398A, and the double mutant C181T/C398A. In addition, the C128V transport fructose similarly as the wild type hSLC2A9b (**Fig. B2F**). Immunohistochemistry and biotinylation indicated that C128V express on the oocytes membrane also similar to wild type protein (**Fig. B2E**).

We speculated that this C128 is a site that might form a disulfide bridge between two hSLC2A9 monomers that allows them to form a dimer during transport. This assumption is possible that Hebert and Carruthers (340) reported the dimerization in hSLC2A1 through disulfide bond to stabilized the transporter structure, thus enhance the hexose transport function. Zottola *et al.* (196) illustrated the N-terminal half of hSLC2A1 contains the necessary residues for dimerization and two cysteines, C347 and C421 on the C-terminal half are critical for intramolecular disulfide formation for tetramerization. Zottola *et al.* illustrated that substitution of cysteine 347 or 421 to serine significantly reduces hSLC2A1

exposure of tetrameric GLUT1-specific epitopes. Therefore, it is very possible that the thiol group of the C128s forms an intramolecular disulfide linkage between the two hSLC2A9 monomers similar as the ones in hSLC2A1, thus enhance the urate transport activity. When we break the linkage by change the cysteine into valine, the thiol groups were no longer present, hence alter the structure of the hSLC2A9 and the urate transport ability. However, future studies need to reveal the details of this dimerization hypothesis in hSLC2A9.

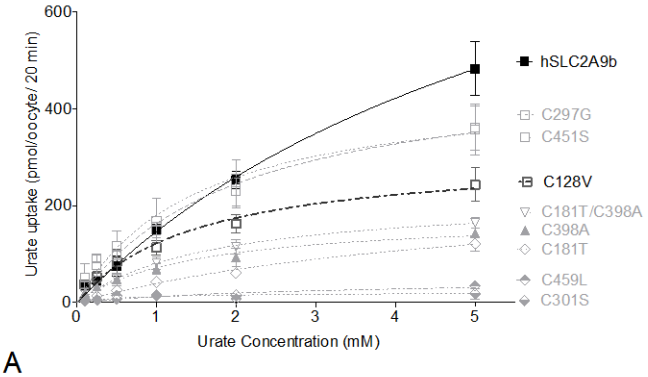

A

B

	hSLC2A9 WT	C128V
$K_{M\ (mM)}$	6.6	1.5
SEM	3.7	0.5
V_{MAX} (pmol/oocyte/20 min)	1122.0	307.1
SEM	388.0	42.9

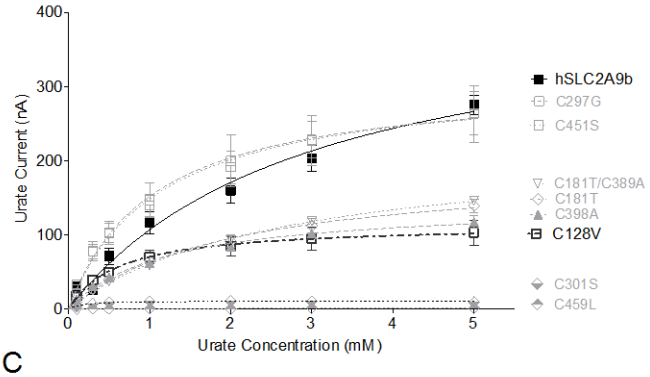

C

D

	hSLC2A9 WT	C128V
$K_{M\ (mM)}$	3.0	0.8
SEM	0.8	0.2
$V_{MAX\ (nA)}$	425.6	172.0
SEM	57.0	15.8

E

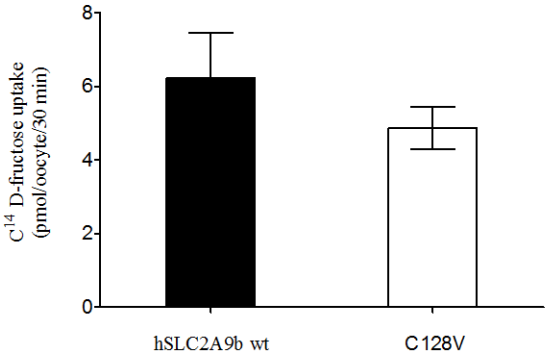

F

Figure B. 2. Urate and fructose transport mediated by WT hSLC2A9b and its C128V mutant.

Panel A. Michaelis-Menten curves of ^{14}C urate kinetics of hSLC2A9b WT (■) and C128V (□). Urate uptake was measured by incubating protein expressing oocytes in 200 µL urate solution ranged from 100 µM to 5 mM for 20 minutes. Uptake activity was corrected for non-specific transport measured in control water injected oocytes from the same batch of oocytes. **Panel B.** ^{14}C urate kinetic constants of the 2 isoforms (n=3). **Panel C.** Michaelis-Menten curves of urate-induced currents of WT hSLC2A9b WT and C128V mutant. Currents were measured by Two Micro-electrode Voltage Clamp (TEVC). Data were collected at the peak of each urate-induced current. Points represent the mean of urate-induced peak outward current for each urate concentration. **Panel D.** Urate-induced current kinetic constants of the WT and C128V mutant (n=15 oocytes from 3 frogs). **Panel E.** Representative pictures of immunohistochemistry and Western blot analysis of protein expression of C128V mutant expressing oocytes. **Panel F.** ^{14}C fructose uptake mediated by hSLC2A9b WT and C128V mutant. Urate uptake was measured by incubating protein expressing oocytes in 200 µL 100 µM fructose solution for 20 minutes. Bar graphs represent fructose uptake activities, which were corrected for non-specific transport measured in control water injected oocytes from the same batch of oocytes (n=3).

Appendix. B3. Second messenger pathways. At the end of this thesis study, we started to look at other possibilities that might also regulate urate transport mediated by hSLC2A9. So far, most studies focus on the relationship of structure and function of hSLC2A9, we would like to test whether the secondary messenger pathway will have an effect on its substrate transport ability. Our formal student, Witkowska, proposed an initial idea that the transport function of hSLC2A9 is perhaps regulated by phosphorylation. Therefore, we performed some primary experiments by applied both phorbol 12-myristate 13-acetate (PMA), a diester of phorbol that activates protein kinase C, and the cyclic adenosine monophosphate (cAMP) that also activates protein kinases.

Method - We mutated two serine residues, S9 and S22, into alanine in the N-terminus of hALS2A9. We tested these two mutants together with the wild type with pre-incubated the proteins expressing oocytes with either PMA and cAMP; then, we performed a simple 14C urate uptake experiments to the pre-treated oocytes. We also applied PMA in the electrophysiology experiments that we clamped the protein expressing oocyte at -30 mV and ran a RAMP protocol from -120 mV to +60 mV to obtain an I-V curve; then, we ran the same RAMP protocol to a PMA pre-incubate oocyte.

Results - Our preliminary data indicate that urate transport was reduced when we applied PMA, however, cAMP did not cause any changes in urate uptake mediated by hSCL2A9 (**Fig. B3.D**). The two serine residues, Serine 9 and 22, on the N-terminus of hALC2A9 showing in **Fig. B.3A**,**B**,**C**, are not the corresponding

sites for the lost urate activity caused PKC activator. Further studies of other residues screening and experiments have to be conduct to further reveal other possible pathways that could affect urate transport mediated by hSLC2A9.

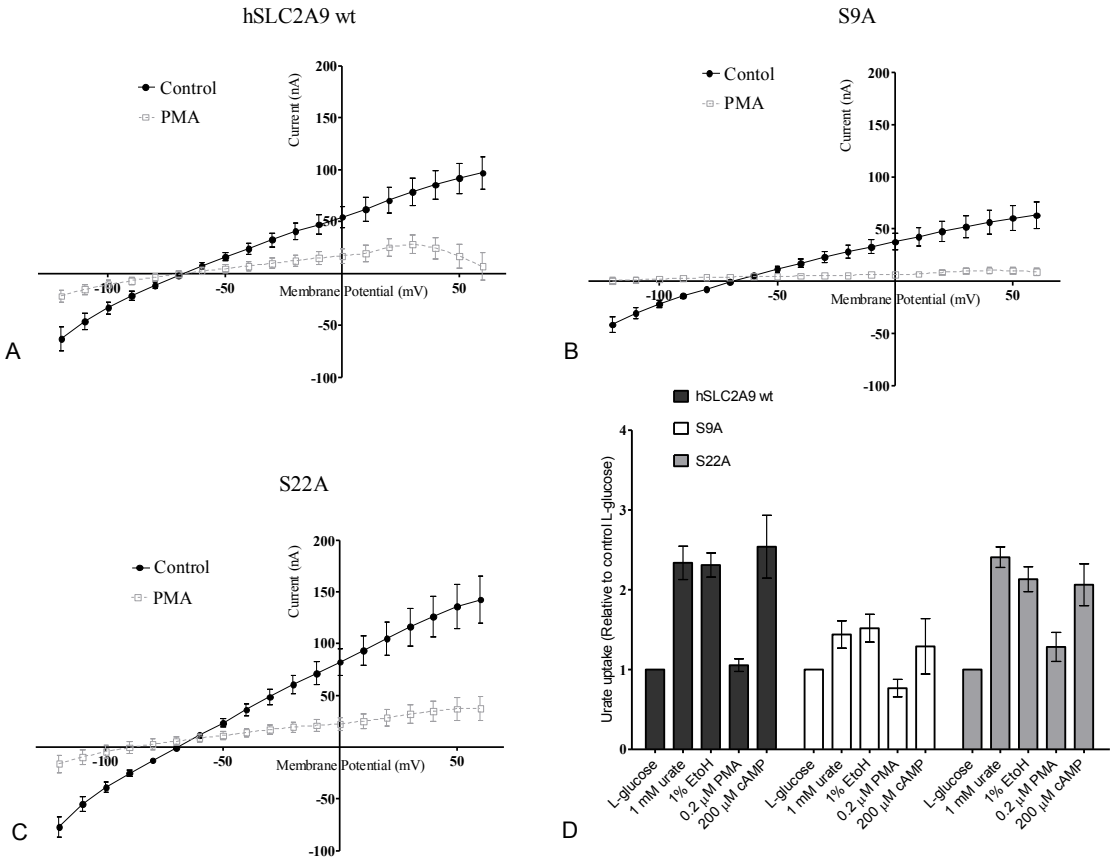

Figure B. 3. Effect of PMA and cAMP on hSLC2A9 and its serine mutants.

Panel A, B & C. Current-Voltage curve before (black)/ after (grey) PMA treatments to hSLC2A9 wt and its mutants expressing oocytes. (n >15 oocytes from 3 frogs). **Panel D**. Trans-stimulation of urate flux in presence of intracellular urate with/without PMA or cAMP treatments to hSLC2A9 wt and its serine to alanine mutants (n=4). GPS 3.0 http://gps.biocuckoo.org/

References

1. Choi, H., Mount, D., and Reginato, A. (2005) Pathogenesis of Gout. *Ann Intern Med*. **143**, 499–516

2. Mclean, L., and Dalbeth, N. (2015) *Rheumatology*, Sixth Edit (Hochberg, M., Silman, A., Smolen, J., Weinblatt, M., and Weisman, M. eds), Elsevier Ltd, **187**, 1555–1568

3. Hediger, M. a, Johnson, R. J., Miyazaki, H., and Endou, H. (2005) Molecular physiology of urate transport. *Physiology (Bethesda).* **20**, 125–33

4. Hayashi, S., Fujiwara, S., and Noguchi, T. (2000) Evolution of Urate-Degrading Enzymes in Animal Peroxisomes. *Cell Biochem. Biophys.* **32**, 123–129

5. Wu, X., Muzny, D. M., Chi Lee, C., and Thomas Caskey, C. (1992) Two independent mutational events in the loss of urate oxidase during hominoid evolution. *J. Mol. Evol.* **34**, 78–84

6. McCarty, D. J. (1970) A historical note: Leeuwenhoek's description of crystals from a gouty tophus. *Arthritis Rheum.* **13**, 414–418

7. Nuki, G., and Simkin, P. a (2006) A concise history of gout and hyperuricemia and their treatment. *Arthritis Res. Ther.* **8 Suppl 1**, S1

8. Eliahou, R., Hidas, G., Duvdevani, M., and Sosna, J. (2010) Determination of Renal Stone Composition with Dual-Energy Computed Tomography: An Emerging Application. *Semin. Ultrasound, CT MRI*. **31**, 315–320

9. Storey, G. D. (2001) Alfred Baring Garrod (1819-1907). *Rheumatology.* **40**, 1189–1190

10. Puig, J. G., and Ruilope, L. M. (1999) Uric acid as a cardiovascular risk factor in arterial hypertension. *J Hypertens.* **17**, 869–872

11. Johson, R.J., Kang, D. H., Feig, D., Kivlighn, S., Kanellis, J., Watanabe, S., Tuttle, K. R., and Rodriguez-Iturbe, B Herrera-Acosta,J. Mazzali, M. (2003) Is there a pathogenetic role for uric acid in hypertension and cardiovascular and renal disease? *Hypertension.* **41**, 1183–1190

12. Onat, A., Uyarel, H., Hergenc, G., Karabulut, A., Albayrak, S., Sari, I., Yazici, M., and I, K. (2006) Serum uric acid is a determinant of metabolic syndrome in a population-based study. *Am J Hertens.* **19**, 1055–1062

13. Bo, S., Cavallo-Perin, P., Gentile, L., Repetti, E., and Pagano, G. (2001) Hypouricemia and hyperuicemia in type 2 Diabetes: two different phenotypes. *Eur J Clin Invest*. **31**, 318–321

14. Center for Disease and Control. Control.http://www.cdc.gov/arthritis/basics/gout.htm

15. Life with arthritis in canada : A personal and public health challenge. http://www.cdc.gov/arthritis/basics/gout.html (2011)

16. Zhu, Y., Pandya, B., and Choi, H. (2011) Prevalence of gout and hyperuricemia in the US general population: The national health and nutrition examination survey 2007–2008. *Arthritis Rheum.* **63**, 3136–3143

17. Feig, D. I., and Johnson, R. J. (2003) Hyperuricemia in childhood primary hypertension. *Hypertension*. **42**, 247–252

18. Presores, J. B., and and Swift, J. . (2012) Adhesion properties of uric acid crystal surfaces. *Langmuir*. **28**, 7401–7406

19. Sorensen, B. L. B., and Ph, D. (1965) Role of the Intestinal Tract in the Elimination of Uric Acid. *Arthritis Rheum.* **8**, 694–706

20. Cheeseman, C. (2009) Solute carrier family 2, member 9 and uric acid homeostasis. *Curr. Opin. Nephrol. Hypertens.* **18**, 428–432

21. Cura AJ, Carruthers, A. J. (2013) The role of monosaccharide transport proteins in carbohydrate assimilation, distribution, metabolism and homeostasis. *Compr Physiol*. **2**, 863–914

22. Bobulescu, I. A., and Moe, O. W. (2012) Renal transport of uric acid: evolving concepts and uncertainties. *Adv. Chronic Kidney Dis.* **19**, 358–71

23. Bannasch, D. L., Ryun, J. R., Bannasch, M. J., Schaible, R. H., Breen, M., and Ling, G. (2004) Exclusion of galectin 9 as a candidate gene for hyperuricosuria in the Dalmatian dog. *Anim. Genet.* **35**, 326–328

24. Lu, Y., Nakanishi, T., and Tamai, I. (2012) Functional cooperation of SMCTs and URAT1 for renal reabsorption transport of urate. *Drug Metab. Pharmacokinet.* **28**, 153–158

25. Paroder, V., Spencer, S. R., Paroder, M., Arango, D., Schwartz, S., Mariadason, J. M., Augenlicht, L. H., Eskandari, S., and Carrasco, N. (2006) Na(+)/monocarboxylate transport (SMCT) protein expression correlates with survival in colon cancer: molecular characterization of SMCT. *Proc. Natl. Acad. Sci. U. S. A.* **103**, 7270–7275

26. You, G. (2002) Structure, function, and regulation of renal organic anion transporters. *Med. Res. Rev.* **22**, 602–16

27. Kuze, K., Graves, P., Leahy, A., Wilson, P., Stuhlmann, H., and You, G. (1999) Heterologous expression and functional characterization of a mouse renal organic anion transporter in mammalian cells. *J. Biol. Chem.* **274**, 1519–1524

28. Zhou, F., and You, G. (2007) Molecular insights into the structure-function relationship of organic anion transporters OATs. *Pharm. Res.* **24**, 28–36

29. You, G., Kuze, K., Kohanski, R. A., Amsler, K., and Henderson, S. (2000) Regulation of mOAT-mediated Organic Anion Transport by Okadaic Acid and Protein Kinase C in LLC-PK 1 Cells. *J. Biol. Chem.* **275**, 10278–10284

30. Lu, R. U. N., Chan, B. S., and Schuster, V. L. (1999) Cloning of the human kidney PAH transporter : narrow substrate specificity and regulation by protein kinase C. *Am J Physiol Ren. Physiol*. **276**, 295–303

31. Hosoyamada, M., Sekine, T., Kanai, Y., and Endou, H. (1999) Molecular cloning and functional expression of a multispecific organic anion transporter from human kidney. *Am J Physiol Ren. Physiol*

32. Race, J. E., Grassl, S. M., Williams, W. J., and Holtzman, E. J. (1999) Molecular cloning and characterization of two novel human renal organic anion transporters (hOAT1 and hOAT3). *Biochem. Biophys. Res. Commun.* **255**, 508–14

33. Bakhiva, A., Bahn, A., Burckhardt, G., and Wolff, N. (2003) Human organiceanioin transporter 3 (hOAT3) can operate as an exchanger and mediate secretory urate flux. *Cell Physiol. Biochem*. **19**, 243–256

34. Channels, I. O. N., Transport, M., and Physiology, I. (2003) Urate transport via human PAH transporter hOAT1 and its gene structure. **63**, 143–155

35. Eraly, S. a, Vallon, V., Rieg, T., Gangoiti, J. a, Wikoff, W. R., Siuzdak, G., Barshop, B. a, and Nigam, S. K. (2008) Multiple organic anion transporters contribute to net renal excretion of uric acid. *Physiol. Genomics*. **33**, 180–92

36. Cha, S. H., Sekine, T., Kusuhara, H., Yu, E., Kim, J. Y., Kim, D. K., Sugiyama, Y., Kanai, Y., and Endou, H. (2000) Molecular Cloning and Characterization of Multispecific Organic Anion Transporter 4 Expressed in the Placenta. *J. Biol. Chem.* **275**, 4507–4512

37. Roch-ramel, F., and Werner, D. (1994) Urate transport in brush-border membrane of human kidney. *Am J physiol Ren. Fluid Electrolyte Physiol.*

38. Roch-Ramel F, Guisan B, S. L. (1996) Indirect coupling of urate and p-aminohippurate transport to sodium in human brush-border membrane vesicles. *Am J physiol Ren. Fluid Electrolyte Physiol.*

39. Hagos, Y., Stein, D., Ugele, B., Burckhardt, G., and Bahn, A. (2007) Human renal organic anion transporter 4 operates as an asymmetric urate transporter. *J. Am. Soc. Nephrol.* **18**, 430–9

40. Nishiwaki, T., Daigo, Y., Tamari, M., Fujii, Y., and Nakamura, Y. (1998) Molecular cloning, mapping, and characterization of two novel human genes, ORCTL3 and ORCTL4, bearing homology to organic-cation transporters. *Cytogenet. Cell Genet.* **83**, 251–255

41. Bahn, A., Hagos, Y., Reuter, S., Balen, D., Brzica, H., Krick, W., Burckhardt, B. C., Sabolic, I., and Burckhardt, G. (2008) Identification of a new urate and high affinity nicotinate transporter, hOAT10 (SLC22A13). *J. Biol. Chem.* **283**, 16332–41

42. Enomoto, A., Kimura, H., and Chairoungdua, A. (2002) Molecular identification of a renal urate – anion exchanger that regulates blood urate levels. *Nature*. **417**, 447–452

43. Ichida, K. (2004) Clinical and Molecular Analysis of Patients with Renal Hypouricemia in Japan-Influence of URAT1 Gene on Urinary Urate Excretion. *J. Am. Soc. Nephrol.* **15**, 164–173

44. Ichida, K., Hosoyamada, M., Kamatani, N., Kamitsuji, S., Hisatome, I., Shibasaki, T., and Hosoya, T. (2008) Age and origin of the G774A mutation in SLC22A12 causing renal hypouricemia in Japanese. *Clin. Genet.* **74**, 243–51

45. Tanaka, M., Itoh, K., Matsushita, K., Matsushita, K., Wakita, N., Adachi, M., Nonoguchi, H., Kitamura, K., Hosoyamada, M., Endou, H., and Tomita, K. (2003) Two male siblings with hereditary renal hypouricemia and exercise-induced ARF. *Am. J. Kidney Dis.* **42**, 1287–1292

46. Tin, A., Woodward, O. M., Kao, W. H. L., Liu, C.-T., Lu, X., Nalls, M. a, Shriner, D., Semmo, M., Akylbekova, E. L., Wyatt, S. B., Hwang, S.-J.,

Yang, Q., Zonderman, A. B., Adeyemo, A. a, Palmer, C., Meng, Y., Reilly, M., Shlipak, M. G., Siscovick, D., Evans, M. K., Rotimi, C. N., Flessner, M. F., Köttgen, M., Cupples, L. A., Fox, C. S., and Köttgen, A. (2011) Genome-wide association study for serum urate concentrations and gout among African Americans identifies genomic risk loci and a novel URAT1 loss-of-function allele. *Hum. Mol. Genet.* **20**, 4056–68

47. Shin, H. J., Takeda, M., Enomoto, A., Fujimura, M., Miyazaki, H., Anzai, N., and Endou, H. (2011) Interactions of urate transporter URAT1 in human kidney with uricosuric drugs. *Nephrology (Carlton).* **16**, 156–62

48. Nishioka, K., Sumida, T., Iwatani, M., Kusumoto, A., Ishikura, Y., Hatanaka, H., Yomo, H., Kohda, H., Ashikari, T., Shibano, Y., and Suwa, Y. (2002) Influence of moderate drinking on purine and carbohydrate metabolism. *Alcohol. Clin. Exp. Res.* **26**, 20S–25S

49. Lu, Y., Nakanishi, T., Fukazawa, M., and Tamai, I. (2014) How Does Whisky Lower Serum Urate Level ? *Phyther. Res.* **790**, 788–790

50. Werner, A., Biber, J., and Murer, H. (1991) Cloning and expression of cDNA for a Na / Pi cotransport system of kidney cortex F7. *Proc Natl Acad Sci*. **88**, 9608–9612

51. Chong, S., K, K., HY, Z., and MR., H. (1993) Molecular cloning of the cDNA encoding a human renal sodium phosphate transport protein and its assignment to chromosome 6p21.3-p23. *Genomics*. **18**, 355–599

52. Ishibashi, K., Matsuzaki, T., Takata, K., and Imai, M. (2003) Indentification of a new member of type I Na/phosphate co-transporter in the rat kidney. *Nephron Physiol.* **94**, 10–18

53. Iharada, M., Miyaji, T., Fujimoto, T., Hiasa, M., Anzai, N., Omote, H., and Moriyama, Y. (2010) Type 1 sodium-dependent phosphate transporter (SLC17A1 Protein) is a Cl--dependent urate exporter. *J. Biol. Chem.* **285**, 26107–13

54. Miyaji, T., Kawasaki, T., Togawa, N., Omote, H., and Moriyama, Y. (2013) Type 1 sodium-denpendent phosphate transporter acts as a membrane potential-driven urate exporter. *Curr. Mol. Pharmacol.* **6**, 88–94

55. Hollis-Moffatt, J. E., Phipps-Green, A. J., Chapman, B., Jones, G. T., van Rij, A., Gow, P. J., Harrison, A. a, Highton, J., Jones, P. B., Montgomery, G. W., Stamp, L. K., Dalbeth, N., and Merriman, T. R. (2012) The renal urate transporter SLC17A1 locus: confirmation of association with gout. *Arthritis Res. Ther.* **14**, R92

56. Dehghan, A., Köttgen, A., Yang, Q., Kao, W. H. L., Rivadeneira, F., Levy, D., Hofman, A., Astor, B. C., Benjamin, E. J., Duijn, C. M. Van, Witteman, J. C., Coresh, J., and Fox, C. S. (2008) Assoiation of the three genetic loci with uric acid concentration and risk of gout: a genome-wide association study. *Lancet.* **372**, 1953–1961

57. Jutabha, P., Anzai, N., Wempe, M. F., Wakui, S., Endou, H., and Sakurai, H. (2011) Apical voltage-driven urate efflux transporter NPT4 in renal proximal tubule. *Nucleosides. Nucleotides Nucleic Acids*. **30**, 1302–11

58. Jutabha, P., Anzai, N., Kimura, T., Taniguchi, A., Urano, W., Yamanaka, H., Endou, H., and Sakurai, H. (2011) Functional Analysis of Human Sodium-Phosphate Transporter 4 (NPT4/SLC17A3) Polymorphisms. *J. Pharmacol. Sci.* **115**, 249–253

59. Jones, P. M., and George, a M. (2004) The ABC transporter structure and mechanism: perspectives on recent research. *Cell. Mol. Life Sci.* **61**, 682–99

60. Kathawala, R. J., Gupta, P., Ashby, C. R., and Chen, Z.-S. (2015) The modulation of ABC transporter-mediated multidrug resistance in cancer: A review of the past decade. *Drug Resist. Updat.* **18**, 1–17

61. Leslie, E. M., Deeley, R. G., and Cole, S. P. C. (2005) Multidrug resistance proteins: Role of P-glycoprotein, MRP1, MRP2, and BCRP (ABCG2) in tissue defense. *Toxicol. Appl. Pharmacol.* **204**, 216–237

62. Ravna, A. W., and Sager, G. (2008) Molecular model of the outward facing state of the human multidrug resistance protein 4 (MRP4/ABCC4). *Bioorg. Med. Chem. Lett.* **18**, 3481–3483

63. Juliano, R. L., and Ling, V. (1976) A surface glycoprotein modulating drug permeability in Chinese hamster ovary cell mutants. *Biochim. Biophys. Acta*. **455**, 152–162

64. Kochel, T. J., and Fulton, A. M. (2014) Multiple drug resistance-associated protein 4 (MRP4), prostaglandin transporter (PGT), and 15-hydroxyprostaglandin dehydrogenase (15-PGDH) as determinants of PGE2 levels in cancer. *Prostaglandins Other Lipid Mediat.* **4**, 2–6

65. Van Aubel, R. a M. H., Smeets, P. H. E., van den Heuvel, J. J. M. W., and Russel, F. G. M. (2005) Human organic anion transporter MRP4 (ABCC4) is an efflux pump for the purine end metabolite urate with multiple allosteric substrate binding sites. *Am. J. Physiol. Renal Physiol.* **288**, F327–33

66. Allikmets, R., Schriml, L. M., Hutchinson, A., Romano-Spica, V., and Dean, M. (1998) A human placenta-specific ATP-binding cassette gene (ABCP) on chromosome 4q22 that is involved in multidrug resistance. *Cancer Res.* **58**, 5337–5339

67. Doyle, L., Yang, W., Abruzzo, L., Krogmann, T., Gao, Y., Rishi, A., and Ross, D. (1998) A multidrug resistance transporter from human MCF-7 breast cancer cells. *Proc. Natl. Acad. Sci.* **95**, 15665–15670

68. Wain, H. M., Wain, H. M., Bruford, E. a, Bruford, E. a, Lovering, R. C., Lovering, R. C., Lush, M. J., Lush, M. J., Wright, M. W., Wright, M. W., Povey, S., and Povey, S. (2002) Guidelines for Human Gene Nomenclature. *Online*. **79**, 464–470

69. Miyake, K., Mickley, L., Litman, T., Zhan, Z., Robey, R., Cristensen, B., Brangi, M., Greenberger, L., Dean, M., Fojo, T., and Bates, S. E. (1999) Molecular cloning of cDNAs which are highly overexpressed in mitoxantrone-resistant cells: Demonstration of homology to ABC transport genes. *Cancer Res.* **59**, 8–13

70. Smeets, P. H. E., van Aubel, R. a M. H., Wouterse, A. C., van den Heuvel, J. J. M. W., and Russel, F. G. M. (2004) Contribution of multidrug resistance protein 2 (MRP2/ABCC2) to the renal excretion of p-aminohippurate (PAH) and identification of MRP4 (ABCC4) as a novel PAH transporter. *J. Am. Soc. Nephrol.* **15**, 2828–35

71. Lee, K., Belinsky, M. G., Bell, D. W., Testa, J. R., and Krulr, G. D. (1998) Advances in Brief Isolation of MOAT-B , a Widely Expressed Multidrug Resistance-associated Canalicular Multispecific Organic Anion Transporter-related Transporter. *Image (Rochester, N.Y.)*. **58**, 2741–2747

72. Smeets, P. H. E., Peters, J. G. P., and Russel, F. G. M. (2002) The MRP4 / ABCC4 Gene Encodes a Novel Apical Organic Anion Transporter in Human Kidney Proximal Tubules : Putative Efflux Pump for Urinary cAMP and cGMP. *J Am Soc Nephrol*. **13**, 595–603

73. Caulfield, M. J., Munroe, P. B., O'Neill, D., Witkowska, K., Charchar, F. J., Doblado, M., Evans, S., Eyheramendy, S., Onipinla, A., Howard, P., Shaw-Hawkins, S., Dobson, R. J., Wallace, C., Newhouse, S. J., Brown, M., Connell, J. M., Dominiczak, A., Farrall, M., Lathrop, G. M., Samani, N. J., Kumari, M., Marmot, M., Brunner, E., Chambers, J., Elliott, P., Kooner, J., Laan, M., Org, E., Veldre, G., Viigimaa, M., Cappuccio, F. P., Ji, C., Iacone, R., Strazzullo, P., Moley, K. H., and Cheeseman, C. (2008) SLC2A9 is a high-capacity urate transporter in humans. *PLoS Med.* **5**, 1509–1523

74. Mou, L., Jiang, L., and Hu, Y. (2014) A novel homozygous GLUT9 mutation cause recurrent exercise-induced acute renal failure and posterior reversible encephalopathy syndrome. *J. Nephrol.* **28**, 387–392

75. Jeannin, G., Chiarelli, N., Gaggiotti, M., Ritelli, M., Maiorca, P., Quinzani, S., Verzeletti, F., Possenti, S., Colombi, M., and Cancarini, G. (2014) Recurrent exercise-induced acute renal failure in a young Pakistani man with severe renal hypouricemia and SLC2A9 compound heterozygosity. *BMC Med. Genet.* **15**, 1–8

76. Dinour, D., Gray, N. K., Campbell, S., Shu, X., Sawyer, L., Richardson, W., Rechavi, G., Amariglio, N., Ganon, L., Sela, B.-A., Bahat, H., Goldman, M., Weissgarten, J., Millar, M. R., Wright, A. F., and Holtzman, E. J. (2010) Homozygous SLC2A9 mutations cause severe renal hypouricemia. *J. Am. Soc. Nephrol.* **21**, 64–72

77. Dinour, D., Gray, N. K., Ganon, L., Knox, A. J. S., Shalev, H., Sela, B. A., Campbell, S., Sawyer, L., Shu, X., Valsamidou, E., Landau, D., Wright, A. F., and Holtzman, E. J. (2012) Two novel homozygous SLC2A9 mutations cause renal hypouricemia type 2. *Nephrol. Dial. Transplant.* **27**, 1035–1041

78. Stiburkova, B., Ichida, K., and Sebesta, I. (2011) Novel homozygous insertion in SLC2A9 gene caused renal hypouricemia. *Mol. Genet. Metab.* **102**, 430–435

79. Stiburkova, B., Taylor, J., Marinaki, A. M., and Sebesta, I. (2012) Acute kidney injury in two children caused by renal hypouricaemia type 2. *Pediatr. Nephrol.* **27**, 1411–1415

80. Brett, K. E., Ferraro, Z. M., Holcik, M., and Adamo, K. B. (2015) Prenatal physical activity and diet composition affect the expression of nutrient transporters and mTOR signaling molecules in the human placenta. *Placenta*. **36**, 204–212

81. Hedicer, A., Budarf, M. L., Emanuel, B. S., Mohandas, T. K., and Wright, E. M. (1989) Assignment of the human intestinal Na + / Glucose cotransporter transporter. *Genomics*. **4**, 297–300

82. Wright, E., Turk, E., Hager, K., Lescale-Matys, L., Hirayama, B., Supplisson, S., and Loo, D. (1992) The Na+/glucose cotransporter (SGLT1). *Acta. Phsiol. Scand. Suppl.* **607**, 201–207

83. Pao, S. S., Paulsen, I. T., and Saier, M. H. (1998) Major facilitator superfamily. *Microbiol. Mol. Biol. Rev.* **62**, 1–34

84. Saier, M. H., Beatty, J. T., Goffeau, a, Harley, K. T., Heijne, W. H., Huang, S. C., Jack, D. L., Jähn, P. S., Lew, K., Liu, J., Pao, S. S., Paulsen, I. T., Tseng, T. T., and Virk, P. S. (1999) The major facilitator superfamily. *J. Mol. Microbiol. Biotechnol.* **1**, 257–279

85. Yan, N. (2013) Structural advances for the major facilitator superfamily (MFS) transporters. *Trends Biochem. Sci.* **38**, 151–159

86. Brown, M. H., and Skurray, R. a (2001) Staphylococcal multidrug efflux protein QacA. *J. Mol. Microbiol. Biotechnol.* **3**, 163–170

87. Kubota, T., Tanaka, Y., Takemoto, N., Hiraga, K., Yukawa, H., and Inui, M. (2014) Identification and expression analysis of a gene encoding a shikimate transporter of Corynebacterium glutamicum. *Microbiology*. **161**, 254–263

88. Zhao, Y., Mao, G., Liu, M., Zhang, L., Wang, X., and Zhang, X. C. (2014) Crystal structure of the E. coli peptide transporter YbgH. *Structure*. **22**, 1152–1160

89. Rivas, C. I., Zúñiga, F. a., Salas-Burgos, a., Mardones, L., Ormazabal, V., and Vera, J. C. (2008) Vitamin C transporters. *J. Physiol. Biochem.* **64**, 357–376

90. Augustin, R. (2010) The protein family of glucose transport facilitators: It's not only about glucose after all. *IUBMB Life*. **62**, 315–33

91. Manolescu, A. R., Witkowska, K., Kinnaird, A., Cessford, T., and Cheeseman, C. (2007) Facilitated hexose transporters: new perspectives on form and function. *Physiology*. **22**, 234–240

92. Kasahara, M., and Hinkle, P. C. (1977) Reconstitution and purificaton of the D-Glucose transporter from human erythrocytes. *J. Biol. Chem.* **252**, 7384–7390

93. Sogin, D. C., and Hinkle, P. C. (1978) Characterization of the glucose transporter from human erythrocytes. *J. Supramol. Struct.* **8**, 447–453

94. Mueckler, M., Caruso, C., Baldwin, S. a, Panico, M., Blench, I., Morris, H. R., Allard, W. J., Lienhard, G. E., and Lodish, H. F. (1985) Sequence and structure of a human glucose transporter. *Science*. **229**, 941–945

95. Thorens, B., Sarkar, H. K., Kaback, H. R., and Lodish, H. F. (1988) Cloning and functional expression in bacteria of a novel glucose transporter present in liver, intestine, kidney, and beta-pancreatic islet cells. *Cell*. **55**, 281–290

96. Fukumoto, H., Kayano, T., and Buse, J. (1989) Cloning and characterization of the major insulin-responsive glucose transporter expressed in human skeletal muscle and other insulin-responsive tissues. *J. Biol. Chem.* **264**, 7776–7779

97. Colville, C. A., Seatter, M. J., Jess, T. J., Gould, G. W., and Thomas, H. M. (1993) Kinetic analysis of the liver-type (GLUT2) and brain-type (GLUT3) glucose transporters in Xenopus oocytes: substrate specificities and effects of transport inhibitors. *Biochem J*. **290**, 701–706

98. Cheeseman, C. (1993) GLUT2 is the transporter for fructose across the rat intestinal basolateral membrane. *Gastroenterology.* **105**, 1050–1056

99. Craik, J. D., and Elliott, K. R. (1979) Kinetics of 3-O-methyl-D-glucose transport in isolated rat hepatocytes. *Biochem. J.* **182**, 503–508

100. Kayanos, T., Fukumotoo, H., Eddyl, R. L., Fan, Y., Byersl, M. G., Showsl, T. B., and Bell, G. I. (1988) Evidence for a Family of Human Glucose Transporter-like Proteins. *Biol. Chem.* **263**, 15245–15248

101. Yano H, Seino Y, Inagaki N, Hinokio Y, Yamamoto T, Yasuda K, Masuda K, Someya Y, I. H. (1991) Tissue distribution and species difference of the brain type glucose transporter (GLUT3). *Biochem Biophys Res Commun.* **174**, 470–477

102. Shepherd, P. R., Gould, G. W., Colville, C. a., McCoid, S. C., Gibbs, E. M., and Kahn, B. B. (1992) Distribution of GLUT3 glucose transporter protein in human tissues. *Biochem. Biophys. Res. Commun.* **188**, 149–154

103. Wu, X., and Freeze, H. H. (2002) GLUT14, a duplicon of GLUT3, is specially expressed in testis as alternative splice forms. *Science*. **80**, 553–557

104. Clancy, B. M., and Czech, M. P. (1990) Hexose transport stimulation and membrane redistribution of glucose transporter isoforms in response to cholera toxin, dibutyryl cyclic AMP, and insulin in 3T3-L1 adipocytes. *J. Biol. Chem.* **265**, 12434–12443

105. Kayano, T., CF, B., Fukumoto, H., Gould, G., Fan, Y., Eddy, R., Byers, M., Shows, T., Seino, S., and Bell, G. (1990) Human facilitative glucose transporters. Isolation, functional characterization, and gene localization of cDNAs encoding an isoform (GLUT5) expressed in small intestine, kidney, muscle, and adipose tissue and an unusual glucose transporter pseudogene-like. **265**, 13276–13282

106. Corpe, C. P., Basaleh, M. M., Affleck, J., Gould, G., Jess, T. J., and Kellett, G. L. (1996) The regulation of GLUT5 and GLUT2 activity in the adaptation of intestinal brush-border fructose transport in diabetes. *Pflugers Arch. Eur. J. Physiol.* **432**, 192–201

107. Waddell, I. D., Zomerschoe, a G., Voice, M. W., and Burchell, A. (1992) Cloning and expression of a hepatic microsomal glucose transport protein. Comparison with liver plasma-membrane glucose-transport protein GLUT 2. *Biochem. J.* **286 (Pt 1)**, 173–177

108. Burchell, A. (1998) A re-evaluation of GLUT 7. *Biochem. J.* **331**, 973

109. Li, Q., Manolescu, A., Ritzel, M., Yao, S., Slugoski, M., Young, J. D., Chen, X.-Z., and Cheeseman, C. I. (2004) Cloning and functional characterization of the human GLUT7 isoform SLC2A7 from the small intestine. *Am. J. Physiol. Gastrointest. Liver Physiol.* **287**, G236–G242

110. Phay, J. E., Hussain, H. B., and Moley, J. F. (2000) Cloning and expression analysis of a novel member of the facilitative glucose transporter family , SLC2A9 (GLUT9). *Genomics*. **66**, 217–220

111. Kimura, T., Takahashi, M., Yan, K., and Sakurai, H. (2014) Expression of SLC2A9 isoforms in the kidney and their localization in polarized epithelial cells. *PLoS One*. **9**, e84996

112. Doege, H., Bocianski, a, Joost, H. G., and Schürmann, a (2000) Activity and genomic organization of human glucose transporter 9 (GLUT9), a novel member of the family of sugar-transport facilitators predominantly expressed in brain and leucocytes. *Biochem. J.* **350 Pt 3**, 771–776

113. Lisinski, I., Schürmann, a, Joost, H. G., Cushman, S. W., and Al-Hasani, H. (2001) Targeting of GLUT6 (formerly GLUT9) and GLUT8 in rat adipose cells. *Biochem. J.* **358**, 517–522

114. Vitart, V., Rudan, I., Hayward, C., Gray, N. K., Floyd, J., Palmer, C. N. a, Knott, S. a, Kolcic, I., Polasek, O., Graessler, J., Wilson, J. F., Marinaki, A., Riches, P. L., Shu, X., Janicijevic, B., Smolej-Narancic, N., Gorgoni, B., Morgan, J., Campbell, S., Biloglav, Z., Barac-Lauc, L., Pericic, M., Klaric, I. M., Zgaga, L., Skaric-Juric, T., Wild, S. H., Richardson, W. a, Hohenstein, P., Kimber, C. H., Tenesa, A., Donnelly, L. a, Fairbanks, L. D., Aringer, M., McKeigue, P. M., Ralston, S. H., Morris, A. D., Rudan, P., Hastie, N. D., Campbell, H., and Wright, A. F. (2008) SLC2A9 is a newly identified urate transporter influencing serum urate concentration, urate excretion and gout. *Nat. Genet.* **40**, 437–442

115. Doege, H., Bocianski, a, Scheepers, a, Axer, H., Eckel, J., Joost, H. G., and Schürmann, a (2001) Characterization of human glucose transporter (GLUT) 11 (encoded by SLC2A11), a novel sugar-transport facilitator specifically expressed in heart and skeletal muscle. *Biochem. J.* **359**, 443–449

116. Doege, H., Schürmann, A., Bahrenberg, G., Brauers, A., and Joost, H. G. (2000) GLUT8, a novel member of the sugar transport facilitator family with glucose transport activity. *J. Biol. Chem.* **275**, 16275–16280

117. Ibberson, M., Uldry, M., and Thorens, B. (2000) GLUTX1, a novel mammalian glucose transporter expressed in the central nervous system and insulin-sensitive tissues. *J. Biol. Chem.* **275**, 4607–4612

118. McVie-Wylie, a J., Lamson, D. R., and Chen, Y. T. (2001) Molecular cloning of a novel member of the GLUT family of transporters, SLC2a10 (GLUT10), localized on chromosome 20q13.1: a candidate gene for NIDDM susceptibility. *Genomics*. **72**, 113–117

119. Dawson, P. a, Mychaleckyj, J. C., Fossey, S. C., Mihic, S. J., Craddock, a L., and Bowden, D. W. (2001) Sequence and functional analysis of GLUT10: a glucose transporter in the Type 2 diabetes-linked region of chromosome 20q12-13.1. *Mol. Genet. Metab.* **74**, 186–199

120. Rogers, S., Macheda, M., Docherty, S., Carty, M., Hendderson, M., Soeller, W., Gibbs, E., James, D., and Best, J. (2002) Identification of a novel glucose transporter-like protein GLUT-12. *Appl. Phys. Endocrinol Metab*. **283**, E733–738

121. Wilson-O'Brien, A. L., DeHaan, C. L., and Rogers, S. (2008) Mitogen-stimulated and rapamycin-sensitive glucose transporter 12 targeting and functional glucose transport in renal epithelial cells. *Endocrinology*. **149**, 917–924

122. Razeghi, P., Young, M. E., Alcorn, J. L., Moravec, C. S., Frazier, O. H., and Taegtmeyer, H. (2001) Metabolic gene expression in fetal and failing human heart. *Circulation*. **104**, 2923–2931

123. Rogers, S., Docherty, S. E., Slavin, J. L., Henderson, M. a., and Best, J. D. (2003) Differential expression of GLUT12 in breast cancer and normal breast tissue. *Cancer Lett.* **193**, 225–233

124. Gude, N. M., Stevenson, J. L., Rogers, S., Best, J. D., Kalionis, B., Huisman, M. a., Erwich, J. J. H. M., Timmer, a., and King, R. G. (2003) GLUT12 expression in human placenta in first trimester and term. *Placenta*. **24**, 566–570

125. Rogers, S., Chandler, J. D., Clarke, A. L., Petrou, S., and Best, J. D. (2003) Glucose transporter GLUT12-functional characterization in Xenopus laevis oocytes. *Biochem. Biophys. Res. Commun.* **308**, 422–426

126. Uldry, M., Ibberson, M., Horisberger, J. D., Chatton, J. Y., Riederer, B. M., and Thorens, B. (2001) Identification of a mammalian H+-myo-inositol symporter expressed predominantly in the brain. *EMBO J.* **20**, 4467–4477

127. Hresko, R. C., Kruse, M., Strube, M., and Mueckler, M. (1994) Topology of the GLUT1 glucose transporter deduced from glycosylation scanning mutagenesis. *J. Biol. Chem.* **269**, 20482–20488

128. Davies, A., Meeran, K., Cairns, M., and Baldwin, S. (1987) Peptide-specific antibodies as probes of the orientation of the glucose transporter in the human erythrocyte membrane. *J. Biol. Chem.* **262**, 9347–9352

129. Mueckler, M. (1994) Facilitative glucose transporters. *Eur. J. Biochem.* **219**, 713–725

130. Cairn, M., Alvarez, J., Panico, M., Gibbs, A., Morris, H., Chapman, D., and Baldwin, S. (1987) Investigation of the structure and function of the human erythrocyte glucose transporter by proteolytic dissection. *Biochim Biophys Acta.* **905**, 295–310

131. Zhao, F.-Q., and Keating, A. F. (2007) Functional properties and genomics of glucose transporters. *Curr. Genomics*. **8**, 113–128

132. Mori, H., Hashiramoto, M., Clark, A. E., Yang, J., Muraoka, A., Tamori, Y., Kasuga, M., and Holman, G. D. (1994) Substitution of tyrosine 293 of GLUT1 locks the transporter into an outward facing conformation. *J. Biol. Chem.* **269**, 11578–11583

133. Moris, H., and Muraokas, A. (1994) Substitution at Pro385 of GLUTl Perturbs the Glucose Transport Function by Reducing Conformational Flexibility. **269**, 2982–2986

134. Schürmann, A., Doege, H., Ohnimus, H., Monser, V., Buchs, A., and Joost, H. G. (1997) Role of conserved arginine and glutamate residues on the cytosolic surface of glucose transporters for transporter function. *Biochemistry*. **36**, 12897–12902

135. Olson, a L., and Pessin, J. E. (1996) Structure, function, and regulation of the mammalian facilitative glucose transporter gene family. *Annu. Rev. Nutr.* **16**, 235–256

136. Thorens, B., and Mueckler, M. (2010) Glucose transporters in the 21st Century. *Am. J. Physiol. Endocrinol. Metab.* **298**, 141–145

137. Mueckler, M., Weng, W., and Kruse, M. (1994) Glutamine 161 of Glut1 glucose transporter is critical for transport activity and exofacial ligand binding. *J. Biol. Chem.* **269**, 20533–20538

138. Doege, H., Schürmann, A., Ohnimus, H., Monser, V., Holman, G. D., and Joost, H. G. (1998) Serine-294 and threonine-295 in the exofacial loop domain between helices 7 and 8 of glucose transporters (GLUT) are involved in the conformational alterations during the transport process. *Biochem. J.* **329**, 289–293

139. Garcia, J. C., Strube, M., Leingang, K., Keller, K., and Mueckler, M. M. (1992) Amino acid substitutions at tryptophan 388 and tryptophan 412 of the HepG2 (Glut1) glucose transporter inhibit transport activity and targeting to the plasma membrane in Xenopus oocytes. *J. Biol. Chem.* **267**, 7770–7776

140. Schürmann, A., Keller, K., Monden, I., Brown, F. M., Wandel, S., Shanahan, M. F., and Joost, H. G. (1993) Glucose transport activity and photolabelling with 3-[125I]iodo-4-azidophenethylamido-7-O-succinyldeacetyl (IAPS)-forskolin of two mutants at tryptophan-388 and -412 of the glucose transporter GLUT1: dissociation of the binding domains of forskolin and gl. *Biochem. J.* **290**, 497–501

141. Seatter, M. J., De La Rue, S. a., Porter, L. M., and Gould, G. W. (1998) QLS motif in transmembrane helix VII of the glucose transporter family interacts with the C-1 position of D-glucose and is involved in substrate selection at the exofacial binding site. *Biochemistry*. **37**, 1322–1326

142. Joost, H., and Thorens, B. (2001) The extended GLUT-family of sugar/polyol transport facilitators: nomenclature, sequence characteristics, and potential function of its novel members (Review). *Mol. Membr. Biol.* **18**, 257–264

143. Manolescu, A. R., Augustin, R., Moley, K., and Cheeseman, C. (2007) A highly conserved hydrophobic motif in the exofacial vestibule of fructose transporting SLC2A proteins acts as a critical determinant of their substrate selectivity. *Mol. Membr. Biol.* **24**, 455–463

144. Manolescu, A., Salas-Burgos, A. M., Fischbarg, J., and Cheeseman, C. I. (2005) Identification of a hydrophobic residue as a key determinant of fructose transport by the facilitative hexose transporter SLC2A7 (GLUT7). *J. Biol. Chem.* **280**, 42978–42983

145. Long, W., Panwar, P., Witkowska, K., Wong, K., O'Neill, D., Chen, X.-Z., Lemieux, M. J., and Cheeseman, C. I. (2015) Critical Roles of Two Hydrophobic Residues within Human Glucose Transporter 9 (hSLC2A9) in Substrate Selectivity and Urate Transport. *J. Biol. Chem.* **290**, 15292–15303

146. Asano, T., Katagiri, H., Takata, K., Lin, J. L., Ishihara, H., Inukai, K., Tsukuda, K., Kikuchi, M., Hirano, H., Yazaki, Y., and Oka, Y. (1991) The role of N-glycosylation of GLUT1 for glucose transport activity. *J. Biol. Chem.* **266**, 24632–24636

147. Alvarez, J., Lee, D. C., Baldwin, S. a, and Chapman, D. (1987) Fourier transform infrared spectroscopic study of the structure and conformational changes of the human erythrocyte glucose transporter. *J. Biol. Chem.* **262**, 3502–3509

148. Chin, J. J., Jung, E. K., Chen, V., and Jung, C. Y. (1987) Structural basis of human erythrocyte glucose transporter function in proteoliposome vesicles: circular dichroism measurements. *Proc. Natl. Acad. Sci. U. S. A.* **84**, 4113–4116

149. Heinze, M., Monden, I., and Keller, K. (2004) Cysteine-scanning mutagenesis of transmembrane segment 1 of glucose transporter GLUT1: extracellular accessibility of helix positions. *Biochemistry*. **43**, 931–936

150. Mueckler, M., and Makepeace, C. (2002) Analysis of transmembrane segment 10 of the Glut1 glucose transporter by cysteine scanning mutagenesis and substituted cysteine accessibility. *J. Biol. Chem.* **277**, 3498–3503

151. Mueckler, M., and Makepeace, C. (1999) Transmembrane segment 5 of the Glut1 glucose transporter is an amphipathic helix that forms part of the sugar permeation pathway. *J. Biol. Chem.* **274**, 10923–10926

152. Mueckler, M., Roach, W., and Makepeace, C. (2004) Transmembrane segment 3 of the Glut1 glucose transporter is an outer helix. *J. Biol. Chem.* **279**, 46876–46881

153. Mueckler, M., and Makepeace, C. (2008) Transmembrane segment 6 of the Glut1 glucose transporter is an outer helix and contains amino acid side chains essential for transport activity. *J. Biol. Chem.* **283**, 11550–11555

154. Hruz, P. W., and Mueckler, M. M. (1999) Cysteine-scanning mutagenesis of transmembrane segment 7 of the GLUT1 facilitative glucose transporter. *Biochemistry*. **274**, 36176–36180

155. Mueckler, M., and Makepeace, C. (2006) Transmembrane segment 12 of the Glut1 glucose transporter is an outer helix and is not directly involved in the transport mechanism. *J. Biol. Chem.* **281**, 36993–36998

156. Mueckler, M., and Makepeace, C. (2005) Cysteine-scanning mutagenesis and substituted cysteine accessibility analysis of transmembrane segment 4 of the Glut1 glucose transporter. *J. Biol. Chem.* **280**, 39562–39568

157. Mueckler, M., and Makepeace, C. (2003) Analysis of Transmembrane Segment 8 of the GLUT1 Glucose Transporter by Cysteine-scanning Mutagenesis and Substituted Cysteine Accessibility. *J. Biol. Chem.* **279**, 10494–10499

158. Mueckler, M., and Makepeace, C. (2009) Model of the exofacial substrate-binding site and helical folding of the human Glut1 glucose transporter based on scanning mutagenesis. *Biocchemistry*. **48**, 5934–5942

159. Hruz, P. W., and Mueckler, M. M. (2001) Structural analysis of the GLUT1 facilitative glucose transporter. *Mol. Membr. Biol.* **18**, 183–193

160. Salas-Burgos, A., Iserovich, P., Zuniga, F., Vera, J. C., and Fischbarg, J. (2004) Predicting the three-dimensional structure of the human facilitative glucose transporter glut1 by a novel evolutionary homology strategy: insights on the molecular mechanism of substrate migration, and binding sites for glucose and inhibitory molecules. *Biophys. J.* **87**, 2990–2999

161. Saier, M. H. (1996) Phylogenetic approaches to the identification and characterization of protein families and superfamilies. *Microb. Comp. Genomics*. **1**, 129–150

162. Abramson, J., Smirnova, I., Kasho, V., Verner, G., Kaback, H. R., and Iwata, S. (2003) Structure and mechanism of the lactose permease of Escherichia coli. *Science*. **301**, 610–615

163. Mueckler, M., and Makepeace, C. (2009) Model of the exofacial substrate-binding site and helical folding of the human Glut1 glucose transporter based on scanning mutagenesis. *Biochemistry*. **48**, 5934–5942

164. Lemieux, M. J. (2007) Eukaryotic major facilitator superfamily transporter modeling based on the prokaryotic GlpT crystal structure. *Mol. Membr. Biol.* **24**, 333–341

165. Dwyer, D. S. (2001) Model of the 3-D structure of the GLUT3 glucose transporter and molecular dynamics simulation of glucose transport. *Proteins*. **42**, 531–541

166. Mohan S, S., Perry, J. J. P., Poulose, N., Nair, B. G., and Anilkumar, G. (2009) Homology modeling of GLUT4, an insulin regulated facilitated glucose transporter and docking studies with ATP and its inhibitors. *J. Biomol. Struct. Dyn.* **26**, 455–464

167. Madej, M. G., Sun, L., Yan, N., and Kaback, H. R. (2014) Functional architecture of MFS D-glucose transporters. *Proc. Natl. Acad. Sci. U. S. A.* **111**, E719–27

168. Clémençon, B., Lüscher, B. P., Fine, M., Baumann, M. U., Surbek, D. V., Bonny, O., and Hediger, M. a. (2014) Expression, Purification, and Structural Insights for the Human Uric Acid Transporter, GLUT9, Using the Xenopus laevis Oocytes System. *PLoS One*. **9**, e108852

169. Chang, G., Spencer, R. H., Lee, a T., Barclay, M. T., and Rees, D. C. (1998) Structure of the MscL homolog from Mycobacterium tuberculosis: a gated mechanosensitive ion channel. *Science*. **282**, 2220–2226

170. Deng, D., Xu, C., Sun, P., Wu, J., Yan, C., Hu, M., and Yan, N. (2014) Crystal structure of the human glucose transporter GLUT1. *Nature*. **510**, 121–5

171. Sun, L., Zeng, X., Yan, C., Sun, X., Gong, X., Rao, Y., and Yan, N. (2012) Crystal structure of a bacterial homologue of glucose transporters GLUT1–4. *Nature*. **490**, 361–366

172. Iancu, C. V, Zamoon, J., Bum, S., Aleshin, A., and Choe, J. (2013) Crystal structure of a glucose / H + symporter and its mechanism of action. *Proc. Natl. Acad. Sci.* **110**, 17862–17867

173. Jayaraj, V., Suhanya, R., Vijayasarathy, M., Anandagopu, P., and Rajasekaran, E. (2009) Role of large hydrophobic residues in proteins. *Bioinformation*. **3**, 409–412

174. Mueckler, M., and Makepeace, C. (1997) Identification of an amino acid residue that lies between the exofacial vestibule and exofacial substrate-binding site of the glutl sugar permeation pathway. *J. Biol. Chem.* **272**, 30141–30146

175. Carruthers, a (1990) Facilitated diffusion of glucose. *Physiol. Rev.* **70**, 1135–1176

176. Wellner, M., Monden, I., and Keller, K. (1995) From triple cysteine mutants to the cysteine-less glucose transporter GLUT1: a functional analysis. *FEBS Lett.* **370**, 19–22

177. Due, A. D., Cook, J. A., Fletcher, S. J., Zhi-Chao, Q., Powers, A. C., and May, James, M. (1995) A “cysteineless” GLUT1 glucose transporter has normal function when expressed in Xenopus oocytes. *Biochem. Biophys. Res. Commun.* **208**, 590–596

178. Fisher, R., and Parsons, D. (1953) Glucose movements across the wall of the rat small intestine. *J Physiol.* **119**, 210–223

179. Fisher, R., and Parsons, D. (1953) Galactose absorption from the surviving small intestine of the rat. *J Physiol*. **119**, 224–232

180. Widdas, W. (1952) Inability of diffusion to accoundt for placental glucose transfer in the sheep and consideration of the kinetics of a possible carrier transfer. *J Physiol*. **118**, 23–39

181. Neame, K., and Richards, T. (1972) *Elementary kinetics of membrane carrier transport.*, 1st Ed., Oxford, Blackwell Scientific Publications, London

182. Naftalin, R., and Holman, G. (1977) *Membrane transport in red cells.* (Ellory, J., and Lew, V. eds), Academic Press, New York

183. Regen, D., and Tarpley, H. (1974) Anomalous transport kinetics and the glucose carrier hypothesis. *Biochem. Biophys. Acta.* **339**, 218–233

184. Eilam, Y. (1975) Two-carrier models for mediated transport. 1. Theoretical analysis of several two-carrier models. *Biochim. Biophys. Acta*. **401**, 349–363

185. Naftalin, R. (1970) Model for sugar transport across red cell membrane without carriers. *Biochim. Biophys. Acta.* **211**, 65–78

186. Lieb, W. R., and Stein, W. D. (1970) Quantitative predictions of a noncarrier model for glucose transport across the human red cell membrane. *Biophys. J.* **10**, 585–609

187. LeFevre, P. G. (1973) A model for erythrocyte sugar transport based on substrate-conditioned “introversion” of binding sites. *J. Membr. Biol.* **11**, 1–19

188. Mueckler, M., and Thorens, B. (2013) The SLC2(GLUT) family of membrane transporters. *Mol Asp. Med*. **34**, 121–138

189. Naftalin, R. J. (2008) Osmotic water transport with glucose in GLUT2 and SGLT. *Biophys. J.* **94**, 3912–3923

190. Cura, A. J., and Carruthers, A. (2012) AMP kinase regulation of sugar transport in brain capillary endothelial cells during acute metabolic stress. *AJP Cell Physiol.* **303**, C806–C814

191. Vollers, S. S. (2013) Identification and Analysis of the Domain Required for Trans-Acceleration Kinetics in the Human Glucose Transporter GLUT1 : A Dissertation. *Univ. Massachusetts Med. Sch. GSBS Diss. Thesis.*

192. Carruthers, A., DeZutter, J., Ganguly, A., and Devaskar, S. U. (2009) Will the original glucose transporter isoform please stand up! *Am. J. Physiol. Endocrinol. Metab.* **297**, E836–E848

193. Toyoda, N., Flanagan, J. E., and Kono, T. (1987) Reassessment of insulin effects on the V(max) and K(m) values of hexose transport in isolated rat epididymal adipocytes. *J. Biol. Chem.* **262**, 2737–2745

194. Taylor, L., and Holman, G. (1981) Symmetrical kinetic parameters for 3-O-methyl-D-glucose transport in adipocytes in the presence and in the absence of insulin. *Biochim Biophys Acta.* **642**, 325–335

195. Pessino, a., Hebert, D. N., Woon, C. W., Harrison, S. a., Clancy, B. M., Buxton, J. M., Carruthers, a., and Czech, M. P. (1991) Evidence that functional erythrocyte-type glucose transporters are oligomers. *J. Biol. Chem.* **266**, 20213–20217

196. Zottola, R., Cloherty, E., Coderre, P., Hansen, A., Hebert, D., and Carruther, A. (1995) Glucose transporter function is controlled by transporter oligomeric structure. A single, intramolecular disulfide promotes GLUT1 tetramerization. *Biochemistry*. **34**, 9734–9747

197. De Zutter, J. K., Levine, K. B., Deng, D., and Carruthers, A. (2013) Sequence determinants of GLUT1 oligomerization: Analysis by homology-scanning mutagenesis. *J. Biol. Chem.* **288**, 20734–20744

198. Lemieux, M. J., Huang, Y., and Wang, D. N. (2005) Crystal structure and mechanism of GlpT, the glycerol-3-phosphate transporter from E. coli. *J. Electron Microsc. (Tokyo).* **54**, 43–46

199. Dang, S., Sun, L., Huang, Y., Lu, F., Liu, Y., Gong, H., Wang, J., and Yan, N. (2010) Structure of a fucose transporter in an outward-open conformation. *Nature*. **467**, 734–738

200. Jardetzky, O. (1966) Simple allosteric model for membrane pumps. *Nature*. **211**, 969–970

201. Park, C. R., Crofford, O. B., and Kono, T. (1968) Mediated (nonactive) transport of glucose in Mammalian cells and its regulation. *J. Gen. Physiol.* **52**, 296–318

202. Rosenberg, T., and Wilbrandt, W. (1957) Uphill transport induced by counterflow. *J Gen Physiol*. **41**, 289–296

203. Maher, F., Davies-Hill, T., and Simpson, I. (1996) Substrate specificity and kinetic parameters of GLUT3 in rat cerebellar granule neurons. *J. Biol. Chem.* **315**, 827–831

204. Vollers, S. S., and Carruthers, A. (2012) Sequence determinants of GLUT1-mediated accelerated-exchange transport: Analysis by homology-scanning mutagenesis. *J. Biol. Chem.* **287**, 42533–42544

205. Liu, Q., Vera, J. C., Peng, H., and Golde, D. W. (2001) The predicted ATP-binding domains in the hexose transporter GLUT1 critically affect transporter activity. *Biochemistry*. **40**, 7874–7881

206. Sweet, I. R., and Matschinsky, F. M. (1997) Are there kinetic advantages of GLUT2 in pancreatic glucose sensing? *Diabetologia*. **40**, 112–9

207. Clark, A. E., Holman, G. D., and Kozka, I. J. (1991) Determination of the rates of appearance and loss of glucose transporters at the cell surface of rat adipose cells. *Biochem. J.* **278**, 235–241

208. Haney, P. M., Slot, J. W., Piper, R. C., James, D. E., and Mueckler, M. (1991) Intracellular targeting of the insulin-regulatable glucose transporter (GLUT4) is isoform specific and independent of cell type. *J. Cell Biol.* **114**, 689–699

209. Hudson, A. W., Ruiz, M., and Birnbaum, M. J. (1992) Isoform-specific subcellular targeting of glucose transporters in mouse fibroblasts. *J. Cell Biol.* **116**, 785–797

210. Piper, R. C., Tai, C., Slot, J. W., Hahn, C. S., Rice, C. M., Huang, H., and James, D. E. (1992) The efficient intracellular sequestration of the insulin-regulatable glucose transporter (GLUT-4) is conferred by the NH2 terminus. *J. Cell Biol.* **117**, 729–743

211. Shibasaki, Y., Asano, T., Lin, J. L., Tsukuda, K., Katagiri, H., Ishihara, H., Yazaki, Y., and Oka, Y. (1992) Two glucose transporter isoforms are sorted differentially and are expressed in distinct cellular compartments. *Biochem. J.* **281**, 829–834

212. Verhey, K. J., Hausdorff, S. F., and Birnbaum, M. J. (1993) Identification of the carboxy terminus as important for the isoform-specific subcellular targeting of glucose transporter proteins. *J. Cell Biol.* **123**, 137–147

213. Riskin, A., Nannegari, V. H., and Mond, Y. (2008) Acute effectors of GLUT1 glucose transporter subcellular targeting in CIT3 mouse mammary epithelial cells. *Pediatr. Res.* **63**, 56–61

214. Czech, M. P., Chawla, A., Woon, C. W., Buxton, J., Armoni, M., Tang, W., Joly, M., and Corvera, S. (1993) Exofacial epitope-tagged glucose transporter chimeras reveal COOH-terminal sequences governing cellular localization. *J. Cell Biol.* **123**, 127–135

215. Andrisse, S., Patel, G. D., Chen, J. E., Webber, A. M., Spears, L. D., Koehler, R. M., Robinson-Hill, R. M., Ching, J. K., Jeong, I., and Fisher, J. S. (2013) ATM and GLUT1-S490 Phosphorylation Regulate GLUT1 Mediated Transport in Skeletal Muscle. *PLoS One*. **8**, e66027–66041

216. Inukai, K., Shewan, A. M., Pascoe, W. S., Katayama, S., James, D. E., and Oka, Y. (2004) Carboxy terminus of glucose transporter 3 contains an apical membrane targeting domain. *Mol. Endocrinol.* **18**, 339–349

217. Yang, J., and Holman, G. D. (1993) Comparison of GLUT4 and GLUT1 subcellular trafficking in basal and insulin-stimulated 3T3-L1 cells. *J. Biol. Chem.* **268**, 4600–4603

218. Yang, J., Clark, A. E., Harrison, R., Kozka, I. J., and Holman, G. D. (1992) Trafficking of glucose transporters in 3T3-L1 cells trafficking proteins. *Biochem J*. **281**, 809–817

219. Egert, S., Nguyen, N., and Schwaiger, M. (1999) Myocardial glucose transporter GLUT1: translocation induced by insulin and ischemia. *J. Mol. Cell. Cardiol.* **31**, 1337–1344

220. El-Jack, a K., Kandror, K. V, and Pilch, P. F. (1999) The formation of an insulin-responsive vesicular cargo compartment is an early event in 3T3-L1 adipocyte differentiation. *Mol. Biol. Cell*. **10**, 1581–1594

221. Mueckler, M. (1992) The molecular biology of mammalian glucose transporters. *Curr. Opin. Nephrol. Hypertens.* **1**, 12–20

222. Roach, W., and Plomann, M. (2007) PACSIN3 overexpression increases adipocyte glucose transport through GLUT1. *Biochem. Biophys. Res. Commun.* **355**, 745–750

223. Nakayama, T., Kamiguchi, H., and Akagawa, K. (2012) Syntaxin 1C, a soluble form of syntaxin, attenuates membrane recycling by destabilizing microtubules. *J. Cell Sci.* **125**, 817–830

224. Caliceti, C., Zambonin, L., Prata, C., Vieceli Dalla Sega, F., Hakim, G., Hrelia, S., and Fiorentini, D. (2012) Effect of plasma membrane cholesterol depletion on glucose transport regulation in leukemia cells. *PLoS One*. **7**, e421461–11

225. Fang, J., Zhou, S., Fan, J., and Yan, S. (2015) Roles of glucose transporter-1 and the phosphatidylinositol 3-kinase/protein kinase B pathway in cancer radioresistance. *Mol. Med. Rep.* **11**, 1573–1578

226. Wofford, J. a, Wieman, H. L., Jacobs, S. R., Zhao, Y., Rathmell, J. C., and Jeffrey, C. (2008) IL-7 promotes Glut1 trafficking and glucose uptake via STAT5-mediated activation of Akt to support T cell survival. *Blood*. **111**, 2101–2112

227. Zambrano, A., Jara, E., Murgas, P., Jara, C., Castro, M. a., Angulo, C., and Concha, I. I. (2010) Cytokine stimulation promotes increased glucose uptake via translocation at the plasma membrane of GLUT1 in HEK293 cells. *J. Cell. Biochem.* **110**, 1471–1480

228. Sommermann, T. G., O'Neill, K., Plas, D. R., and Cahir-McFarland, E. (2011) IKKβ and NF-κB transcription govern lymphoma cell survival through AKT-induced plasma membrane trafficking of GLUT1. *Cancer Res.* **71**, 7291–7300

229. Gonnella, R., Santarelli, R., Farina, A., Granato, M., D'Orazi, G., Faggioni, A., and Cirone, M. (2013) Kaposi sarcoma associated herpesvirus (KSHV) induces AKT hyperphosphorylation, bortezomib-resistance and GLUT-1 plasma membrane exposure in THP-1 monocytic cell line. *J. Exp. Clin. Cancer Res.* **32**, 79

230. Jacobs, S. R., Herman, C. E., Maciver, N. J., Wofford, J. a, Wieman, H. L., Hammen, J. J., and Rathmell, J. C. (2008) Glucose uptake is limiting in T cell activation and requires CD28-mediated Akt-dependent and independent pathways. *J. Immunol.* **180**, 4476–4486

231. Stockli, J., Fazakerley, D. J., and James, D. E. (2011) GLUT4 exocytosis. *J. Cell Sci.* **124**, 4147–4159

232. Belman, J. P., Habtemichael, E. N., and Bogan, J. S. (2014) A proteolytic pathway that controls glucose uptake in fat and muscle. *Rev Endocr Metab Disord.* **15**, 55–66

233. Alvim, R. O., Cheuhen, M. R., and Machado, S. R. (2015) General aspects of muscle glucose uptake. *Ann. Brazilian Acad. Sci.* **87**, 351–368

234. Millar, C. a., Powell, K. a., Hickson, G. R. X., Bader, M. F., and Gould, G. W. (1999) Evidence for a role for ADP-ribosylation factor 6 in insulin-stimulated glucose transporter-4 (GLUT4) trafficking in 3T3-L1 adipocytes. *J. Biol. Chem.* **274**, 17619–17625

235. Van Dam, E. M., Govers, R., and James, D. E. (2005) Akt activation is required at a late stage of insulin-induced GLUT4 translocation to the plasma membrane. *Mol. Endocrinol.* **19**, 1067–1077

236. Backer, J. M., Myers, M. G., Shoelson, S. E., Chin, D. J., Sun, X. J., Miralpeix, M., Hu, P., Margolis, B., Skolnik, E. Y., and Schlessinger, J. (1992) Phosphatidylinositol 3'-kinase is activated by association with IRS-1 during insulin stimulation. *EMBO J.* **11**, 3469–3479

237. White, M. F., and Kahn, C. R. (1994) The insulin signaling system. *J. Biol. Chem.* **269**, 1–4

238. Zorzano, a., Munoz, P., Camps, M., Mora, C., Testar, X., and Palacin, M. (1996) Insulin-induced redistribution of GLUT4 glucose carriers in the muscle fiber: In search of GLUT4 trafficking pathways. *Diabetes*. **45**, SUPPL. 1

239. Steinbusch, L. K. M., Schwenk, R. W., Ouwens, D. M., Diamant, M., Glatz, J. F. C., and Luiken, J. J. F. P. (2011) Subcellular trafficking of the substrate transporters GLUT4 and CD36 in cardiomyocytes. *Cell. Mol. Life Sci.* **68**, 2525–2538

240. Capilla, E., Suzuki, N., Pessin, J. E., and Hou, J. C. (2007) The glucose transporter 4 FQQI motif is necessary for Akt substrate of 160-kilodalton-dependent plasma membrane translocation but not Golgi-localized (gamma)-ear-containing Arf-binding protein-dependent entry into the insulin-responsive storage compartmen. *Mol. Endocrinol.* **21**, 3087–3099

241. Khan, A. H., Capilla, E., Hou, J. C., Watson, R. T., Smith, J. E., and Pessin, J. E. (2004) Entry of newly synthesized GLUT4 into the insulin-responsive storage compartment is dependent upon both the amino terminus and the large cytoplasmic loop. *J. Biol. Chem.* **279**, 37505–37511

242. Tsuchiya, A., Kanno, T., and Nishizaki, T. (2013) Diacylglycerol promotes GLUT4 translocation to the cell surface in a PKCε-dependent and PKCλ/ι and -ζ-independent manner. *Life Sci.* **93**, 240–246

243. Asano, T., Kanda, A., Katagiri, H., Nawano, M., Ogihara, T., Inukai, K., Anai, M., Fukushima, Y., Yazaki, Y., Kikuchi, M., Hooshmand-Rad, R., Heldin, C. H., Oka, Y., and Funaki, M. (2000) p110B Is up-regulated during differentiation of 3T3-L1 cells and contributes to the highly insulin-responsive glucose transport activity. *J. Biol. Chem.* **275**, 17671–17676

244. Waller, A., Kohler, K., Burns, T., Mudge, M., Belknap, J., and Lacombe, V. (2011) Naturally-occuring compensated insulin resistance selectively alters glucose transporters in visceral and subcutaneous adipose tissue without change in AS 160 activation. *Biochim Biophys Acta*. **1812**, 1098–1103

245. Tsuchiya, Y., Hatakeyama, H., Emoto, N., Wagatsuma, F., Matsushita, S., and Kanzaki, M. (2010) Palmitate-induced down-regulation of sortilin and impaired GLUT4 trafficking in C2C12 Myotubes. *J. Biol. Chem.* **285**, 34371–34381

246. Hong, Y. H., Betik, A. C., and McConell, G. K. (2014) Role of nitric oxide in skeletal muscle glucose uptake during exercise. *Exp. Physiol.* **99**, 1569–1573

247. Li, Q., Zhu, X., Ishikura, S., Zhang, D., Gao, J., Sun, Y., Contreras-Ferrat, A., Foley, K. P., Lavandero, S., Yao, Z., Bilan, P. J., Klip, A., and Niu, W. (2014) Ca2+ signals promote GLUT4 exocytosis and reduce its endocytosis in muscle cells. *Am. J. Physiol. Endocrinol. Metab.* **307**, e209–224

248. Kellett, G. L., and Helliwell, P. a (2000) The diffusive component of intestinal glucose absorption is mediated by the glucose-induced recruitment of GLUT2 to the brush-border membrane. *Biochem J*. **350**, 155–162

249. Tobin, V., Gall, M. Le, Fioramonti, X., Stolarczyk, E., Blazquez, A. G., Klein, C., Prlgent, M., Serradas, P., Cuif, M. H., Magnan, C., Leturque, A., and Brot-Laroche, E. (2008) Insulin internalizes GLUT2 in the enterocytes of healthy but not insulin-resistant mice. *Diabetes*. **57**, 555–562

250. Helliwell, P., Richardson, M., Affleck, J., and Kellett, G. (2000) Stimulation of fructose transport across the intestinal brush-border membrane by PMA is mediated by GLUT2 and dynamically regulated by protein kinase C. *Biochem J*. **350**, 149–154

251. Mace, O. J., Lister, N., Morgan, E., Shepherd, E., Affleck, J., Helliwell, P., Bronk, J. R., Kellett, G. L., Meredith, D., Boyd, R., Pieri, M., Bailey, P. D., Pettcrew, R., and Foley, D. (2009) An energy supply network of nutrient absorption coordinated by calcium and T1R taste receptors in rat small intestine. *J. Physiol.* **587**, 195–210

252. Cheeseman, C. I., and O'Neill, D. (1998) Basolateral D-glucose transport activity along the crypt-villus axis in rat jejunum and upregulation induced by gastric inhibitory peptide and glucagon-like peptide-2. *Exp. Physiol.* **83**, 605–616

253. Shepherd, E. J., Helliwell, P. a, Mace, O. J., Morgan, E. L., Patel, N., and Kellett, G. L. (2004) Stress and glucocorticoid inhibit apical GLUT2-trafficking and intestinal glucose absorption in rat small intestine. *J. Physiol.* **560**, 281–290

254. Habold, C., Foltzer-Jourdainne, C., Le Maho, Y., Lignot, J.-H., and Oudart, H. (2005) Intestinal gluconeogenesis and glucose transport according to body fuel availability in rats. *J. Physiol.* **566**, 575–586

255. Wiśniewski, J., Friedrich, A., Keller, T., Mann, M., and Koepsell, H. (2015) The Impact of High-Fat Diet on Metabolism and Immune Defense in Small Intestine Mucosa. *J. Proteome Res.* **14**, 353–365

256. Cohen, M., Kitsberg, D., Tsytkin, S., Shulman, M., Aroeti, B., and Nahmias, Y. (2014) Live imaging of GLUT2 glucose- dependent trafficking and its inhibition in polarized epithelial cysts. *Open Biol.* **4**, 140091

257. Greenlee, W., Heather, M., Uemura, E., Carpenter, S. L., Doyle, R. T., and Buss, J. E. (2003) Glucose uptake in PC12 cells: GLUT3 vesicle trafficking and fusion as revealed with a novel GLUT3-GFP fusion protein. *J. Neurosci. Res.* **73**, 518–525

258. McClory, H., Williams, D., Sapp, E., Gatune, L. W., Wang, P., DiFiglia, M., and Li, X. (2014) Glucose transporter 3 is a rab11-dependent trafficking cargo and its transport to the cell surface is reduced in neurons of CAG140 Huntington's disease mice. *Acta Neuropathol. Commun.* **2**, 1–9

259. Pinto, A. B., Carayannopoulos, M. O., Hoehn, A., Dowd, L., and Moley, K. H. (2002) Glucose transporter 8 expression and translocation are critical for murine blastocyst survival. *Biol. Reprod.* **66**, 1729–1733

260. Carayannopoulos, M. O., Chi, M. M., Cui, Y., Pingsterhaus, J. M., McKnight, R. a, Mueckler, M., Devaskar, S. U., and Moley, K. H. (2000) GLUT8 is a glucose transporter responsible for insulin-stimulated glucose uptake in the blastocyst. *Proc. Natl. Acad. Sci.* **97**, 7313–7318

261. Piroli, G. G., Grillo, C. a., Charron, M. J., McEwen, B. S., and Reagan, L. P. (2004) Biphasic effects of stress upon GLUT8 glucose transporter expression and trafficking in the diabetic rat hippocampus. *Brain Res.* **1006**, 28–35

262. Piroli, G. G., Grillo, C. a., Hoskin, E. K., Znamensky, V., Katz, E. B., Milner, T. a., McEwen, B. S., Charron, M. J., and Reagan, L. P. (2002) Peripheral glucose administration stimulates the translocation of GLUT8 glucose transporter to the endoplasmic reticulum in the rat hippocampus. *J. Comp. Neurol.* **452**, 103–114

263. Augustin, R., Riley, J., and Moley, K. H. (2005) GLUT8 contains [DE]XXXL[LI] sorting motif and localizes to a late endomosal/lysosomal compartment. *Traffic*. **6**, 1196–1212

264. Flessner, L., and Moley, K. (2010) Similar [DE]XXX[LI] motifs differentially target GLUT8 and GLUT12 in Chinese Hamster Ovary cells. *Traffic*. **10**, 324–333

265. Aerni-Flessner, L., Abi-Jaoude, M., Koenig, A., Payne, M., and Hruz, P. W. (2012) GLUT4, GLUT1, and GLUT8 are the dominant GLUT transcripts expressed in the murine left ventricle. *Cardiovasc. Diabetol.* **11**, 63–73

266. Augustin, R., Carayannopoulos, M. O., Dowd, L. O., Phay, J. E., Moley, J. F., and Moley, K. H. (2004) Identification and characterization of human glucose transporter-like protein-9 (GLUT9): Alternative splicing alters trafficking. *J. Biol. Chem.* **279**, 16229–16236

267. De Vivo, D., Trifiletti, R., Jacobson, R., Ronen, G., Behmand, R., and SI, H. (1991) Deffective glucose transport across the blood-brain barrier as a cause of persistent hypoglycorrhachia, seizures, and development delay. *N. Engl. J. Med.* **325**, 703–709

268. Sen, S., Keough, K., and Gibson, J. (2015) Clinical Reasoning : Novel GLUT1-DS mutation Refractory seizures and ataxia. *Am. Acad. Neurol.* **84**, e111–114

269. Raja, M., and Kinne, R. K. H. (2015) Pathogenic mutations causing glucose transport defects in GLUT1 transporter: The role of intermolecular forces in protein structure-function. *Biophys. Chem.* **200-201**, 9–17

270. Yang, H., Wang, D., Engelstad, K., Bagay, L., Wei, Y., Rotstein, M., Aggarwal, V., Levy, B., Ma, L., Chung, W. K., and De Vivo, D. C. (2011) Glut1 deficiency syndrome and erythrocyte glucose uptake assay. *Ann. Neurol.* **70**, 996–1005

271. Rohr, K. (1949) Familial panmyelophthisis, Fanconi syndrome in adults. *Blood*. **4**, 130–141

272. Santer, R., Schneppenheim, R., Dombrowske, A., Gotzer, H., Steinmann, B., and Schaub, J. (1997) Mutation in GLUT2, the gene for the liver-type

glucose transporter, in patients with Fanconi-Bickel syndrome. *Nat. Genet.* **15**, 57–61

273. Ohtsubo, K., Takamatsu, S., Gao, C., Korekane, H., Kurosawa, T. M., and Taniguchi, N. (2013) N-glycosylation modulates the membrane sub-domain distribution and activity of glucose transporter 2 in pancreatic beta cells. *Biochem. Biophys. Res. Commun.* **434**, 346–351

274. De los Angeles García, M., Millán, C., Balmaceda-Aguilera, C., Castro, T., Pastor, P., Montecinos, H., Reinicke, K., Zúñiga, F., Vera, J. C., Oñate, S. a., and Nualart, F. (2003) Hypothalamic ependymal-glial cells express the glucose transporter GLUT2, a protein involved in glucose sensing. *J. Neurochem.* **86**, 709–724

275. Abbasi, F., Azizi, F., Javaheri, M., Mosallanejad, A., Ebrahim-Habibi, A., and Ghafouri-Fard, S. (2015) Segregation of a novel homozygous 6 nucleotide deletion in GLUT2 gene in a Fanconi–Bickel syndrome family. *Gene*. **557**, 103–105

276. Matsuo, H., Chiba, T., Nagamori, S., Nakayama, A., Domoto, H., Phetdee, K., Wiriyasermkul, P., Kikuchi, Y., Oda, T., Nishiyama, J., Nakamura, T., Morimoto, Y., Kamakura, K., Sakurai, Y., Nonoyama, S., Kanai, Y., and Shinomiya, N. (2008) Mutations in Glucose Transporter 9 Gene SLC2A9 Cause Renal Hypouricemia. *Am. J. Hum. Genet.* **83**, 744–751

277. DeBosch, B., Kluth, O., Kujiwara, H., Schürmann, A., and Moley, K. (2015) Early-onset metabolic syndrome in mice lacking the intestinal uric acid transporter SLC2A9. *Nat. Commun.* **5**, 4642

278. Racker, E., and Spector, M. (1981) Warburg effect revisited: merger of biochemistry and molecular biology. *Science*. **213**, 303–307

279. Warburg, O. (1956) On the origin of cancer cells. *Oncologia.* **9**, 75–83

280. Wang, H., Li, D., Liu, S., Liu, R., Yuan, H., Krasnoperov, V., Shan, H., Conti, P. S., Gill, P. S., and Li, Z. (2015) Small animal PET imaging of pancreatic cancer xenografts using 64Cu labeled monoclonal antibody MAb159. *J. Nucl. Med.* **56**, 908–913

281. Kepka, L., and Socha, J. (2015) PET-CT use and the occurrence of elective nodal failure in involved field radiotherapy for non-small cell lung cancer: A systematic review. *Radiother. Oncol.* **115**, 151–156

282. Koo, H. R., Park, J. S., Kang, K. W., Han, W., Park, I. A., and Moon, W. K. (2015) Correlation between 18F-FDG uptake on PET/CT and prognostic factors in triple-negative breast cancer. *Eur. Radiol.* In Press.

283. Weber, W. A., Gatsonis, C. A., Mozley, P. D., Hanna, L. G., Shields, A. F., Aberle, D. R., Govindan, R., Torigan, D. A., Karp, J. S., Yu, J. Q., Subramaniam, R. M., Halvorsen, R. A., and Siegel, B. A. (2015) Repeatability of 18F-FDG PET/CT in Advanced Non-small Cell Lung Cancer: Prospective Assessment in Two Multicenter Trials. *J. Nucl. Med.* In Press.

284. Levi, J., Cheng, Z., Gheysens, O., Patel, M., Chan, C. T., Wang, Y., Namavari, M., and Gambhir, S. (2007) Fluorescent fructose derivatives for imaging breast cancer cells. *Bioconjug Chem*. **18**, 628–634

285. Zamora-León, S. P., Golde, D. W., Concha, I. I., Rivas, C. I., Delgado-López, F., Baselga, J., Nualart, F., and Vera, J. C. (1996) Expression of the fructose transporter GLUT5 in human breast cancer. *Proc. Natl. Acad. Sci. U. S. A.* **93**, 1847–1852

286. Wuest, M., Trayner, B. J., Grant, T. N., Jans, H. S., Mercer, J. R., Murray, D., West, F. G., McEwan, A. J. B., Wuest, F., and Cheeseman, C. I. (2011) Radiopharmacological evaluation of 6-deoxy-6-[18F]fluoro-d-fructose as a radiotracer for PET imaging of GLUT5 in breast cancer. *Nucl. Med. Biol.* **38**, 461–475

287. Trayner, B. J., Grant, T. N., West, F. G., and Cheeseman, C. I. (2009) Synthesis and characterization of 6-deoxy-6-fluoro-d-fructose as a potential compound for imaging breast cancer with PET. *Bioorganic Med. Chem.* **17**, 5488–5495

288. Neves, F. A., Cortez, E., Bernardo, A. F., Mattos, A. B. M., Vieira, A. K., de O. Malafaia, T., Thole, A. A., Alessandra, A. C., Garcia-Souza, É. P., Sichieri, R., and Moura, A. S. (2014) Heart energy metabolism impairment in Western-diet induced obese mice. *J. Nutr. Biochem.* **25**, 50–57

289. Pereira, R. O., Wende, A. R., Olsen, C., Soto, J., Rawlings, T., Zhu, Y., Anderson, S. M., and Abel, E. D. (2013) Inducible overexpression of GLUT1 prevents mitochondrial dysfunction and attenuates structural remodeling in pressure overload but does not prevent left ventricular dysfunction. *J. Am. Heart Assoc.* **2**, e000301

290. Craveiro, M., Clerc, I., Sitbon, M., and Taylor, N. (2013) Metabolic pathways as regulators of HIV infection. *Curr. Opin. HIV AIDS*. **8**, 182–9

291. Loisel-Meyer, S., Swainson, L., Craveiro, M., Oburoglu, L., Mongellaz, C., Costa, C., Martinez, M., Cosset, F.-L., Battini, J.-L., Herzenberg, L. a., Herzenberg, L. a., Atkuri, K. R., Sitbon, M., Kinet, S., Verhoeyen, E., and Taylor, N. (2012) Glut1-mediated glucose transport regulates HIV infection. *Proc. Natl. Acad. Sci.* **109**, 2549–2554

292. Palmer, C. S., Anzinger, J. J., Zhou, J., Gouillou, M., Landay, a., Jaworowski, a., McCune, J. M., and Crowe, S. M. (2014) Glucose Transporter 1-Expressing Proinflammatory Monocytes Are Elevated in Combination Antiretroviral Therapy-Treated and Untreated HIV+ Subjects. *J. Immunol.* **193**, 5595–5603

293. McBrayer, S. K., Cheng, J. C., Singhal, S., Krett, N. L., Rosen, S. T., and Shanmugam, M. (2012) Multiple myeloma exhibits novel dependence on GLUT4, GLUT8, and GLUT11: Implications for glucose transporter-directed therapy. *Blood*. **119**, 4686–4697

294. Aravinthan, A., Challis, B., Shannon, N., Hoare, M., Heaney, J., and Alexander, G. J. M. (2015) Selective insulin resistance in hepatocyte senescence. *Exp. Cell Res.* **331**, 38–45

295. Garvey, W. T., Maianu, L., Zhu, J. H., Brechtel-Hook, G., Wallace, P., and Baron, A. D. (1998) Evidence for defects in the trafficking and translocation of GLUT4 glucose transporters in skeletal muscle as a cause of human insulin resistance. *J. Clin. Invest.* **101**, 2377–2386

296. Favaretto, F., Milan, G., Collin, G. B., Marshall, J. D., Stasi, F., Maffei, P., Vettor, R., and Naggert, J. K. (2014) GLUT4 Defects in Adipose Tissue Are Early Signs of Metabolic Alterations in Alms1GT/GT, a Mouse Model for Obesity and Insulin Resistance. *PLoS One*. **9**, e109540

297. Shikhman, A. R., Brinson, D. C., and Lotz, M. K. (2004) Distinct pathways regulate facilitated glucose transport in human articular chondrocytes during anabolic and catabolic responses. *Am. J. Physiol. Endocrinol. Metab.* **286**, E980–E985

298. Hirai, T., Heymann, J. a W., Maloney, P. C., and Subramaniam, S. (2003) Structural model for 12-helix transporters belonging to the major facilitator superfamily. *J. Bacteriol.* **185**, 1712–1718

299. Cannon, P. J., Stason, W. B., Demartini, F. E., Sommers, S. C., and Laragh, J. H. (1996) Hyperuricemia in primary and renal hypertension. *N Engl J Med.* **275**, 457–464

300. Witkowska, K., Smith, K. M., Yao, S. Y. M., Ng, A. M. L., O'Neill, D., Karpinski, E., Young, J. D., and Cheeseman, C. I. (2012) Human SLC2A9a and SLC2A9b isoforms mediate electrogenic transport of urate with different characteristics in the presence of hexoses. *Am. J. Physiol. Renal Physiol.* **303**, F527–39

301. Keskanokwong, T., Shandro, H. J., Johnson, D. E., Kittanakom, S., Vilas, G. L., Thorner, P., Reithmeier, R. A. F., Akkarapatumwong, V.,

Yenchitsomanus, P. T., and Casey, J. R. (2007) Interaction of integrin-linked kinase with the kidney chloride/bicarbonate exchanger, kAE1. *J. Biol. Chem.* **282**, 23205–23218

302. Zhang, Y. (2008) I-TASSER server for protein 3D structure prediction. *BMC Bioinformatics*. **9**, 40

303. Laskowski, R. A., MacArthur, M. W., Moss, D. S., and Thornton, J. M. (1993) Procheck: a program to check the stereochemical quality of protein structures. *J. Appl. Crystallogr.* **26**, 283–291

304. Sievers, F., Wilm, A., Dineen, D., Gibson, T. J., Karplus, K., Li, W., Lopez, R., McWilliam, H., Remmert, M., Söding, J., Thompson, J. D., and Higgins, D. G. (2011) Fast, scalable generation of high-quality protein multiple sequence alignments using Clustal Omega. *Mol. Syst. Biol.* **7**, 539

305. Robert, X., and Gouet, P. (2014) Deciphering key features in protein structures with the new ENDscript server. *Nucleic Acids Res.* **42**, 320–324

306. Dietvorst, J., Karhumaa, K., Kielland-brandt, M. C., and Brandt, A. (2010) Amino acid residues involved in ligand preference of the Snf3 transporter-like sensor in Saccharomyces cerevisiae. *Yeast*. **27**, 131–138

307. Stein, W. D. (1972) The mechanism of sugar transfer across erythrocyte membranes. *Ann. N. Y. Acad. Sci.* **195**, 412–428

308. Anzai, N., Ichida, K., Jutabha, P., Kimura, T., Babu, E., Chun, J. J., Srivastava, S., Kitamura, K., Hisatome, I., Endou, H., and Sakurai, H. (2008) Plasma urate level is directly regulated by a voltage-driven urate efflux transporter URATv1 (SLC2A9) in humans. *J. Biol. Chem.* **283**, 26834–26838

309. Smirnova, I., Kasho, V., and Kaback, H. R. (2011) Lactose permease and the alternating access mechanism. *Biochemistry.* **50**, 9683–9693

310. Huang, Y., Lemieux, M. J., Song, J., Auer, M., and Wang, D.-N. (2003) Structure and mechanism of the glycerol-3-phosphate transporter from Escherichia coli. *Science*. **301**, 616–620

311. Rasmussen, T., Edwards, M. D., Black, S. S., Rasmussen, A., Miller, S., and Booth, I. R. (2010) Tryptophan in the pore of the mechanosensitive channel MscS: assessment of pore conformations by fluorescence spectroscopy. *J. Biol. Chem.* **285**, 5377–84

312. Williams, J. K., Zhang, Y., Schmidt-Rohr, K., and Hong, M. (2013) pH-dependent conformation, dynamics, and aromatic interaction of the gating

tryptophan residue of the influenza M2 proton channel from solid-state NMR. *Biophys. J.* **104**, 1698–708

313. Katagiri, H., Asano, T., Shibasaki, Y., Lin, J. L., Tsukuda, K., Ishihara, H., Akanuma, Y., Takaku, F., and Oka, Y. (1991) Substitution of leucine for tryptophan 412 does not abolish cytochalasin B labeling but markedly decreases the intrinsic activity of GLUT1 glucose transporter. *J. Biol. Chem.* **266**, 7769–7773

314. Katagiri, H., Asano, T., Ishihara, H., Lin, J. L., Inukai, K., Shanahan, M. F., Tsukuda, K., Kikuchi, M., Yazaki, Y., and Oka, Y. (1993) Role of tryptophan-388 of GLUT1 glucose transporter in glucose-transport activity and photoaffinity-labelling with forskolin. *Biochem. J.* **291**, 861–867

315. Komoda, F., Sekine, T., Inatomi, J., Enomoto, A., Endou, H., Ota, T., Matsuyama, T., Ogata, T., Ikeda, M., Awazu, M., Muroya, K., Kamimaki, I., and Igarashi, T. (2004) The W258X mutation in SLC22A12 is the predominant cause of Japanese renal hypouricemia. *Pediatr. Nephrol.* **19**, 728–33

316. Krishnamurthy, H., Piscitelli, C. L., and Gouaux, E. (2009) Unlocking the molecular secrets of sodium-coupled transporters. *Nature*. **459**, 347–355

317. Emmerson, B. . (1974) Effect of oral fructose on urate production. *Ann. Dis. Rheum.* **33**, 276–280

318. Komala, M. G., Panchapakesan, U., Pollock, C., and Mather, A. (2012) Sodium glucose cotransporter 2 and the diabetic kidney. *Curr. Opin. Nephrol. Hypertens.* **22**, 113–119

319. Johnson, R. J., Sanchez-Lozada, L. G., and Nakagawa, T. (2010) The effect of fructose on renal biology and disease. *J. Am. Soc. Nephrol.* **21**, 2036–2039

320. Stein, W. D. (1986) *Transport and diffusion across cell membranes.*, Academic Press, San Diego

321. Bibert, S., Hess, S. K., Firsov, D., Thorens, B., Geering, K., Horisberger, J.-D., and Bonny, O. (2009) Mouse GLUT9: evidences for a urate uniporter. *Am. J. Physiol. Renal Physiol.* **297**, F612–F619

322. Torres, R. J., de Miguel, E., Bailen, R., Banegas, J. R., and Puig, J. G. (2014) Tubular Urate Transporter Gene Polymorphisms Differentiate Patients with Gout Who Have Normal and Decreased Urinary Uric Acid Excretion. *J. Rheumatol.* **41**, 1863–1870

323. Li, S., Sanna, S., Maschio, A., Busonero, F., Usala, G., Mulas, A., Lai, S., Dei, M., Orrù, M., Albai, G., Bandinelli, S., Schlessinger, D., Lakatta, E., Scuteri, A., Najjar, S. S., Guralnik, J., Naitza, S., Crisponi, L., Cao, A., Abecasis, G., Ferrucci, L., Uda, M., Chen, W.-M., and Nagaraja, R. (2007) The GLUT9 gene is associated with serum uric acid levels in Sardinia and Chianti cohorts. *PLoS Genet.* **3**, e194

324. Keembiyehetty, C., Augustin, R., Carayannopoulos, M. O., Steer, S., Manolescu, A., Cheeseman, C. I., and Moley, K. H. (2006) Mouse glucose transporter 9 splice variants are expressed in adult liver and kidney and are up-regulated in diabetes. *Mol. Endocrinol.* **20**, 686–697

325. Bibee, K. P., Illsley, N. P., and Moley, K. H. (2011) Asymmetric syncytial expression of GLUT9 splice variants in human term placenta and alterations in diabetic pregnancies. *Reprod. Sci.* **18**, 20–27

326. Silverman, M. (1991) Structure and function of hexose transporters. *Annu. Rev. Biochem.* **60**, 757–794

327. Walmsley, A. R. (1988) The dynamics of the glucose transporter. *Trends Biochem. Sci.* **13**, 226–231

328. Li, C., Wen, A., Shen, B., Lu, J., Huang, Y., and Chang, Y. (2011) FastCloning: a highly simplified, purification-free, sequence- and ligation-independent PCR cloning method. *BMC Biotechnol.* **11**, 92–102

329. Wellner, M., Monden, I., and Keller, K. (1994) The role of cysteine residues in glucose-transporter-GLUT1-mediated transport and transport inhibition. *Biochem. J.* **299 (Pt 3**, 813–817

330. Yao, S. Y., Sundaram, M., Chomey, E. G., Cass, C. E., Baldwin, S. a, and Young, J. D. (2001) Identification of Cys140 in helix 4 as an exofacial cysteine residue within the substrate-translocation channel of rat equilibrative nitrobenzylthioinosine (NBMPR)-insensitive nucleoside transporter rENT2. *Biochem. J.* **353**, 387–393

331. Vaziri, H., Baldwin, S. a, Baldwin, J. M., Adams, D. G., Young, J. D., and Postis, V. L. G. (2013) Use of molecular modelling to probe the mechanism of the nucleoside transporter NupG. *Mol. Membr. Biol.* **30**, 114–28

332. Park, J. S., and Hammond, J. R. (2012) Cysteine Residues in the Transmembrane (TM) 9 to TM11 Region of the Human Equilibrative Nucleoside Transporter Subtype 1 Play an Important Role in Inhibitor Binding and Translocation Function. *Mol. Pharmacol.* **82**, 784–94

333. Thornton, J. M. (1981) Disulphide bridges in globular proteins. *J. Mol. Biol.* **151**, 261–287

334. Pallaghy, P. K., Nielsen, K. J., Craik, D. J., and Norton, R. S. (1994) A common structural motif incorporating a cystine knot and a triple-stranded beta-sheet in toxic and inhibitory polypeptides. *Protein Sci.* **3**, 1833–1839

335. Craik, D. J. (2012) Protein folding: Turbo-charged crosslinking. *Nat. Chem.* **4**, 600–602

336. Preitner, F., Bonny, O., Laverrière, A., Rotman, S., Firsov, D., Da Costa, A., Metref, S., and Thorens, B. (2009) Glut9 is a major regulator of urate homeostasis and its genetic inactivation induces hyperuricosuria and urate nephropathy. *Proc. Natl. Acad. Sci. U. S. A.* **106**, 15501–15506

337. Preitner, F., Laverriere-Loss, A., Metref, S., Da Costa, A., Moret, C., Rotman, S., Bazin, D., Daudon, M., Sandt, C., Dessombz, A., and Thorens, B. (2013) Urate-induced acute renal failure and chronic inflammation in liver-specific Glut9 knockout mice. *Am. J. Physiol. Renal Physiol.* **305**, F786–95

338. Bjornstad, P., Lanaspa, M. A., Ishimoto, T., Kosugi, T., Kume, S., Jalal, D., Maahs, D. M., Snell-Bergeon, J. K., Johnson, R. J., and Nakagawa, T. (2015) Fructose and uric acid in diabetic nephropathy. *Diabetologia*. **58**, 1993–2002

339. Lanaspa, M. A., Ishimoto, T., Cicerchi, Christina Tamura, Y., Roncal-Jimenez, C. A., Chen, W., Tanabe, K., Andres-Hernando, Ana Orlicky, D. J., Finol, E., Inaba, S., Li, N., Rivard, C. J., Kosugi, T., Sanchez-Lozada, L. G., Petrash, J. M., Sautin, Y. Y., Ejaz, A. A., Kitagawa, W., Garcia, G. E., Bonthron, D. T., Asipu, A., Diggle, C. P., Rodriguez-Iturbe, B., Nakagawa, T., and Johnson, R. J. (2014) Endogenous fructose production and fructokinase activation mediate renal injury in diabetic nephropathy. *J. Am. Soc. Nephrol.* **25**, 2526–2538

340. Hebert, D. N., and Carruthers, a. (1992) Glucose transporter oligomeric structure determines transporter function. Reversible redox-dependent interconversions of tetrameric and dimeric GLUT1. *J. Biol. Chem.* **267**, 23829–23838